THE ROLE OF AUTOPHAGY MACHINERY IN OSTEOCLAST DISEASE PATHOGENESIS

Sing-Wai Wong

A dissertation submitted to the faculty of the University of North Carolina at Chapel Hill in Curriculum of Oral and Craniofacial Biomedicine.

Chapel Hill
2019

Approved by:

J. Timothy Wright

Ching-Chang Ko

Jennifer Martinez

Henry Tseng

Patricia Miguez

ABSTRACT

Sing-Wai Wong: The role of autophagy machinery in osteoclast disease pathogenesis
(Under the direction of Ching-Chang Ko and Jennifer Martinez)

Osteoclast disease, such as Paget's disease of the bone and osteoporosis, are pathological conditions of excessive bone resportion caused by disproportionate generation or over-activation of osteoclasts. They represent some of the most common chronic diseases that result in morbidity and disability in the elderly population with an estimation of more than 60 million people in the US currently affected with osteoclast diseases. My dissertation research focuses on studying the role of autophagy machinery in osteoclast differentiation and osteoclast disease pathogenesis.

In the second chapter, we investigate the role autophagy receptor Optineurin (OPTN) in the pathogenesis of Paget's disease of the bone (PDB). We identify that OPTN acts as an intrinsic negative modulator for osteoclast development, as it restrains osteoclast differentiation *in vitro* and protects against the development of PDB *in vivo*. While the absence of OPTN results in a defective type I interferon responses in osteoclasts, exogenous supplementations of recombinant IFNβ completely reverse the hyperactivity observed in OPTN deficient osteoclasts. Therefore, we propose that IFNβ could serve a novel pharmacotherapy for PDB.

In the third chapter, we investigate the role of autophagy machinery in osteoclast differentiation. We reveal that certain upstream autophagy core proteins, such Beclin-1, VPS34, ATG14 and FIP200 are required for osteoclast development, which seems to be dispensable of autophagic flux. Moreover, we uncovered the noncanonical roles of autophagy protein Beclin-1 in osteoclast differentiation – nuclear Beclin-1 protects against DNA damages and cell death to main-

tain sufficient noncanonical NF-kB responses during osteoclastogenesis. Since mice with myeloid restricted *Becn1* deficiency exhibit insignificant age-related bone loss, Beclin1 may be a novel therapeutic target for osteoporosis.

Taken together, my research adds knowledge to our current understanding of osteoclast development - the entire autophagy pathway is instrumental for osteoclast differentiation, through different components exert different control over the differentiation process. Targeting the autophagy and its effector pathways may be a novel anti-resorptive regimen for patients with osteoclast disease, and may potential benefit them in a multifaceted way.

To my parents **Y Wong** and **F Tse** who gave me the life.

To my grandparents **S Zhang** and **S Xie** who raised me.

ACKNOWLEDGEMENTS

I would like to give my deepest gratitude to my two PhD supervisors, Dr. Ching-Chang Ko and Dr. Jennifer Martinez, who mentored me during past 4 years. Thank you Dr. Ko for being a wonderful mentor. Your commitment to patients and devotion to science has illuminated my career path. Thank you for always taking care of me and for your utmost guidance and support during my PhD. Thank you Dr. Martinez for introducing the immunology world and for teaching me to become a scientist. Thank you for always motivating me whenever I had a failed experiment or a downhill of the life, and for your unreserved support for whatever decision I have made.

Besides my advisors, I would also like to thank my thesis committee members. Thank you Dr. Wright for leading my PhD progress and for contributing invaluable insights from the genetic aspect, which I always interested in. Thank you Dr. Tseng for providing me the knockout mice and for your great comments, which made think outside the box. Thanks for Dr. Miguez for insightful suggestions from bone aspects and for providing me numerous chances on my career development.

It is great to be a PhD student in UNC OCBM program. Thank you Dr. Phillips for recruiting me into this fantastic program and for providing me endless support. I would like to thank all OCBM students, including Kevin, Ning, Sehrish and Aatish for the great friendship and many joyful conversations. I want to thank my qualify exam committee members, Drs. Amelio, Yamauchi and Everett who taught me critical thinking abilities, and to thank Dr. Styner of UNC

SOM for teaching me the experiment technique. Thank you Dr. Hong of NIEHS for providing me a chance for lab rotation.

I am very fortunate to conduct my dissertation research at NIEHS, where I was nourished by many phenomenal NIH scientists. Thank you Drs. Cook and Fessler for your constructive suggestions on my research and for your careful help on my manuscript. I want to thank my NIEHS fellow labmates, Joy, Payel, Trey and Ginger for the stimulating discussions and brainstorms and for all the fun during my time in the lab. Also, I would like to thank my UNC fellow labmates, DJ, Peng, and lab manage, John, for your sincere help and support during my PhD study.

I want to take this opportunity to show my gratitude's for my master thesis mentor Dr. Hailan Feng, who opened me a door to the life a clinician-scientist.

Finally yet importantly, I would like to thank my friends. I am grateful for having many awesome friends during PhD like Shengjie, Jason, Bo-wen, Allen, Nuo, Yuanfan, Qiuyu and Xuhui, who made my PhD life colorful, joyful and meaningful

TABLE OF CONTENTS

LIST OF TABLES

LIST OF FIGURES

LIST OF ABBREVIATIONS

AMPK	AMP-activated protein kinase
ATG	Autophagy
BSA	Bovine serum albumin
DMEM	Dulbecco's modified eagle medium
ECM	Extra cellular matrix
FBS	Fetus bovine serum
FIP200	FAK-interacting protein of 200 kDA
GAPDH	Glyceraldehyde 3-phosphate dehydrogenase
GWAS	genome-wide association studies
IFN	Interferon
IL	Interleukin
IL6	Interleukin 6
IRF	interferon regulatory factor
JNK	c-Jun N-terminal Kinase
LAP	Lymphoid enhancer-binding factor 1

LC3	LC3-associated phagocytosis
LPS	Lipopolysaccharide
MAPK	Mitogen-activated protein kinase
MCP-1	Monocyte chemoattractant protein-1
MMPs	Matrix metalloproteases
NADPH	Nicotinamide adenine dinucleotide phosphate
NEMO	NF-kappa-B essential modulator
NF-kB	Nuclear factor kappa-light-chain-enhancer of activated B cells
OPTN	Optineurin
PBS	Phosphate buffered saline
PDB	Paget's disease of the bone
PE	Phosphatidylethanolamine
PI(3)P	phosphatidylinositol 3-phosphate
PI3KC3	class III PI3K complex
SNP	single nucleotide polymorphism

TNF-α	Tumor necrosis factor alpha
ULK1/2	Unc-51-like autophagy activating kinase
UVRAG	UV radiation resistance-associated gene
VPS34	Vacuolar protein sorting 34
Wnt	Wingless-type MMTV integration site family Member

CHAPTER 1: INTRODUCTION [1]

Osteoclast diseases

Osteoclast disease, such as osteopenia, osteoporosis and Paget's disease of the bone, are pathological conditions of excessive bone resorption caused by disproportionate generation of activation of osteoclasts, the multi-nucleated cells that degrade bone. They represent some of the most common chronic disease that result in morbidity and disability in the elderly population (Bilezikian 2019). It is estimated that more than 60 million people in the US are currently affected with osteoclast disease (Johnell and Kanis 2006), which result in disability, death and decreased quality of life, and places a huge burden on the patients, healthcare systems and the entire society.

Osteoporosis

The clinical definition of osteoporosis is "a systemic disease characterized by low bone mass and microarchitectural deterioration of bone tissue, with a consequent increase in bone fragility and susceptibility" (Peck et al. 1993). Osteoporosis was first named during the last century based on the histological diagnosis, "porous bone". In 1994, the World Health Organization, defined the diagnosis of osteoporosis as dependent on bone mineral density and previous facture history (Bilezikian 2019). It has been estimated that more than 10 million

[1] This chapter is partial extracted from previous published articles in *Frontiers in Immunology* and the *FEBS (Federation of European Biochemical Societies) Journal*. The original citations are as follows:
Wong SW, Sil P, Martinez J. "Rubicon: LC3-associated phagocytosis and beyond." *FEBS J* 285(8) (April 2018): 1379-1388.
Sil P, Wong SW, Martinez J. "More Than Skin Deep: Autophagy Is Vital for Skin Barrier Function". *Front Immunol* 25; 9 (Jun 2018): 1376

American people over 50 years of age have osteoporosis, that leads to approximately 1.5 million bone fractures annually (Bilezikian 2019).Osteoporosis is diagnosed with a decrease of bone-mineral density (BMD) of more than 2.5 standard deviations below the average of young adults (T score < 2.5), assessed by dual x-ray absorptiometry (DXA) (Kanis et al. 1994). Bone fracture is the main consequence of osteoporosis, and commonly occurrs in the spine, hip or wrist. After a bone fracture of the low extremities, the mortality of osteoporotic patients can reach up to 20% due to adverse complications, such thromboembolism and pneumonia.

It is widely accepted that, from the pubertal growth spurt, when the peak bone mass is attained, to the very early middle age, these is no significant change in BMD or microarchitecture. Beginning in the third decade of life, the trabecular bone starts to be lost in both males and females, suggesting that aging is a critical confounding factor for osteoclastic bone resorption. After the age of 50 years, the volumetric BMD exhibits a linear declination, which is greater in females than in males (Bilezikian 2019; Khosla and Riggs 2005). It has been estimated that about 40% of postmenopausal women are affected with osteoporosis. After menopausal, serum estrogen concentrations decrease dramatically (85% to 90% reduction of serum estradiol levels), and this reduction is in parallel with a rapid systemic bone resorption (Khosla et al. 1997). While the rates of bone formation and resorption are approximately equivalent before menopause, a menopausal associated estradiol reduction results in a disequilibrium of bone homostasis by increasing both bone resorption and formation, with bone resorption outpacing bone formation (Garnero et al. 1996). Mechanistically, estrogen has been showed to suppress RANKL, receptor activator of nuclear factor kB ligand, a key cytokine for osteoclastogenesis (Eghbali-Fatourechi et al. 2003) and promotes the expression of osteoprotegerin (OPG), a decoy receptor for RANKL and an osteoclastogenic inhibitor (Hofbauer et al. 1999). With the decrease of the estrogen level, the ratio

of RANKL/OPG is increased, which favors osteoclast differentiation and subsequent bone resorption (Bilezikian 2019). Compared to postmenopausal females, aged males have less bone reduction (Riggs et al. 1998) and less frequency of bone fractures due to the involvement of both testosterone and estrogen in bone preservation (Khosla et al. 1998).

Paget's diseases of the bone

Paget disease of bone (PDB) is featured by focal areas of irregular bone remodeling in the elderly population. It is the second most common bone disease after osteoporosis in the United States, with a prevalence rate of 2.32% in people over 65 years of age (Altman et al. 2000). Paget's disease commonly affects axial bones, including the pelvis, femur, spine, skull and tibia. Based on the number of affected sites, this disease can be monostotic (only affect a single bone) or polystotic (involvement of two or more bones). The majority of Paget's disease patient are asymptomatic and were usually diagnosed during routine X-ray exams. With disease progression, however, signs and symptoms appear. The common clinical manifestation of PDB are bone pain, bone deformity, bone fracture, spinal stenosis/cord compression. In rare situations (less than 1%), a Pagetic lesion undergoes malignant degeneration and can be transformed to bone tumors, such as osteosarcomas or fibrosarcomas (Bilezikian 2019).

The earliest change in a Pagetic lesion is an increase formation of osteoclasts, which cause bone resorption in the affected regions. Compared to normal osteoclasts, osteoclasts in Pagetic lesions exhibit a hyper-activated signature – the number, size, actively and nuclei number of Pagetic osteoclasts are all increased (Rebel et al. 1980; Singer et al. 2006; Teramachi et al. 2016). As skeletal homeostasis breaks and bone resorption initiates, an early osteolytic lesion is formed and it manifests as a radiolucency on radiographs (Bilezikian 2019). After the osteolytic phase,

osteoblasts are recruited to the resorptive site for a compensative bone repair. Due to the rapid nature of bone formation, the structure, quality and shapes of newly formed bones are abnormal, and its phase is named as hypertrophic or mixed phase lesion of PBD. At the final stage, the affected bone may exhibits decreased hypercellularity, which changes to a sclerotic, mosaic lesion in which active bone turnover is absent, naming burned out Paget's disease (Bilezikian 2019).

Multiple lines of evidence indicate that both environmental and genetic factors have been involved in the etiopathogenesis of PDB. While environmental challenges such as, toxins, animal exposures, viral infections have been occasionally reported to be associated with PDB (Singer 2015), numerous studies showed a strong genetic predisposition of PDB (Singer 2015). Approximately 20% PDB patient have a positive family history and about a half of familial PDB patients harbor a mutation in the *SQSTM1* gene, which encodes p62, an autophagy receptor protein (Singer 2015). To date, about 30 different mutations in *SQSTM1* have been reported to cause PDB, with most of the mutations located in the ubiquitin-associated domain (Singer 2015). Some *in vitro* functional studies demonstrate that these PDB-associated mutants enhance NF-kB activation, and hence increase osteoclast differentiation. As only one tenth of patients with PDB demonstrate a mutation in *SQSTM1,* genome-wide association studies (GWAS) have explored new candidate genes associated with PDB (Albagha et al. 2010; Singer 2015). Among 15 known susceptibility loci for Paget's disease discovered by GWAS, 4 risk loci, including *CSF1*, *OPTN*, *TM7SF4* and *TNFRSF11A*, showed the strongest links to PDB and contributes to 67% of the genetic risks (Albagha et al. 2010; Chung et al. 2010).

Signaling pathways involved osteoclast differentiation

Osteoclasts are multi-nucleated bone-resorbing cells derived from monocytic lineage cells of hematopoietic cells, and the process of osteoclast differentiation is called osteoclastogenesis (Suda et al. 1999). Since the discovery of RANKL in 1990s, the molecular mechanisms that govern osteoclast differentiation continue to be elucidated (Anderson et al. 1997). It has been widely accepted that the differentiation of osteoclast depends exclusively on RANKL, an essential osteoclastogenic cytokine produced from osteoblastic cells, mesenchymal stem cells and immune cells. RANKL binds to its receptor, RANK, on the monocyte/macrophage lineage cell surfaces to induce osteoclastogenesis programme (Theill et al. 2002).

Upon RANKL stimulations, TRAF6 (Darnay et al. 1998; Naito et al. 1999) is activated and ubiquitinated for the recruitment of TAB1 (TGF-β-activated kinase 1-binding protein 1) and TAB2 to form RANK-TRAF6-TAB1-TAB2 complex, which activates TAK1 (activate mitogen-activated kinase kinase kinase) (Mizukami et al. 2002). The activation of TAK1 results in both canonical and noncanonical NF-kB activations (Lamothe et al. 2012; Swarnkar et al. 2015). For canonical NF-kB responses, the IKK complex comprising IKKα, IKKβ, and NEMO (NF-κB essential modulator) (Swarnkar et al. 2016) induces the phosphorylation and subsequent degradation of IκB. After IκB degradation, the NF-κB complex, p65/p50, is activated and translocated into the nucleus to transactivate its downstream genes. Unlike canonical NF-kB responses, noncanonical NF-kB activations requires the formation of an IKKα homodimer, which is induced by NIK (kinase NF-κB-inducing kinase). The IKKα homodimer then induce the processing from p100 to to p52 to form a RelB/p52 heterodimer (Iotsova et al. 1997). Similar to the canonical NF-κB complex, the noncanonical heterodimer, RelB/p52 is subsequently activated and translocated into the nucleus to trans-activate its effector genes (Okamoto et al. 2017).

In addition to NF-kB responses, RANKL also activates MAP kinases activations during osteoclastogenesis. *In vitro* studies showed that pharmacological inhibition of the MAP kinase, p38, blocks osteoclast differentiation (Li et al. 2002). While JNK1 and JNK2, MAP kinases are both highly expressed in osteoclasts, only JNK1 is indispensable for *in vitro* osteoclastogenesis (David et al. 2002). Although ERK1/2 is activated in RANKL induced osteoclastogenesis, its role osteoclast differentiation is inconclusive (Okamoto et al. 2017). Activated MAP kinase activate and phosphorylate the transcription factor, AP-1, for osteoclast differentiation. AP-1 is a heterodimer formed by c-Fos (Grigoriadis et al. 1994) and c-Jun proteins, and the RANKL induced the c-Fos expression is mediated by CREB (CaMK/cAMP responsive element binding protein) (Sato et al. 2006), PPARγ (peroxisome proliferator activated receptor γ) (Wan et al. 2007) and NF-κB pathways (Yamashita et al. 2007). While c-Fos is an essential component for osteoclast differentiation established by the finding that c-Fos deficient mice exhibit osteoclastopenia (Grigoriadis et al. 1994), the role of c-Jun family of proteins in osteoclast differentiation is not well studied (Okamoto et al. 2017).

NFATc1 has been considered a master regulator for osteoclast differentiation (Takayanagi et al. 2002a), and it is trans-activated by c-Fos, canonical and noncaonical NF-kB. While the above-mentioned pathways are thought to be the main resources for NFATc1 inductions, studies demonstrate other transcription factors, such as ATF4 (activating transcription factor 4) (Cao et al. 2010), LRF (leukemia/lymphoma-related factor) (Tsuji-Takechi et al. 2012), Jdp2 (Jun dimerization protein) (Maruyama et al. 2012) and Blimp1 (B lymphocyte-induced maturation protein 1) (Miyauchi et al. 2010) are also involved in the trans-activation of NFATc1. Once activated, NFATc1 can be recruited to its own promoter site to promote its auto-amplification (Asagiri et al. 2005), maintaining its expression in a high level and transactivation the promoters

of downstream osteoclastogenic genes, such as *CTSK* (cathepsin K) (Saftig et al. 1998), *ACP5* (tartrate-resistant acid phosphatase 5b) (Hayman et al. 1996), *ITGB3* (integrin β3) (McHugh et al. 2000), *OSCAR* (osteoclast-associated receptor), *DC-STAMP* (dendritic cell-specific transmembrane protein) (Yagi et al. 2005), *OC-STAMP* (osteoclast stimulatory transmembrane protein) (Miyamoto et al. 2012), *Atp6v0d2* (v-type proton ATPase subunit d2) (Lee et al. 2006).

Autophagy

Autophagy means *self* (auto) *eating* (phagy) and is a highly conserved cellular process across eukaryotes, which allows cells to recycle cytoplasmic materials *via* the lysosome and survive periods of nutrient deprivation. The term autophagy is derived from ancient Greek, but the word first garnered attention when Christian de Duve not only coined it but also won the Nobel prize in Physiology or Medicine in 1974 for his work on lysosomes (De Duve and Wattiaux 1966). More recently, Dr. Yoshinori Oshumi, described the autophagy-related genes (ATG) in yeast in 1993 (Takeshige et al. 1992) and received the Nobel prize in 2016. His pioneering work led to the discovery of other ATG genes and its human orthologs. Autophagy pathways include macroautophagy (canonical autophagy/autophagy), microautophagy, and chaperone-mediated autophagy (CMA). Traditionally, autophagy is orchestrated by the group of ATG proteins, which precisely control the autophagic process. The process kickstarts the formation of the pre-initiation complex, followed by generation of the phagophore, autophagosome, and autolysosome, leading to cargo degradation (Figure 1.2). Mammalian target of rapamycin complex 1 inhibition leads to the induction of autophagy and assembles ULK1/2, ATG13, and FIP200 to form the pre-initiation complex at the phagophore (Figure 1.1). Once activated, it targets the Class III phosphatidylinositol-3-kinase (PI3K) complex (Beclin1, VPS34, VPS15, and ATG14) which

recruits downstream conjugation ATG proteins. During autophagosome elongation, E3(Ubiquitin)-ligase ATG7 mediates ATG5–ATG12–ATG16L1 complex formation and is recruited to the autophagosome membrane. Ubiquitin-conjugating/E2-like enzyme ATG10 mediates covalent conjugation of the ubiquitin-like ATG12–ATG5. E2-like enzyme ATG3 forms ATG12–ATG3 conjugate, controls mitochondrial homeostasis. ATG7 can recruit ATG3 and ATG10 forming ATG7–ATG3 and ATG10–ATG3, respectively. Mice lacking ULK1/2, ATG3, ATG5, ATG7, ATG12, or ATG16L1 are embryonic lethal mutations. ATG12-conjugation is essential for the formation of preautophagosomes. ATG3 aids in conjugation of LC3-I with phosphatidylethanolaminie (PE) required for the formation of autophagosomes. This facilitates the LC3 lipidation with PE and forms LC3-PE (or LC3-II). LC3-PE embeds into the mature autophagosome which finally fuses with the lysosome, wherein the cargo is degraded and recycled. The autophagy pathway is not only limited to the processes of degradation and survival during starvation but is also active in regulating other cellular functions. This bolsters the need for investigating autophagy's widespread influence on different biological mechanisms.

PI3KC3s

Recent studies have described three functionally, molecularly, and location distinct Class III PI3K complexes (herein called PI3KC3) that operate during autophagy. PI3KC3s commonly contain VPS34, the catalytic subunit, Beclin 1, and VPS15 (also called p150), and the specificity of PI3KC3 are determined by different complex components which bind Beclin 1 (Sun et al. 2011). The PI3KC3 containing ATG14 (also called Barkor or ATG14L) is required for starvation-induced autophagy and is targeted to form autophagosomes. In addition, ATG14 has been shown to

augment PI(3)P production by VPS34, indicating that during canonical autophagy, ATG14 serves as both a localization agent and activity regulator of PI3KC3 (Burman and Ktistakis 2010).

A second PI3KC3 lacks ATG14 but contains UVRAG (UV radiation resistance-associated gene), a Beclin 1-binding protein that promotes Beclin 1–VPS34 interactions as well as Vps34 activity (Liang et al. 2006). The role of the UVRAG-containing PI3KC3 has been controversial (Liang et al. 2006; Song et al. 2014), as some studies have supported its role in autophagosome formation while other studies have challenged this role and rather highlighted this PI3KC3's major role in endocytosis, endosomal trafficking, autophagosome maturation via its interaction with class C-VPS/HOPS (Itakura et al. 2008; Liang et al. 2008).

The third PI3KC3 contains both UVRAG and Rubicon, and unlike the preceding two PI3KC3, this complex is a negative regulator of autophagy, interacting at multiple steps in the autophagic pathway. This inhibitory complex is partly induced by the master autophagy negative regulator, mTORC1. Under nutrient-rich conditions, mTORC1 binds and phosphorylates UVRAG, amplifying the association of UVRAG with Rubicon and the inhibition of autophagy (Kim et al. 2015). Originally identified as a Beclin 1-binding partner localizing at the early and late endosomes, Rubicon was also described as a VPS34-binding partner via its RUN domain, and this interaction inhibited VPS34 lipid kinase activity and autophagosome formation (Zhong et al. 2009). Thus, Rubicon-deficient cells demonstrate increased autophagic activity, with increased ATG16L puncta, decreased levels of p62, $LC3^{+}$ puncta, and LC3-II conversion (Matsunaga et al. 2009; Zhong et al. 2009). However, Rubicon also plays a role in inhibiting the autophagosomal maturation stage, as Rubicon-deficient cells showed a higher ratio of autophagolysosomes to autophagosomes, compared to control cells (Itakura et al. 2008).

Selective autophagy

To ensure proper scrutiny, the autophagy machinery takes on specialized roles that selectively targets and digests intracellular components and is called selective or non-canonical autophagy (Martinez et al. 2015; Munch and Dikic 2018). Depending on the cargo engulfed, it can be classified into CMA (heat-shock cognate 70 stress protein mediated target of the substrate), aggrephagy (clearance of protein aggregates), macrolipidophagy (the degradation of lipids), pexophagy (autophagic degradation of peroxisomes), ER-phagy (endoplasmic reticulum autophagy), mitophagy (damaged mitochondria), xenophagy (intracellular pathogens), and LC3-associated phagocytosis (LAP) (efferocytosis and pathogen phagocytosis) (Martinez et al. 2015; Munch and Dikic 2018). Selective autophagy receptors/adaptors p62/Sqstm1 (*Sequestome1*), OPTN (*Optineurin*), TAX1BP1 (T-cell leukemia virus type I binding protein 1), NDP52/CALCOCO2 (calcium binding and coiled-coil domain 2), and NBR1 (neighbor of BRCA1 gene 1) coordinate and mediate degradation of ubiquitinated cargos by delivering them to LC3-containing phagophores (Deosaran et al. 2013; Lamark et al. 2009; Richter et al. 2016; Viret et al. 2018; Whang et al. 2017). Mitophagy involves degradation of redundant and distressed mitochondria and normally occurs in a Parkin-PINK1-dependent manner. After ubiquitination, autophagy adaptors, OPTN and NDP52, can recognize and deliver them to LC3-positive autophagosomes for degradation (Lazarou et al. 2015; Padman et al. 2019). Similarly, in xenophagy, cytosolic pathogens or pathogen-contained vacuole can be ubiquitinated by ubiquitin ligases. Subsequently, ubiquitinated pathogens or their substrates are recruited by autophagy receptors for autophagosomal degradation (Alexander and Leib 2008; Mao and Klionsky 2017; Sil et al. 2018). However, when an extracellular pathogen is phagocytosed and it engages pathogen recognition receptor (PRR), as a result it activates a specialized autophagy process called LAP

(Wong et al. 2018). The LAP pathway is also utilized for the clearance of dead cells triggered by wounds, pathogen exposure, or environmental triggers (Wong et al. 2018).

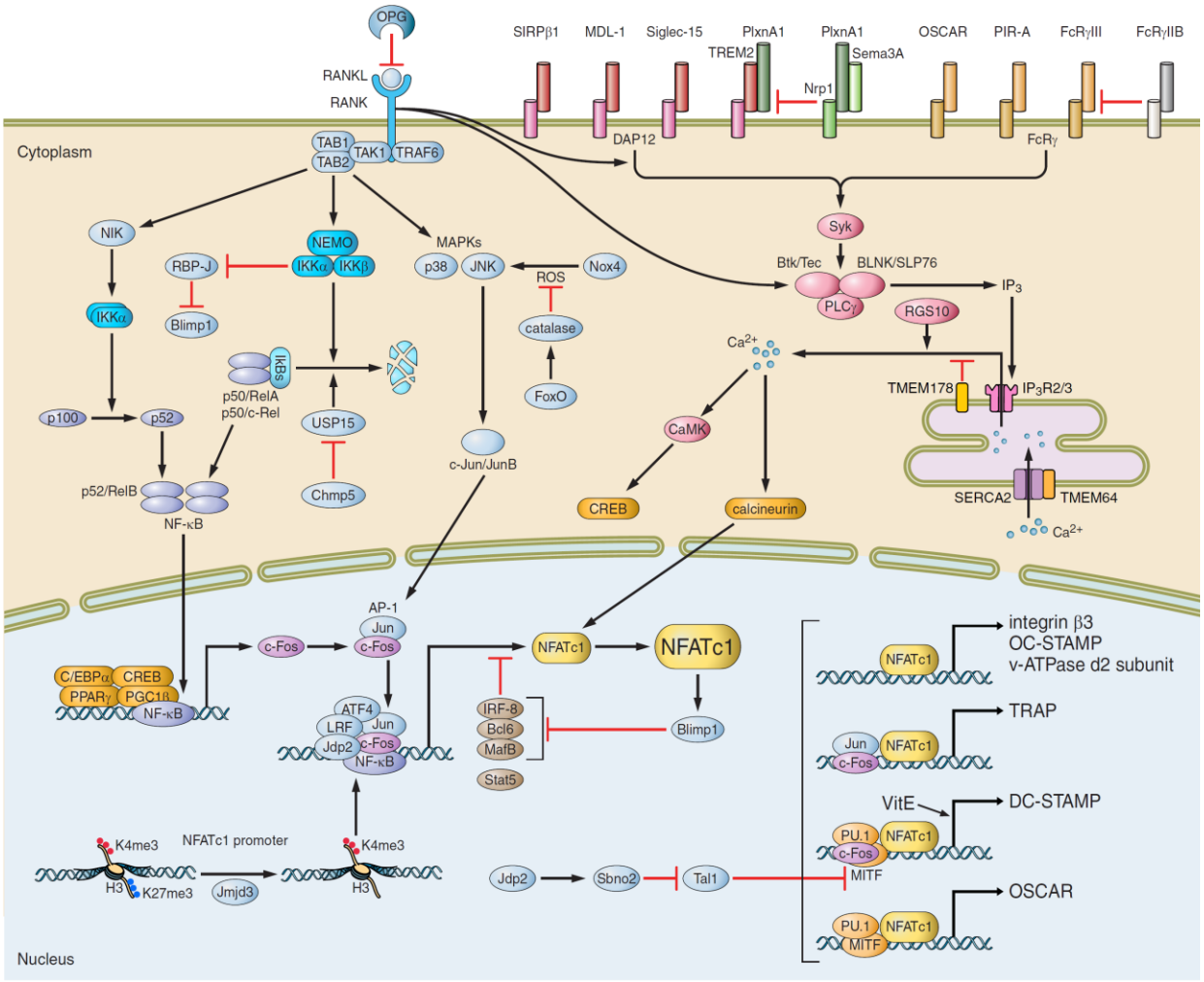

Figure 1.1 Known signaling pathway networks involved in osteoclastogenesis.

(Figure from Kazuo Okamoto et al. *Physiol Rev*, 2017)

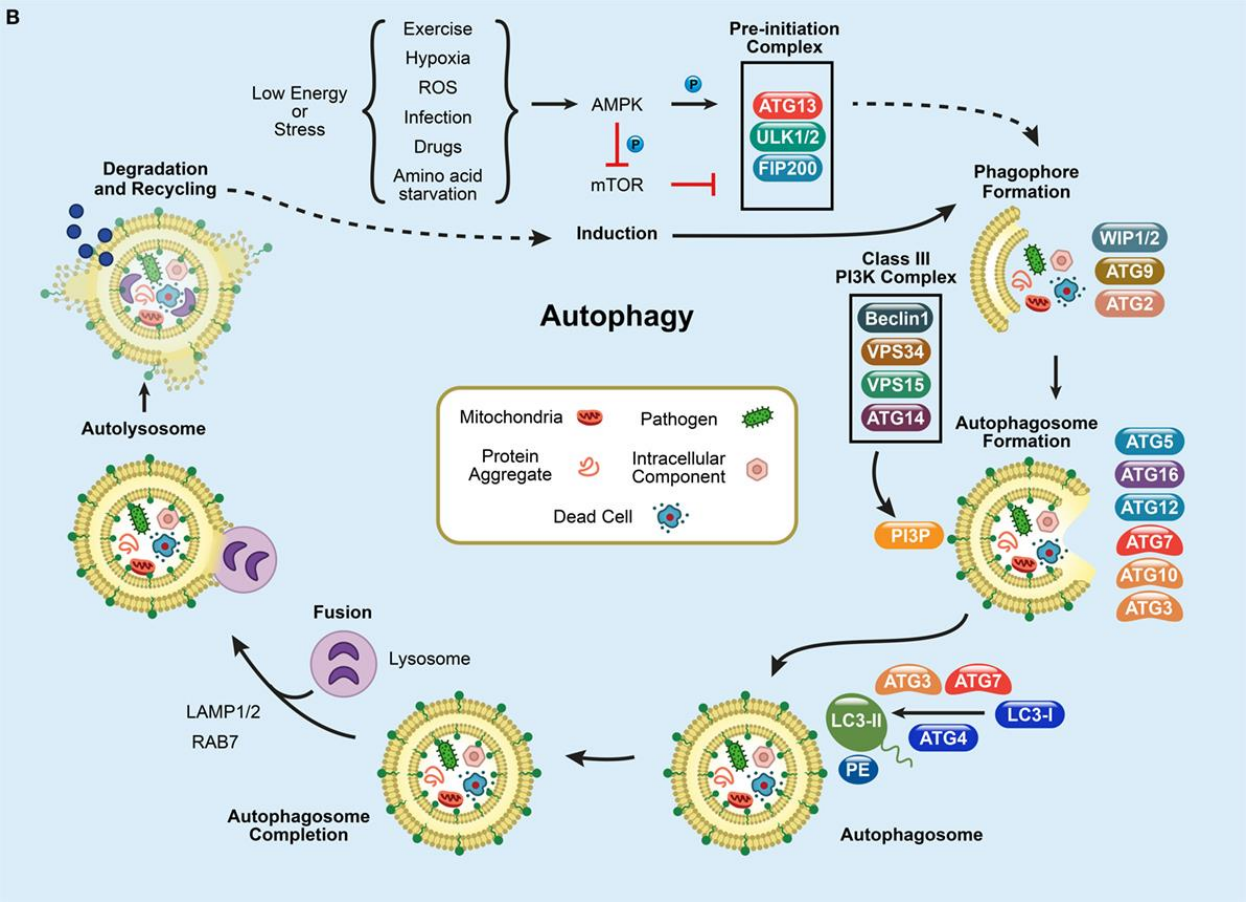

Figure 1.2 Process of autophagy. mTOR inhibition triggers the activation of AMPK and initiates an autophagy-inducing signals during a low energy state such as starvation, ROS, exercise, infection, drugs, and hypoxic stress. This initiates the formation of pre-initiation complex (ULK1/2, ATG13, and FIP200) in the presence of unwanted cargo (such as, mitochondria, pathogens, protein aggregates, and intracellular components). This will, in turn activates the Class III phosphatidylinositol-3-kinase (PI3K) complex, composed of ATG14 (UVRAG)-VPS15-VPS34-Beclin1. The Class III PI3K complex completes the autophagosome formation by producing PI3P which recruits downstream ubiquitin-like conjugation systems (ATG5–12) and converts LC3-I to form LC3-PE. Finally, lysosome fuses with the autophagosome to form the autolysosome to degrade the enclosed cargo. The degraded cargo is finally assimilated and recycled (Sil et al. 2018).

Chapter 2: THE ROLE OF AUTOPHAGY RECEPTOR, OPTINEURIN IN OSTEOCLASTOGENSIS AND THE PATHOGENESIS OF PAGET'S DISEASE OF THE BONE[2]

Introduction

Paget's disease of the bone (PDB) is an age-dependent bone disease wherein patients exhibit symptoms of focal areas of bone fragility, bone deformity, pathological fracture, and nerve root compression. PDB pathology has been attributed to osteoclast hyperactivation, leading to excessive bone resorption and irregular bone remodeling (Teramachi et al. 2016). Compared to normal osteoclasts, Pagetic osteoclasts are increased in number, nuclei, activity, and function (Kukita et al. 1990; Rebel et al. 1976). Furthermore, Pagetic osteoclast precursors display heightened osteoclastogenic potential, as they have an increased responsiveness to RANKL, a critical cytokine for osteoclast differentiation (Menaa et al. 2000). The molecular mechanisms that underlie hyper-activation of Pagetic osteoclasts, however, remain unknown.

While environmental factors, such as viral infections and toxins, can contribute to the etiology of PDB, recent evidence indicates that genetic factors also play a predominant role in PDB pathogenesis (Albagha 2015; Ralston and Albagha 2014). Mutations in *Sqstm1*, which encodes the autophagy receptor p62, have been repeatedly reported among familial PDB patients (Morissette et al. 2006), and p62 dysfunction results in increased generation and activity of

[2] This chapter is extracted from a submitted manuscript in *Cell Death & Differentiation*. The original citation is as follows:
Wong SW, Huang BW, Kim EH, Hu XX, Kolb JP, Padilla RJ, Xue P, Wang L, Oguin TH,. Miguez PA, Tseng HC, Ko CC, and Martinez J. "Global deletion of Optineurin results in altered type I IFN signaling and abnormal bone remodeling in a model of Paget's disease." *Cell Death Differ*.(accepted)

osteoclasts *in vitro* (Sundaram et al. 2011). Recent genome-wide association studies (GWAS) have identified another autophagy receptor, Optineurin (*OPTN*), that is genetically linked to PDB (Albagha et al. 2010), with the PDB-associated *OPTN* variant resulting in a decreased gene expression (Obaid et al. 2015). OPTN is ubiquitously expressed and mediates the delivery of ubiquitinated cargos, such as damaged organelles, protein aggregates, and intracellular pathogens, to autophagosomes during selective autophagy (Slowicka et al. 2016b). OPTN also functions in multiple non-autophagic processes, including vesicle trafficking, Golgi organization, and modulation of the NF-κB pathway (Chibalina et al. 2010; Chibalina et al. 2008; Meena et al. 2016; Munitic et al. 2013; Zhu et al. 2007). In addition to PDB, genetic mutations in *OPTN* underlie primary open-angle glaucoma (POAG) and amyotrophic lateral sclerosis (ALS). While the impacts of OPTN in POAG and ALS have been intensively studied (Chalasani et al. 2007; Ito et al. 2016; Toth and Atkin 2018), the specific role of OPTN in PDB remains to be established.

A recent study demonstrated that while siRNA-mediated knockdown of *Optn* increased osteoclastogenesis *ex vivo*, only approximately 10% of 15- to 18-month old mice harboring a loss-of-function mutation in the ubiquitin binding domain ($Optn^{D477N/D477N}$) developed PDB lesions (Obaid et al. 2015). However, the role of OPTN in molecular pathways beyond ubiquitin binding has not be examined in relation to PDB pathogenesis. Therefore, we generated *Optn* global knockout ($Optn^{-/-}$) mice and performed detailed bone phenotyping analysis. We discovered that $Optn^{-/-}$ mice spontaneously develop late-onset polyostotic osteolytic lesions that are reminiscent of clinical findings in PDB patients. Similarly, we observed an increased capacity for osteoclast differentiation with elevated cFos expression in the absence of *Optn ex vivo*. Mechanistically, OPTN's inhibition of osteoclastogenesis is two-fold. $Optn^{-/-}$ osteoclasts produce significantly decreased levels of IFNβ, a known negative regulator of c-Fos (Obaid et al. 2015), as well as

display a previously undescribed defect in signaling through the IFNα/βR. This defective IFNα/βR signaling also resulted in decreased cell death and hence increased survival. Thus, we have generated and characterized a novel and clinically relevant mouse model of PDB and identified a novel OPTN-type I IFN axis in PDB pathogenesis.

Material and Methods

Animals

Optn$^{flox/flox}$ mice on a C57BL/6 background were generated using a targeting vector-inserted LoxP site that flanks the first coding exon and a neomycin selection cassette (Figure 2.1). We crossed *Optn*$^{flox/flox}$ mice with *CMV-Cre* mice (Jackson Laboratories, Bar Harbor, ME USA) to generate *CMV-Cre; Optn*$^{flox/wt}$ mice, which were used as breeding pairs. Global *Optn* knockout (*CMV-Cre; Optn*$^{flox/flox}$) mice are hereafter referred to as *Optn*$^{-/-}$ mice, and the primers used for genotyping are listed below.

Primer Set	Forward	Reverse
A-B3	taggacctgttaccatgtccca	ccctgttcattcaggcccaaag
A-D1	taggacctgttaccatgtccca	cttggctggacgtaaactcctc
G2-H2	gcccggtaccatcaagtcta	aacacctctccagtgcaacc

Female *Optn*$^{-/-}$ mice were aged for up to 22 months, as aged male mice are more susceptible to spontaneous osteoarthritis, to minimize the influence of age-related osteoarthritis on phenotype (20, 21). *Ifnar*$^{-/-}$ mice were a generous gift from Dr. Michael Fessler (NIEHS). All animal procedures were approved by Institutional Animal Care and Use Committees at the University of North Carolina, Duke University, and NIEHS.

Micro-CT Scanning and Dual Energy X-Ray Absorptiometry (DEXA)

Bones were harvested, fixed in 4% paraformaldehyde, and scanned by MicroCT Scanco 40 (Scanco Medical, Bassersdorf, Switzerland) in 10 μm resolution (E = 70kVa; I = 145 μA). Regions of interest of the cortical and trabecular bone was measured 0.7 mm proximal to the distal tibiofubular junction, and 0.7 mm distal to metaphysis of tibia, respectively. The reconstructed solid 3D images were used for visualizing bone morphology and microarchitecture. We measured bone mineral content (BMC) and bone mineral density (BMD) of lumbar spines and femurs by DEXA using LUNAR PIXImus bone densitometer (GE Healthcare, Fairfield, CT USA).

Slide staining

Bones were decalcified in 10% EDTA for 3 weeks and then processed, paraffin embedded, and sectioned at thickness of 5 μm. Sections were stained with hematoxylin and eosin (H&E) for general histology, and with tartrate-resistant acid phosphatase (TRAP) activity to detect osteoclasts, with safranin O for cartilage. For immunohistochemistry staining, enzymatic antigen retrieval was performed on decalcified sections. After overnight incubation with the primary antibody, sections were incubated with the biotinylated secondary antibody (1:1000; Vector Laboratories, Burlingame, CA USA). The sections were then immersed in a solution containing avidin-biotin peroxidase complex (Vector Laboratories, Burlingame, CA USA), and 3,3'-diaminobenzidine was used as the chromogen.

Serum measurement of PDB biomarkers

Sera was isolated from whole blood by centrifugation of 3000 rpm at 4 ℃ for 15 minutes. Serum ALP level was measured by ALP Assay Kit (Abcam, Cambridge, UK). Serum

concentrations of IL-6 was measured by Milliplex Multiplex Assay (EMD Millipore, Burlington, MA USA). C-terminal propeptide (sCTx) was measured using ELISA kits (Immunodiagnostic Systems, Boldon, UK).

Osteoclast differentiation and resorptive assay *in vitro*

After euthanasia by CO_2, tibias and femurs were harvested from 8-12 weeks old mice. Bone marrow cells were flushed into phenol free α-MEM medium, supplemented with 10% FBS, L-Glutamine, non-essential amino acids, and penicillin/streptomycin. Non-adherent cells were harvested after 24 hours and re-plated at a density of 1.5×10^5 cells/cm^2 with 30 ng/mL M-CSF (R&D Systems, Minneapolis, MN USA). After two days, the medium was replenished with 30 ng/mL M-CSF and 10 ng/mL RANKL (R&D Systems Minneapolis, MN USA) for osteoclast differentiation. After 3 days of culture, cells were fixed and stained with tartrate-resistant acid phosphatase (TRAP) to detect osteoclasts (Xiu et al. 2014a). Bone marrow osteoclast precursors were plated and differentiated into equal numbers of osteoclasts (see above) on Osteo Assay Surface plates (Corning Lifesciences, Tewksburg, MA USA) for resorption assay. At day 5, the plate was bleached, and areas of resorption pits were quantified using NIH Image J.

In vitro IFNβ and anti-IFNaR antibody treatment

Bone marrow osteoclast precursors were treated with 1U IFNβ (R&D Systems, Minneapolis, MN USA) in the osteoclastogenic medium (30 ng/mL M-CSF and 10 ng/mL RANKL) for 3 days. Similarly, bone marrow osteoclast precursors were treated with anti-IFNAR antibody or control antibody a working concentration of 5 μg (Leinco, Fenton, MO USA) in the

osteoclastogenic medium for 3 days. Cells were fixed and stained for TRAP activity to evaluate osteoclastogenesis.

Antibodies and Western Blot Analysis

The following antibodies were from Cell Signaling (Beverly, MA USA): c-Fos (Cat. #4384), LC3B (Cat. #2775), p62 (Cat. #5114), ATG5 (Cat. #12994), ATG7 (Cat. #2631), p65 (Cat. #8242), phos-p65 (Cat. #3033), p100/p52 (Cat. #4882), IκBα (Cat. #4814), phos-p38 (Cat. #9215), p38 (Cat. #9212), phos-ERK1/2 (Cat. #4370), ERK1/2 (Cat. #4695), phos-JNK (Cat. #4668), JNK (Cat. #9252), phos-CREB (Cat. #9198), CREB (Cat. #4820), phos-STAT1 (Cat. #9167), STAT1 (Cat. #9172), STAT2 (Cat. #72604), SOCS3 (Cat. #2932), phos-TBK1 (Cat. #5483), TBK1 (Cat. #3504), phos-IRF3 (Cat. #4947), IRF3 (Cat. #4302), and RIPK1 (Cat. #3493). The following antibodies were from Santa Cruz Biotechnology Inc. (Dallas, TX USA): NFATc1 (Cat. #sc-7294), OPTN (Cat. #sc-166576), and Actin (Cat. #sc-1616). Anti-OPTN antibodies were from ProteinTech (Rosemont, IL USA; Cat. #10837-1-AP) and Cayman Chemical (Ann Arbor, MI USA; Cat. #100000). The myosin VI antibody was from Proteus (Ramona, CA USA; Cat. #25-6791); Huntingtin antibody was from Millipore (Burlington, MA USA; Cat. #MAB2166); Rab8a antibody was from BD Biosciences (San Jose, CA USA; Cat. #610845); phos-STAT2 antibody was from Abcam (Cambridge, MA USA; Cat. #ab53132). Secondary antibodies were from Jackson Immuno-Research (West Grove, PA, USA).

Proteins were harvested, and protein concentration was measured as previously described (Lee et al. 2015). 5-10 µg of total protein lysate was resolved by Criterion TGX precast gel (Biorad, Hercules, CA, USA) and transferred to nitrocellulose membrane using the Trans-Blot Turbo Transfer System (Bio-rad, Hercules, CA, USA) and immunodetected using appropriate primary

and peroxidase-coupled secondary antibodies (Jackson Immunoresearch, West Grove, PA USA). Proteins were visualized by enhanced chemiluminescence (ECL, Amersham Bioscience, Little Chalfont, UK).

Osteoblast differentiation *in vitro*

MC3T3-E1 pre-osteoblasts (Subclone 14, CRL-2594) were obtained from ATCC (Manassas, VA USA). The cells were seeded at 2 X 10^5 cells per 35mm dish, expanded in growth media (α-MEM containing 10% fetal bovine serum (FBS) and 1% penicillin/streptomycin), and differentiated with growth media supplemented with 10mM β-glycerophosphate and 0.2 mmol/L 21 ascorbic acid. The media was changed every 3 days. After 7, 14, and 21 days, the cells were fixed with 75% cold ethanol for 30 minutes and then stained with 1% Alizarin Red (Acros Organics, Geel, Belgium) solution (pH 4.2) for 10 minutes at RT.

Fluorochrome labeling for *in vivo* bone formation

Two fluorochromes (Sigma-Aldrich, St. Louis, MO USA), calcein (20mg/kg) and alizarin red (30mg/kg), were used to label *in vivo* bone formation by intraperitoneal injection. The calcein and alizarin red were administered 5 days and 2 days prior to euthanasia, respectively. Mineral Apposition Rate (MAR, μm/day), was calculated as the distance between two sequential labels divided by the interlabeling period (days).

RNA isolation and qPCR

Total RNA was isolated using the RNeasy plus mini kit (Qiagen, Hilden, Germany) and was reverse-transcribed using the iScript DNA synthesis kit (Biorad, Hercules, CA, USA). qPCR was performed using Taqman Universal PCR master Mix (ThermoFisher, Waltham, MA USA)

with Taqman probes (*Gapdh*: Cat. #4331182, *Ifnb1*: Cat. #4331182). The transcript level of *Ifnb1* was normalized to the level of *Gapdh* within each sample using the ΔΔCt method.

Microarray

RNA was isolated from day 2 $Optn^{+/+}$ and $Optn^{-/-}$ bone-marrow-derived osteoclasts as described above, and gene expression analysis was conducted using Affymetrix Mouse Genome 430 2.0 GeneChip® arrays (Affymetrix, Santa Clara, CA). Arrays were scanned in an Affymetrix Scanner 3000 and preliminary analyses were performed with OmicSoft Array Studio (Version 9.0) software.

Flow Cytometry

To assess cell death, osteoclast precursors were harvested 24 and 48 hours after treatment with RANKL in the presence or absence of IFNβ and stained with Annexin-V (1:50), Zombie-Red (1:1000), and CD45 (1:200), as previously described (Dillon et al. 2014). All antibodies were from Biolegend (San Diego, CA USA).

Statistical Analysis

For all *in vitro* studies, three independent experiments were performed. Data are presented as mean ± SD. Student's T test or Analysis of Variance (ANOVA) was used to determine the differences among groups. A *p value* less than 0.05 is considered statistically significant.

Results

Optineurin is highly expressed in the bone marrow and is upregulated during *in vitro* osteo-

clastogenesis.

To explore the relevance of OPTN in bone biology, we first examined its expression pattern in the long bone by immunohistochemistry. OPTN was most highly expressed in the bone marrow (BM) but was also expressed in osteocytes and chondrocytes (Figure 2.2). We next examined the temporal expression of OPTN during *in vitro* osteoclastogenesis, using both bone marrow cells (Figure 2.2B) and RAW 264.7 cells (Figure 2.2C) as osteoclast precursors. Osteoclasts were fully differentiated on Days 3 and 4 post-RANKL stimulation of BM cells and RAW 264.7 cells, respectively, as determined by Tartrate-resistant acid phosphatase (TRAP) staining. Expression of OPTN increased during osteoclast differentiation, peaking at Days 3 and 2 post-RANKL stimulation in BM cells and RAW 264.7 cells, respectively (Figures 2.2B-C). Immunofluorescence staining further demonstrated that OPTN was localized in the cytoplasm and perinuclear space of fully differentiated osteoclasts (Figures 2.2B-C).

Young *Optn*$^{-/-}$ mice do not display gross skeletal defects *in vivo*

To study the role of *Optn* during bone homeostasis *in vivo*, we generated *CMV-Cre:Optn*$^{flox/flox}$ (*Optn* global knockout mice), hereafter referred to *Optn*$^{-/-}$ mice, (Figure 2.1A-B). Western blot analysis confirmed that OPTN was dramatically decreased in multiple organs of *Optn*$^{-/-}$ mice, confirming global deficiency of this protein (Figure 2.1C). At 3 months of age, *Optn*$^{-/-}$ mice were phenotypically normal and did not have gross anatomical abnormalities or body size differences compared to *Optn*$^{+/+}$ littermates (Figure 2.3A). Furthermore, skeletal phenotyping using micro-computerized tomography (μCT) scanning revealed that 3-month old *Optn*$^{-/-}$ mice did not display overt PDB-like lesions in the long bones (Figure 2.3B). Young *Optn*$^{-/-}$ mice also had normal bone morphometric parameters of trabecular and cortical bones compared to *Optn*$^{+/+}$

littermates (Figure S3C). Similarly, serum levels of alkaline phosphatase (ALP) activity and C-terminal telopeptide (CTX-1), both biomarkers indicative of bone turnover, were not significantly elevated between *Optn*$^{+/+}$ and *Optn*$^{-/-}$ mice at 3 months of age (Figure 2.3D).

Optineurin deficiency *in vivo* results in PDB-like lesions in aged mice.

We next performed skeletal phenotyping of the mice at 8, 12, and 16 months of age. Similar to 3-month old mice, neither genotype displayed any skeletal abnormalities or lesions at 8 or 12 months of age (Figure 2.4A-B, Table 2). At 16 months of age, however, 50% of *Optn*$^{-/-}$ mice had developed incipient, monostotic, localized osteolytic lesions in the tibiae (Figure 2.4C). While there was no significant difference in serum ALP levels between *Optn*$^{+/+}$ and *Optn*$^{-/-}$ mice at 8, 12, and 16 months, serum ALP levels had significantly increased in *Optn*$^{-/-}$ mice between 8 and 16 months, signaling an age-induced onset of PDB in the absence of *Optn* (Figure 2.4D).

Because PDB primarily affects the elderly population with a peak incidence between 70 and 80 years of age (25), we next performed skeletal phenotyping of 22-month old mice, which is equivalent to humans at 70 years old (26). Strikingly, 100% of aged *Optn*$^{-/-}$ mice had developed polyostotic, localized osteolytic lesions in femurs, tibiae (Figures 2.5A-B), calvaria (Figure 2.5C), lumbar vertebra (Figure 2.5D), and fibulas (Figure 2.5E), which are the most commonly affected bones of PDB, and these lesions phenotypically resembled the early or osteolytic stage of PDB (Table 2). Additionally, 20% of *Optn*$^{-/-}$ mice exhibited facial deformities (Figure 2.5C) and bone hypertrophic lesions (Figure 2.5E), pathologies associated with the intermediate or osteoblastic stage of PDB (Table 2). Furthermore, spinal cord/nerve root compression (Figure 2.5D) and pathological fractures (Figure 2.5E) were also seen in affected bones of 40% of aged *Optn*$^{-/-}$ mice (Table 2). Aged *Optn*$^{-/-}$ mice also contained decreased cortical bone components in unaffected

bones (Figure 2.4F) and displayed a decrease in bone mineral density (BMD) (Figure 2.4G). Taken together, these results demonstrate that *Optineurin*-deficiency results in age-dependent, localized bone lesions that are phenotypically consistent with PDB.

Pagetic lesions in *Optn*$^{-/-}$ animals are characterized by hyper-osteoclastogenesis

The osteolytic lesions observed in *Optn*$^{-/-}$ mice are characteristic of disproportionate bone turnover, indicating that OPTN exerts its effect by either enhancing bone resorptive activity by osteoclasts or reducing bone formation activity by osteoblasts. Although OPTN is induced during osteogenesis *in vitro* (Figure 2.6A), we did not observe any difference *in vivo* bone formation as determined by mineral apposition rate (MAR) between young *Optn*$^{+/+}$ and *Optn*$^{-/-}$ mice (Figure 2.6B). Thus, we hypothesized that osteolytic lesions observed in aged *Optn*$^{-/-}$ mice were a result of altered osteoclast activity.

We next performed histological analysis of bones of aged *Optn*$^{+/+}$ and *Optn*$^{-/-}$ mice. H&E and TRAP staining of the distal femur of *Optn*$^{-/-}$ mice confirmed osteolytic lesions and revealed increased bone resorption, with osteoclast-filled pits within the compact bone of *Optn*$^{-/-}$ mice, while bones from age-matched *Optn*$^{+/+}$ mice lacked these pathological features (Figure 2.7A). Cross-sectional analysis of a mixed osteoscleorotic-osteolytic lesion in the proximal tibia of an *Optn*$^{-/-}$ mouse shows that these lesions are comprised of numerous osteoclasts located within the inner surface of cortical bone and adjacent trabecular surfaces (Figure 2.7B,C). In addition, the mixed lesion also displayed secondary endochondrial bone formation (Figure 2.7B). Focal lesions in affected bones from *Optn*$^{-/-}$ mice contained significantly more osteoclasts per area examined compared to *Optn*$^{+/+}$ mice (Figure 2.7D), and each *Optn*$^{-/-}$ osteoclast contained more nuclei than *Optn*$^{+/+}$ osteoclasts, indicative of increased osteoclast activity (Figure 2.7E).

The gold standard for clinical diagnosis of PDB in human patients is increased serum levels of ALP, in response to increased osteoclastic bone resorption (Al Nofal et al. 2015). Similar to PDB patients, we found that aged *Optn*$^{-/-}$ mice had significantly increased ALP activity in their serum, compared to age-matched *Optn*$^{+/+}$ mice, and thus recapitulate the classical diagnostic biomarker for PDB (Figure 2.7F). Furthermore, serum levels of CTX-1, the bone resorption biomarker, were significantly increased in aged *Optn*$^{-/-}$ mice compared to *Optn*$^{+/+}$ littermate mice (Figure 2F). However, serum levels of IL-6, a cytokine that has been associated with PDB (Teramachi et al. 2014), were not affected by loss of OPTN in aged animals (Figure 2.6C). Taken together, our data demonstrate that *Optn*$^{-/-}$ mice exhibit serum and histological features of PDB associated with increased osteoclastogenesis, and the *Optn*$^{-/-}$ mice represent a novel and clinically relevant mouse model for PDB.

OPTN deficiency enhances *in vitro* osteoclastogenesis

We next explored the mechanisms by which deficiency of OPTN augments osteoclast formation. *Optn*$^{-/-}$ bone marrow osteoclast precursors generated significantly increased numbers of osteoclasts *ex vivo*, compared to *Optn*$^{+/+}$ bone marrow precursors (Figure 2.8A). Furthermore, *Optn*$^{-/-}$ osteoclasts differentiated *ex vivo* on calcium phosphate-coated plates displayed increased resorptive activity, as indicated by larger resorption pit areas compared to *Optn*$^{+/+}$ osteoclasts (Figure 2.8B). Finally, *Optn*$^{-/-}$ precursor cells expressed significantly higher levels of c-Fos and NFATc1, two important osteoclast differentiation factors, post-RANKL treatment (Figure 2.8C). Collectively, these data demonstrate that OPTN is a key negative regulator of osteoclastogenesis.

As autophagy has been shown to be involved in osteoclast differentiation (Lin et al. 2013) and OPTN is an autophagy receptor, we first asked if the absence of OPTN alters autophagic

induction during osteoclastogenesis. Intriguingly, *Optn*$^{-/-}$ osteoclasts had a similar transformation of the autophagy marker LC3-I to LC3-II and degradation of p62, as well as expression of ATG5 and ATG7, compared to *Optn*$^{+/+}$ osteoclasts, suggesting that autophagy is unaffected in *Optn*$^{-/-}$ osteoclasts under osteoclastogenic conditions (Figure 2.8D). Activation of the c-Fos-NFATc1 axis for osteoclastogenesis involves the NF-κB pathway (Abu-Amer 2013). As OPTN has been shown to suppress NF-κB activation (Zhu et al. 2007), we examined the phosphorylation of p65, a member of the canonical NF-κB pathway, in *Optn*$^{+/+}$ and *Optn*$^{-/-}$ osteoclast precursors after RANKL treatment. The level of phosphorylated p65 in *Optn*$^{-/-}$ osteoclast precursors was similar to that in *Optn*$^{+/+}$ osteoclast precursors at both early time points (Figure 2.8E) and late time points (Figure 2.8F). Similarly, the degradation of the IκBα, a negative regulator of canonical NF-κB activation, was equivalent in *Optn*$^{+/+}$ and *Optn*$^{-/-}$ cells after RANKL treatment (Figure 2.8E). While previous studies utilized the *Optn*$^{D477N/D477N}$ model, which results in OPTN protein that is unable to bind Ly63-linked ubiquitin chains but can still interact with other proteins via its other un-mutated domains (Obaid et al. 2015), our constitutive knockout model displayed no differences in NF-κB activation during osteoclastogenesis. Collectively, these data indicate that while defects in OPTN's ability to bind ubiquitin can alter NF-κB activation, the absence of OPTN does not.

In addition, we also assessed non-canonical NF-κB activation by examining the processing of p100 to p52 during osteoclastogenesis. *Optn*$^{-/-}$ osteoclast precursors displayed similar levels of the cleaved p52 protein compared to *Optn*$^{+/+}$ osteoclast precursors (Figure 2.8F). These results demonstrate that OPTN regulates osteoclast differentiation independently of autophagy, canonical, or non-canonical NF-κB activation.

We next evaluated other possible signaling pathways implicated in osteoclastogenesis and observed equivalent phosphorylated levels of JNK1/2, ERK1/2, p38, and CREB (Figure 2.9A, B)

in *Optn*$^{+/+}$ and *Optn*$^{-/-}$ osteoclast precursors post-RANKL treatment. We further examined the expression of known OPTN binding partners, RAB8A, Myosin VI, and Huntingtin (HTT) in *Optn*$^{-/-}$ osteoclasts relative to *Optn*$^{+/+}$ osteoclasts, and we found that their expression levels were comparable (Figure 2.9C). Therefore, OPTN deficiency does not affect classical osteoclastogenic pathways in osteoclast precursors during RANKL treatment.

OPTN is required for both the production of type I IFN and signaling via the IFNα/βR

To investigate potential transcriptional differences between *Optn*$^{+/+}$ and *Optn*$^{-/-}$ osteoclasts, genome-wide transcriptional profiling was performed at day 3 of osteoclast differentiation *ex vivo*. Microarray revealed that many critical pathways were upregulated in *Optn*$^{-/-}$ osteoclasts, including genes regulating cytoskeletal rearrangements, cell cycle, cytokine and chemokine expression, and osteoclast differentiation and function, compared to *Optn*$^{+/+}$ osteoclasts (Figure 2.9D). Consistent with our protein results, the transcription of *Rab8a/b*, *Myosin VI*, and *Htt* was equivalent between and *Optn*$^{+/+}$ and *Optn*$^{-/-}$ osteoclasts (Figure 2.9D). Additionally, there was no difference in transcription of other components known to interact with OPTN, such as *Ripk1*, *Cyld*, *Sqstm1*, and *Hace1*, between *Optn*$^{+/+}$ and *Optn*$^{-/-}$ osteoclasts (Figure 2.9D).

We did, however, observe a significant difference in the expression of genes associated with the type I interferon (IFN) signature. Genes such as *Ifitm10*, *Ifitm5*, *Ifna1*, *Irf7*, and *Ifnar2* were dramatically reduced in *Optn*$^{-/-}$ osteoclasts compared to *Optn*$^{+/+}$ osteoclasts (Figure 2.10A). Conversely, expression of *Socs3*, a negative regulator of type I IFN signaling (Krebs and Hilton 2000), was significantly upregulated in *Optn*$^{-/-}$ osteoclasts compared to *Optn*$^{+/+}$ osteoclasts (Figure 2.10A). Engagement of the IFNα/βR with type I IFN (typically IFNβ in myeloid derived cells, such as osteoclasts) results in the phosphorylation of STAT1 (Lehtonen et al. 1997). In response

to RANKL treatment, *Optn*$^{-/-}$ osteoclast precursors displayed lower levels of total and phosphorylated STAT1 and higher levels of SOCS3, suggesting that *Optn* deficiency confers a reduced activation of the type I IFN response in response to RANKL (Figure 2.10B).

We next explored whether this reduced type I IFN signaling in *Optn*$^{-/-}$ osteoclasts resulted from decreased IFNβ production or defective IFNα/βR signaling, or both. We first observed that *Optn*$^{-/-}$ osteoclast precursors generated significantly lower levels of *Ifnb1* in response to RANKL treatment (Figure 2.10C), compared to *Optn*$^{+/+}$ precursors. RANKL-induced IFNβ production does not require canonical TBK1 and IRF3 machinery (Takayanagi et al. 2002b), and we indeed observed that RANKL failed to activate IRF3 in osteoclast precursors and induced a comparable level of TBK1 phosphorylation, which is required for NF-κB activities, between *Optn*$^{+/+}$ and *Optn*$^{-/-}$ precursors (Figure 2.9E). Next, we examined signaling downstream of IFNβ engagement of IFNα/βR during IFNβ treatment. Strikingly, *Optn*$^{-/-}$ osteoclast precursors displayed defective IFNα/βR signaling in response to IFNβ stimulation, as evidenced by decreased total and phosphorylated STAT1/2 (Figure 2.10D). As expected, IFNα/βR-deficient (*Ifnar*$^{-/-}$) osteoclast precursors displayed a completely abolished type I interferon signaling in response to RANKL or IFNβ (Figure 2.9F-G). Taken together, these results demonstrate that OPTN is critical for both the production of type I IFN and efficient signaling via IFNα/βR pathway.

Type I IFN signaling can also promote RIPK3-mediated necroptosis (Dillon et al. 2014), therefore we next examined if defects in IFNβ production by *Optn*$^{-/-}$ osteoclasts conferred a survival advantage compared to *Optn*$^{+/+}$ osteoclasts. Treatment of *Optn*$^{-/-}$ osteoclast precursors with RANKL, a member of the TNF superfamily (Hanada et al. 2011), resulted in significantly increased survival at both 24 and 48 hours post-RANKL treatment, compared to *Optn*$^{+/+}$ precursors (Figure 2.11A). In order to determine if exogenous IFNβ treatment during

osteoclastogenesis could modulate cell death in *Optn*$^{-/-}$ osteoclast precursors, we differentiated *Optn*$^{+/+}$ and *Optn*$^{-/-}$ precursors into osteoclasts with RANKL in the absence or presence of IFNβ. The survival advantage observed in *Optn*$^{-/-}$ osteoclast precursors was partially rescued at 24 and 48 hours compared to *Optn*$^{+/+}$ precursors at 24 and 48 hours post-RANKL/IFNβ treatment (Figure 2.11B, 2.12A).

As IFNβ is also an established negative regulator of osteoclastogenesis (Takayanagi et al. 2002b), we next asked if exogenous IFNβ treatment during osteoclastogenesis could rescue the hyper-differentiation observed in *Optn*$^{-/-}$ osteoclasts. Recombinant IFNβ was sufficient to inhibit the number of osteoclasts generated by *Optn*$^{-/-}$ precursors, as evidenced by TRAP staining (Figure 2.11C). Furthermore, antibody-mediated inhibition of IFNα/βR signaling (αIFNAR) resulted in a significant increase in osteoclastogenesis of both *Optn*$^{+/+}$ and *Optn*$^{-/-}$ precursors (Figure 2.11C). Importantly, IFNα/βR signaling blockade had a larger effect on *Optn*$^{+/+}$ precursors, essentially normalizing the *Optn*$^{-/-}$ osteoclastogenic phenotype (Figure 2.11C). This suggests that the excess OC differentiation of *Optn*$^{-/-}$ cells is mediated by a deficit in native IFN signaling.

Collectively, we have described the *Optn*$^{-/-}$ mouse as a novel and clinically relevant model for PDB *in vivo* and have demonstrated that OPTN is required to maintain homeostatic levels of osteoclastogenesis *in vivo* and *ex vivo*, the absence of which results in hyperactive osteoclast differentiation and activity. In addition, we demonstrate that OPTN functions on two levels to regulate osteoclast differentiation – the production of type I IFN and signaling of type I IFN through the IFNα/βR (Figure 2.13), and the net effect of this defect is increased osteoclastogenesis, as well as defects in cell death, opening the door for possible interferon intervention for the treatment of PDB.

Discussion

Recent advances in the underlying genetic influences on the onset and severity of PDB have shed light onto the root causes of this disease and opened up avenues for deeper biological understanding. Here, we performed extensive *in vivo* skeleton characterization of the *Optn*-deficient mouse, which exhibits full penetrance and multiple key clinical manifestations of PDB in an age-dependent manner, in contrast to the $Optn^{D477N/D477N}$ mutant mice, in which only 10% of 15-month old mice develop PDB lesions (Obaid et al. 2015; Slowicka et al. 2016a). Therefore, this *Optn*-deficient mouse represents a novel and useful mouse model to study PDB pathogenesis, and potentially, other pathologies associated with OPTN dysfunction, such as primary open-angle glaucoma (POAG) and amyotrophic lateral sclerosis (ALS).

While multiple studies have explored the molecular mechanisms by which OPTN dysfunction underlies disease pathogenesis, these studies have mainly focused on POAG and ALS (Toth and Atkin 2018). Studies have demonstrated that the POAG-associated OPTN mutant (E50K) could selectively induce ROS-associated cell death of retinal ganglion cells *in vitro* (Chalasani et al. 2007), and OPTN E50K knock-in mice exhibit loss of retinal ganglion cells *in vivo* (Tseng et al. 2015). Further, in response to TNFα signaling, OPTN deficiency leads to persistent RIPK1 signaling and uncontrolled necroinflammation in the spinal cord, resulting in axonal degeneration and ALS (Ito et al. 2016). However, in contrast to the pathophysiology of *Optn*-dependent POAG and ALS, which is characterized by the loss of ganglion cells or neurons (Ito et al. 2016; Tseng et al. 2015), PDB is highlighted by a 'gain' of osteoclasts (Roodman and Windle 2005), suggesting that the molecular mechanisms implicated in the pathogenesis of PDB is dissimilar to POAG and ALS. While *Optn*-deficient osteoclasts did not display any difference in RIPK1 expression at either mRNA and protein levels, it is possible that activation of necroptotic

machinery is altered in *Optn*-deficient osteoclasts. A recent study has identified MK2 has a critical negative regulator of RIPK1 activity, wherein MK2 phosphorylates RIPK1 at Ser321 to inhibit its ability to induce RIPK1-dependent apoptosis and necroptosis (Jaco et al. 2017). Interestingly, *MK2*$^{-/-}$ mice display a significant decrease in osteoclastogenesis, which could suggest that an increase in functionally active RIPK1 results in decreased osteoclast survival (Herbert et al. 2015). The role that OPTN plays in modulating the MK2-RIPK1 axis in response to type I IFN remains to be elucidated.

Although OPTN has been shown to be a potent inhibitor of NF-κB activity (Slowicka et al. 2016b), our data showed that *Optn*-deficient osteoclasts do not have altered NF-κB activation *ex vivo*, consistent with recent reports (Meena et al. 2016; Munitic et al. 2013; Slowicka et al. 2016a). We did, however, observe a significant and two-pronged defect in the execution of the negative feedback loop mediated by IFNβ. In the absence of OPTN, both production of IFNβ and signaling downstream of the IFNα/βR are impaired. While previous studies have described a role for OPTN in IFNβ production during osteoclastogenesis (Obaid et al. 2015), here we demonstrate for the first time that OPTN is also required for optimal signaling downstream of IFNβ engagement of the IFNα/βR (Figure 2.13). This defect manifests itself in a failure to upregulate anti-osteoclastogenic factors, as well as promote cell survival. Thus, OPTN limits osteoclastogenesis at two distinct nodes and is a critical factor in restricting uncontrolled bone resorption.

Moreover, a defect in type I IFN production could in fact account for the defect in IFNα/βR signaling, as type I IFN upregulates expression of key components of the IFNα/βR signaling pathway (Ivashkiv and Donlin 2014). It's possible that *Optn*-deficient osteoclasts fail to produce amounts of type I IFN necessary to properly establish an IFNα/βR signaling platform, as indicated by decreased levels of total STAT1 and STAT2 in *Optn*-deficient precursors. In addition,

supplementation with recombinant IFNα/β rescues the hyper-osteoclastogenic phenotype in *Optn*-deficient osteoclasts as it upregulates components of the IFNα/βR signaling pathway, such as STAT1 and STAT2, as well as inhibit cFos-mediated osteoclast differentiation. Furthermore, blocking IFNα/βR signaling with anti-IFNAR Ab had a more profound effect on $Optn^{+/+}$ osteoclasts, suggesting that defects in IFNα/βR signaling prevented antibody blockade from being fully effective in $Optn^{-/-}$ osteoclasts.

Interestingly, while *Optn*-deficient osteoclasts exhibit a defective type I IFN pathway, the measles virus, which elicits a robust type I IFN response, is strongly correlated to PDB development (Kurihara et al. 2006). Indeed, this association could support why individuals harboring the *OPTN* variant are prone to develop PDB, as their intrinsic defects in the type I IFN pathway permit them to be more susceptible to measles virus infection. Because of Optineurin's dual function in maintaining bone homeostasis and antiviral type I IFN signaling, IFNβ could be a novel pharmacotherapy for PDB, as it provides restoration of dysregulated bone resorption in addition to anti-viral functions.

Taken together, our results allow us to propose a possible mechanistic model of OPTN-associated PDB pathogenesis. At the molecular level, OPTN plays dual role in the negative regulation of osteoclastogenesis - the production of type I IFN and signaling of the type I IFN through the IFNα/βR to maintain bone homeostasis. Deficiency in OPTN fails to execute the proper inhibitory functions of type I IFN signaling, leading to hyperactivation of osteoclastogenesis and development of osteolytic lesions observed in PDB

Genotype	Pathology	3 months	8 months	12 months	16 months	22 months
Optn$^{+/+}$	Skeletal abnormalities	0%	0%	0%	0%	0%
	Osteolytic lesions	0%	0%	0%	0%	0%
	Osteoscleorotic-osteolytic lesion	0%	0%	0%	0%	0%
	Spinal cord/nerve root compression	0%	0%	0%	0%	0%
	Facial Deformity	0%	0%	0%	0%	0%
Optn$^{-/-}$	Skeletal abnormalities	0%	0%	0%	0%	100%
	Osteolytic lesions	0%	0%	0%	50%	100%
	Osteoscleorotic-osteolytic lesion	0%	0%	0%	0%	40%
	Spinal cord/nerve root compression	0%	0%	0%	0%	40%
	Facial Deformity	0%	0%	0%	0%	20%

Table 2: Phenotypic analysis of skeletal abnormalities in 3-, 8-, 12-, 16-, and 22-month old *Optn*$^{+/+}$ and *Optn*$^{-/-}$ mice

A

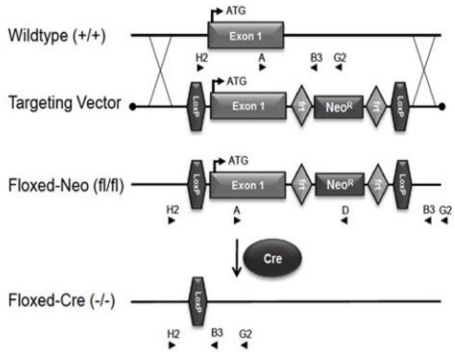

B

***Optn*$^{+/-}$ x *Optn*$^{+/-}$**

	Expected	Observed
***Optn*$^{+/+}$**	41.5 (25%)	34 (20.5%)
***Optn*$^{+/-}$**	83 (50%)	86 (51.8%)
***Optn*$^{-/-}$**	41.5 (25%)	46 (27.7%)
Total	166 (100%)	166 (100%)

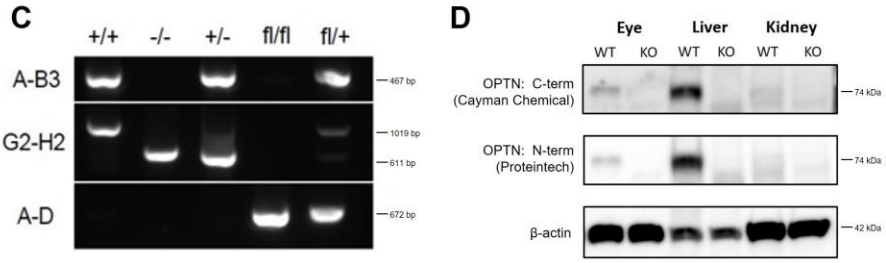

Figure 2.1 Generation of the Global *Optn* knockout mouse. (A) Targeting strategy for the deletion of exon 1 of *Optn* via Cre-mediation excision of LoxP-flanked exon 1. Neomycin cassette (Neo^R) is flanked by frt sites for selection. Cre expression facilitates the deletion of the LoxP-flanked portion of Optn, included the Neo^R cassette. Genotyping primer positions are indicated by arrowheads (A, B3, G2, and H2). (B) Expected and observed frequency of offspring from *Optn*$^{+/-}$ x *Optn*$^{+/-}$ crosses of mice. All genotypes were observed at Mendelian ratios. (C) Genotyping PCR of DNA from (+/+), (-/-), (+/-), (fl/fl), and (fl/+) animals using primers A-B3, G2-H2, and A-D. (D) Western blot analysis of OPTN expression after CMV-mediated deletion in eye, liver, and kidney.

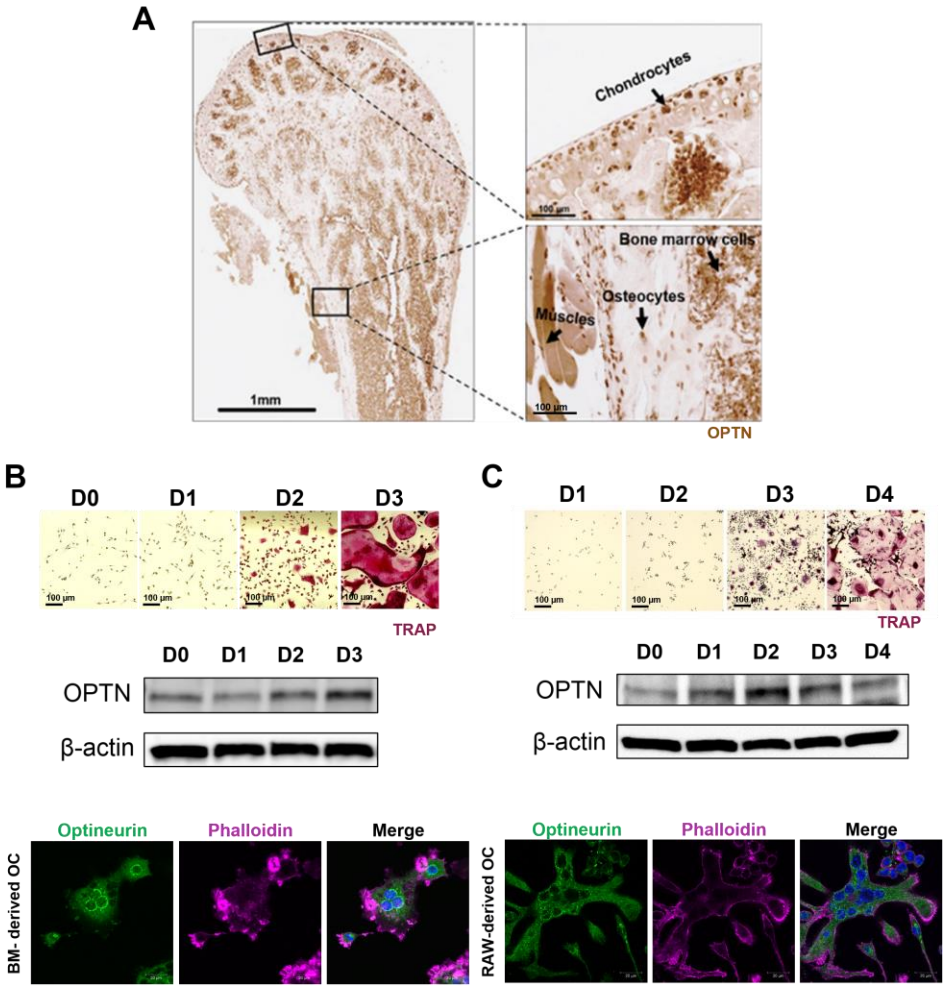

Fig 2.2. Expression of OPTN in bone and osteoclasts. (A) Immunohistochemistry for OPTN in the femurs of a 10-wk-old mouse. Chondrocytes, bone marrow, muscle, and osteocytes are indicated by arrows. (B) TRAP staining, immunoblot, and immunofluorescent staining of OPTN (green) expression during Days 0-3 of RANKL-induced *in vitro* osteoclast differentiation of bone marrow (BM) cells. BM-derived OC were co-stained with phalloidin (pink) and DAPI (blue). (C) TRAP staining, immunoblot, and immunofluorescent staining of OPTN (green) expression during days 0-4 of RANKL-induced *in vitro* osteoclast (OC) differentiation of RAW 264.7 cells. RAW-derived OC were co-stained with phalloidin (pink) and DAPI (blue).

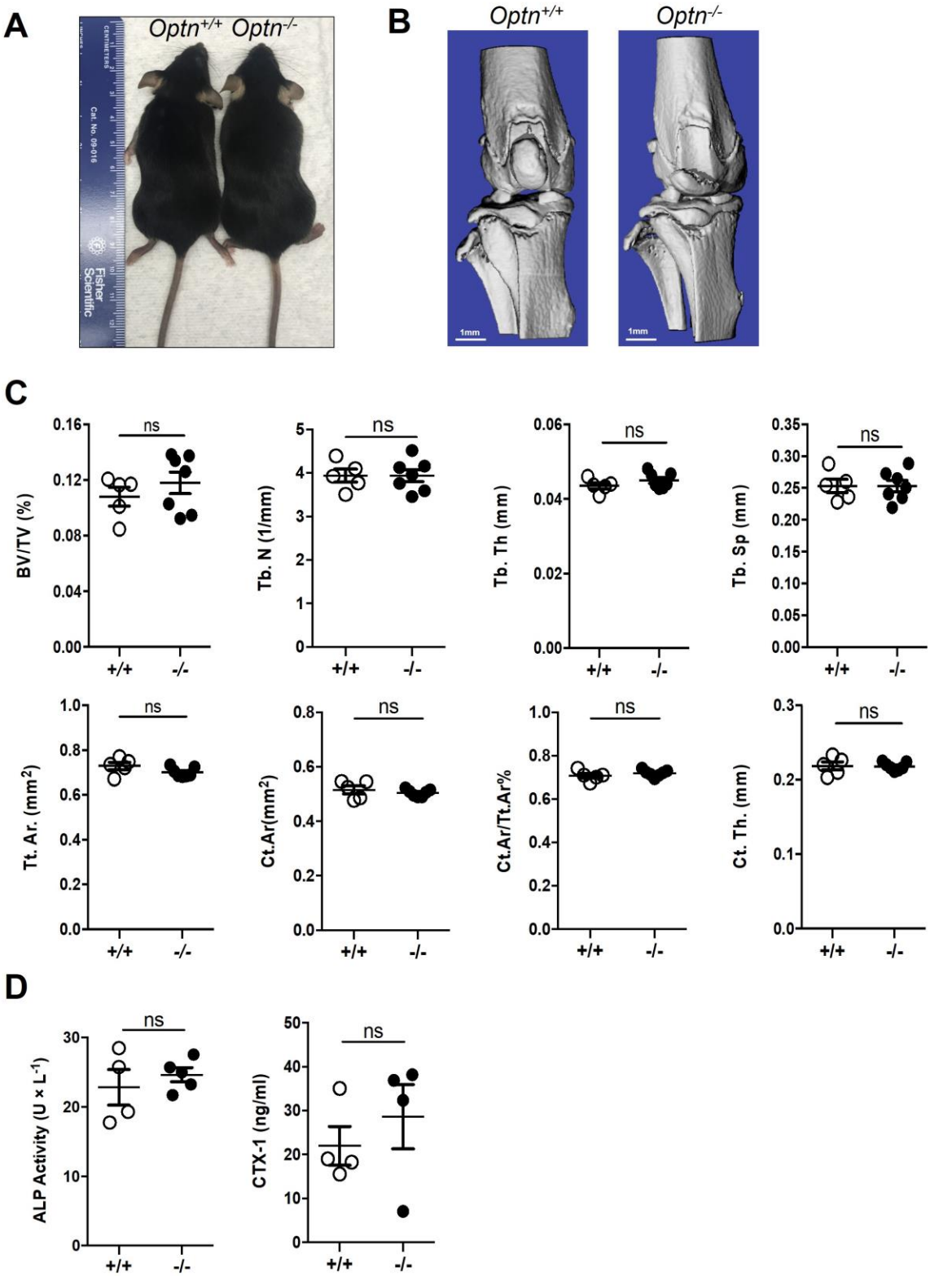
A
Optn+/+ Optn-/-
B
Optn+/+
Optn-/-
1mm
1mm
C
BV/TV (%)
Tb. N (1/mm)
Tb. Th (mm)
Tb. Sp (mm)
Tt. Ar. (mm2)
Ct.Ar(mm2)
Ct.Ar/Tt.Ar%
Ct. Th. (mm)
ns
+/+
-/-
D
ALP Activity (U × L-1)
CTX-1 (ng/ml)

Figure 2.3. *Optn*$^{-/-}$ mice are phenotypically normal at 3 months of age. (A) 3-month old *Optn*$^{+/+}$ and *Optn*$^{-/-}$ mice. (B) Representative micro CT 3D reconstructed images of tibia trabecular bones of *Optn*$^{+/+}$ and *Optn*$^{-/-}$ mice. (C) Trabecular and cortical bone morphometric analysis of *Optn*$^{+/+}$ and *Optn*$^{-/-}$ mice. BV/TV, bone volume / total volume; Tb. N, trabecular number; Tb. Th, trabecular thickness; Tb. Sp, trabecular spacing; Tt. Ar, total area; Ct. Ar, cortical area; Ct. Ar/Tt. Ar, cortical area / total area; Ct. Th, cortical thickness. (n=5-7 female mice per genotype) (D) Serum levels of alkaline phosphatase (ALP) and C-terminal telopeptide (CTX-1) in 3-month old *Optn*$^{+/+}$ (+/+) and *Optn*$^{-/-}$ (-/-) mice (n=4 mice per genotype).

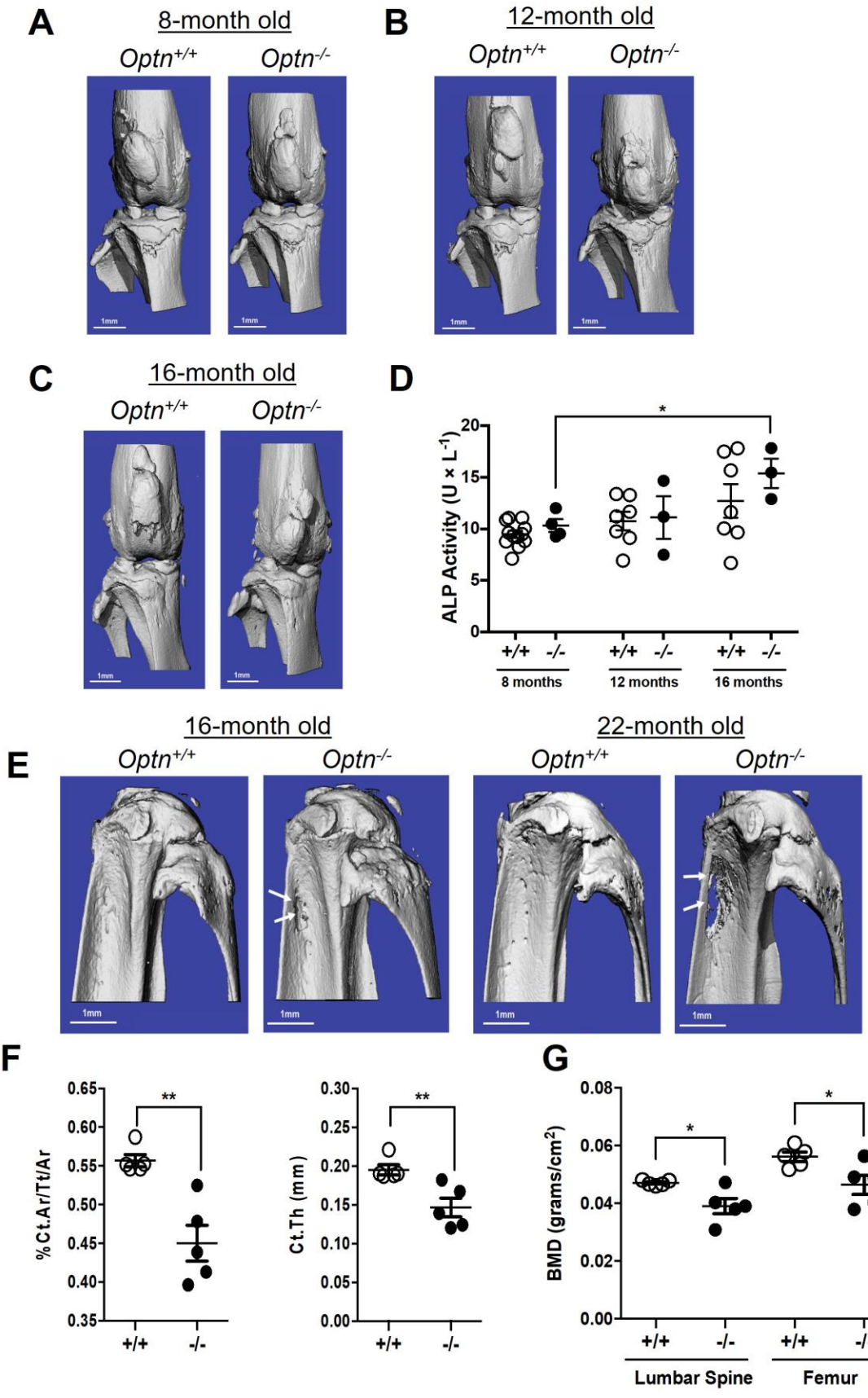
A
8-month old
Optn+/+
Optn-/-
B
12-month old
Optn+/+
Optn-/-
C
16-month old
Optn+/+
Optn-/-
D
ALP Activity (U × L-1)
8 months
12 months
16 months
E
16-month old
22-month old
Optn+/+
Optn-/-
F
%Ct.Ar/Tt/Ar
Ct.Th (mm)
G
BMD (grams/cm2)
Lumbar Spine
Femur

Figure 2.4. *Optn*$^{-/-}$ mice begin displaying PDB characteristics at 16 months of age. (A-C) Representative micro CT 3D reconstructed images of tibia trabecular bones of *Optn*$^{+/+}$ and *Optn*$^{-/-}$ mice at 8 (A), 12 (B), and 16 months of age (C). (D) Serum levels of alkaline phosphatase (ALP) in 8-, 12-, and 16-month old *Optn*$^{+/+}$ (+/+) and *Optn*$^{-/-}$ (-/-) mice (n=3-8 mice per genotype). (E) Incipient, monostotic, localized osteolytic lesions (white arrows) present in the proximal tibia of both 16-month and 22-month old *Optn*$^{-/-}$ mice. (F) Cortical bone morphometric analysis (Cortical thickness [Ct.Th] and % cortical area of total area [%Ct.Ar/Tt.Ar]) of unaffected tibiae of 22-month old *Optn*$^{+/+}$ and *Optn*$^{-/-}$ mice. (G) Bone mineral density (BMD) of lumbar spine and femur of 22-month old *Optn*$^{+/+}$and *Optn*$^{-/-}$ mice. (* $p< 0.05$, ** $p< 0.01$, n = 5 female mice per genotype).

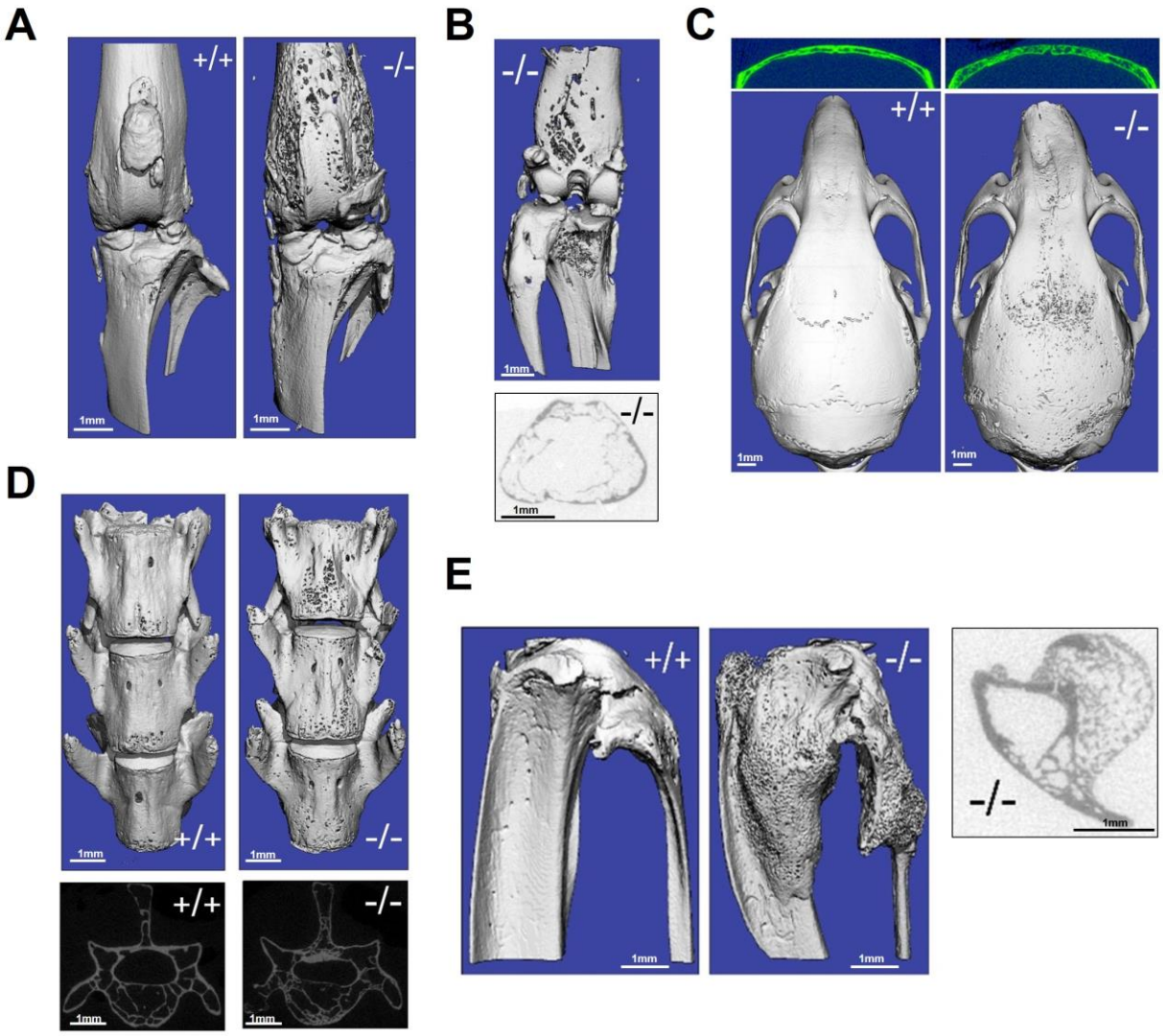

Figure 2.5. Aged *Optn*$^{-/-}$ mice develop Pagetic lesions and exhibit osteoporosis. (A-E) Representative micro CT 3D reconstructed images of osteolytic lesions in the distal femur (A, B), proximal tibia (B), calvaria (C), and lumbar vertebral body (D) of 22-month old female *Optn*$^{-/-}$ mice (-/-), compared to age-matched female *Optn*$^{+/+}$ mice (+/+). Irregular bone remodeling in the calvaria and facial deformity (C) was observed in *Optn*$^{-/-}$ mice (-/-). The affected L4 of lumbar vertebral body displayed a chaotic trabecular structure, which causes spinal stenosis and spinal cord/nerve root compression (D). (E) Aged *Optn*$^{-/-}$ mice had mixed stage lesions in the proximal tibia and fibula, and the affected fibula displayed a pathological fracture. (n=9 mice per genotype).

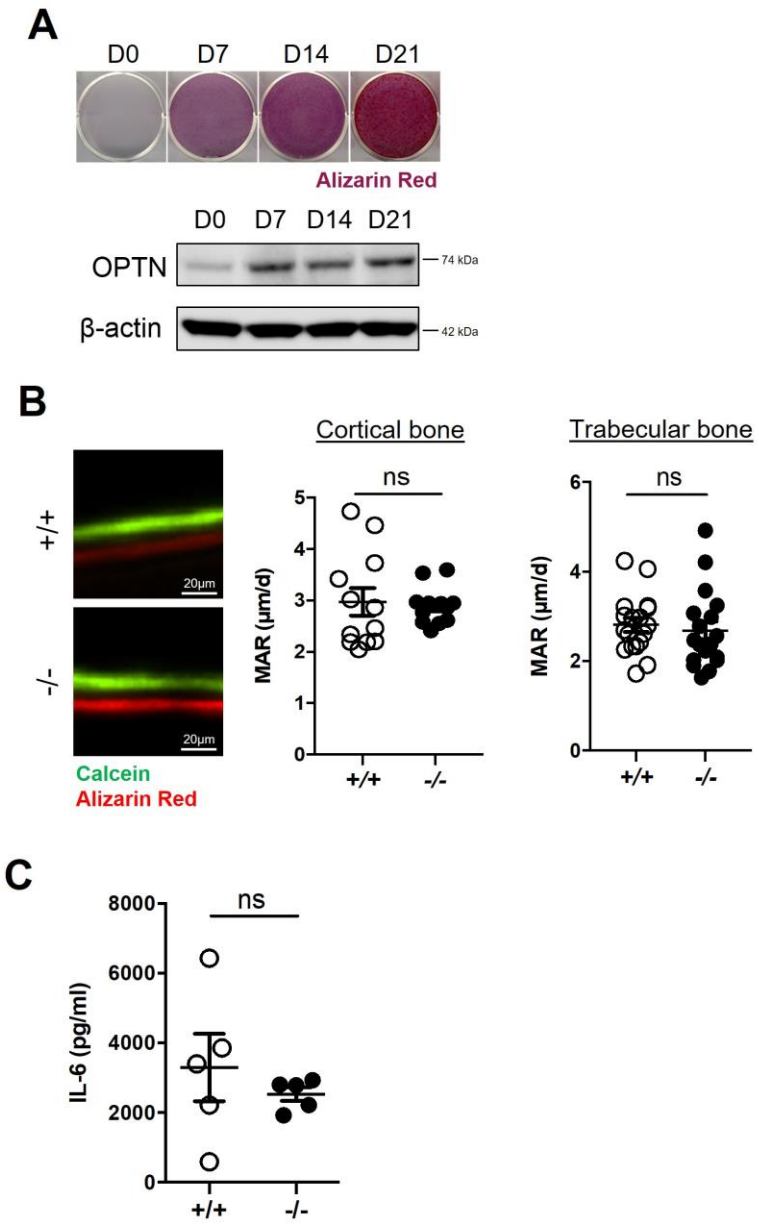

Figure 2.6 *Optn*$^{-/-}$ mice do not display any osteoblastic defects. (A) Alizarin Red staining and immunoblot of OPTN expression during Days 0, 7, 14, and 21 of *in vitro* osteogenesis of MC3T3-E1 pre-osteoclasts. (B) Representative images of *in vivo* bone formation in 3-month old *Optn*$^{+/+}$ (+/+) and *Optn*$^{-/-}$ (-/-) mice, Alizarin (red), Calcein (green). Quantification of measuring mineral apposition rate (MAR) in cortical and trabecular bone (n=4 mice per genotype). (C) Serum levels of IL-6 in 22-month old *Optn*$^{+/+}$ (+/+) and *Optn*$^{-/-}$ (-/-) mice (n=5 mice per genotype).

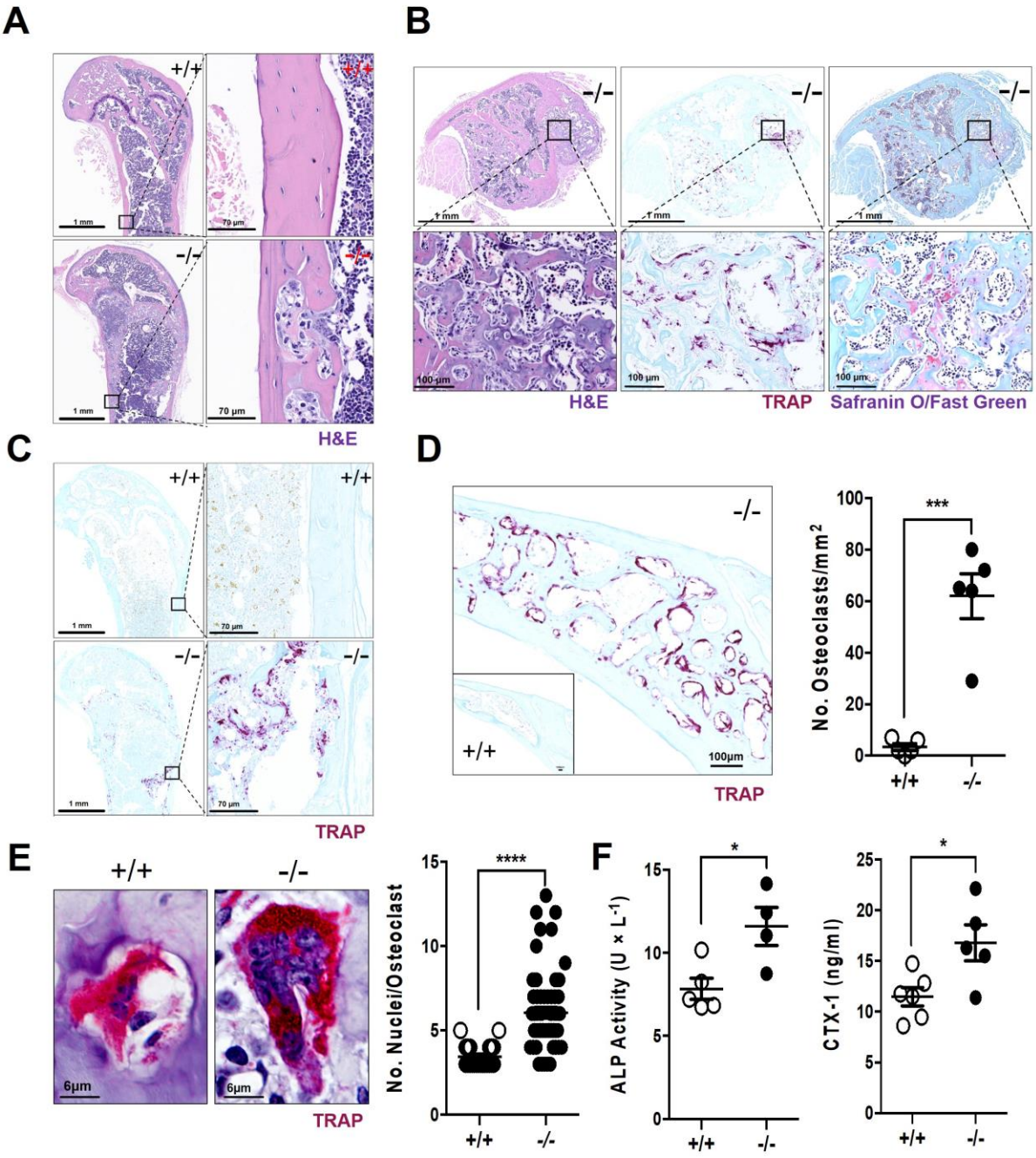

Figure 2.7 Increased osteoclastogenesis in aged *Optn*$^{-/-}$ mice. (A) H&E staining of the distal femur of 22-month old female *Optn*$^{+/+}$ (+/+) and *Optn*$^{-/-}$ (-/-) mice. (B) Staining of a mixed osteoscleorotic-osteolytic lesion in the proximal tibia of 22-month old *Optn*$^{-/-}$ (-/-) mouse with H&E (left), TRAP (middle), and Safranin O/Fast Green (right). (C-D) TRAP staining in distal femur (C) and parietal bone (D) in 22-month old *Optn*$^{+/+}$ (+/+) and *Optn*$^{-/-}$ (-/-) mice.

Quantification of osteoclasts per mm^2 of unaffected bones of *Optn*$^{+/+}$ (+/+) and *Optn*$^{-/-}$ (-/-) mice (*** $p < 0.001$, $n = 5$ mice). (E) Representative images of multi-nucleated osteoclast in the lesion of 22-month old *Optn*$^{+/+}$ (+/+) and *Optn*$^{-/-}$ (-/-) mice. Quantification of number of nuclei per osteoclast in 22-month old *Optn*$^{+/+}$ (+/+) and *Optn*$^{-/-}$ (-/-) mice (**** $p < 0.0001$, $n = 60$ osteoclasts). (F) Serum levels of alkaline phosphatase (ALP) and collagen type I C-telopeptide (CTX-1) in 22-month old *Optn*$^{+/+}$ (+/+) and *Optn*$^{-/-}$ (-/-) mice (* $p < 0.05$, *** $p < 0.001$, $n = 4$-6 per genotype).

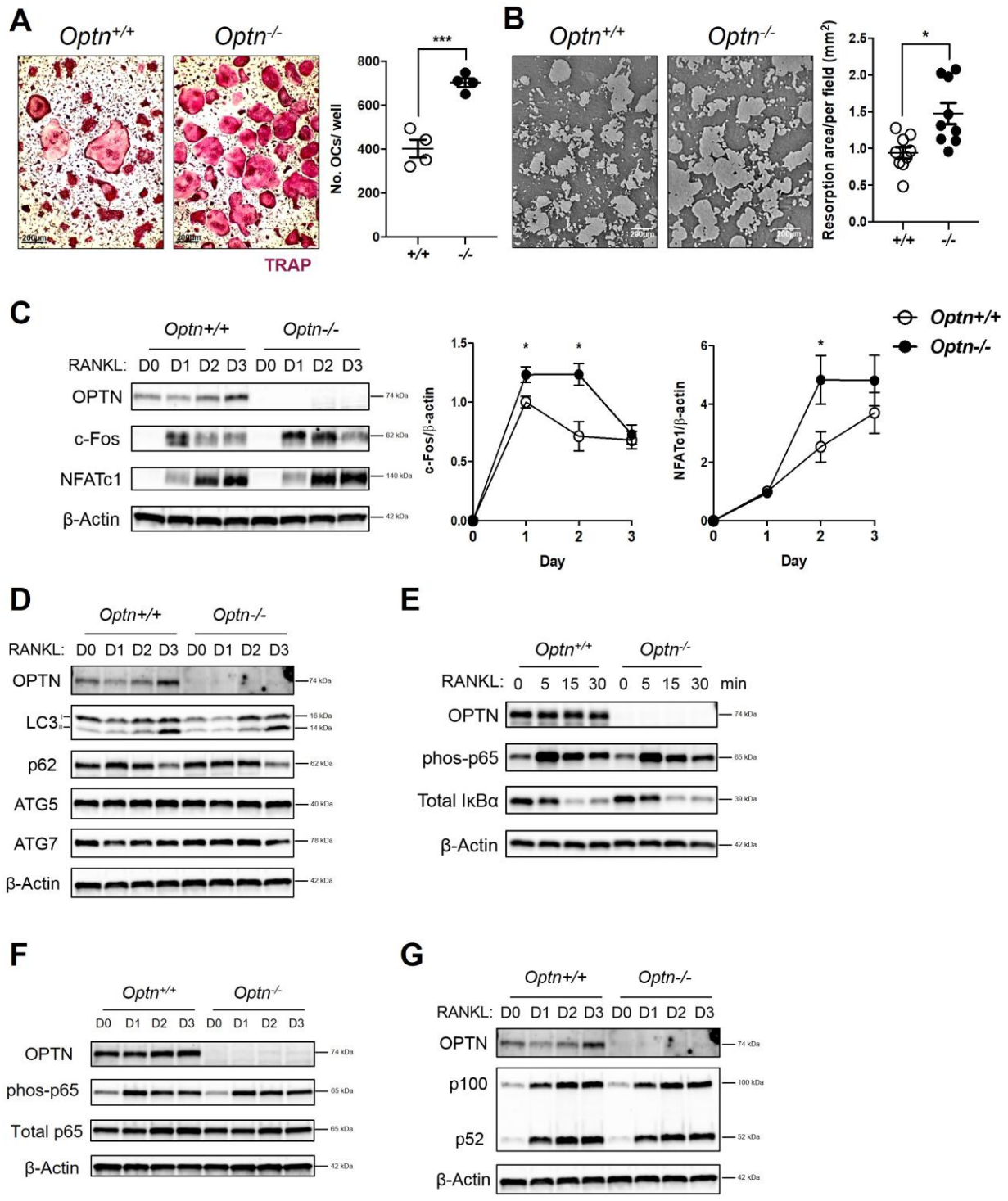

Figure 2.8 OPTN deficiency promotes osteoclastogenesis *in vitro*. (A) *Optn*$^{+/+}$ and *Optn*$^{-/-}$ bone marrow-derived precursors from 8-12 week old mice were cultured under osteoclastogenic conditions, and osteoclast (OC) differentiation was assessed by quantification of the number of

multi-nucleated TRAP-positive cells on day 3 post-RANKL treatment. Representative images are shown. (*** $p < 0.001$, n = 4 wells). (B) *Optn*$^{+/+}$ and *Optn*$^{-/-}$ bone marrow-derived precursors from 8-12 week old mice were cultured under osteoclastogenic conditions on Osteo Assay Surface plates, and resorptive activity was quantified on day 5 post-RANKL treatment. Representative images are shown. (* $p < 0.05$, n = 9 wells). (C) Western blot of OPTN, c-Fos, and NFATc1 in *Optn*$^{+/+}$ and *Optn*$^{-/-}$ OC at days 0-3 of OC differentiation. Densitometry was calculated with ImageJ (* $p < 0.05$, n = 3 blots). (D) *Optn*$^{+/+}$ and *Optn*$^{-/-}$ bone marrow-derived precursors were cultured under osteoclastogenic conditions, and autophagic activity was assessed by Western blot on days 0-3 post-RANKL treatment. Cells were probed for OPTN, LC3, p62, ATG5, and ATG7. (E-G) *Optn*$^{+/+}$ and *Optn*$^{-/-}$ bone marrow-derived precursors were cultured with RANKL for 0-60 minutes or 0-3 days, to assess the activation of canonical and noncanonical NF-κB signaling, respectively, by Western blot. Cells were probed for OPTN (E-G), phos-p65 (E-F), Total p65 (F), Total IκB (E), and p100/p52 (F).

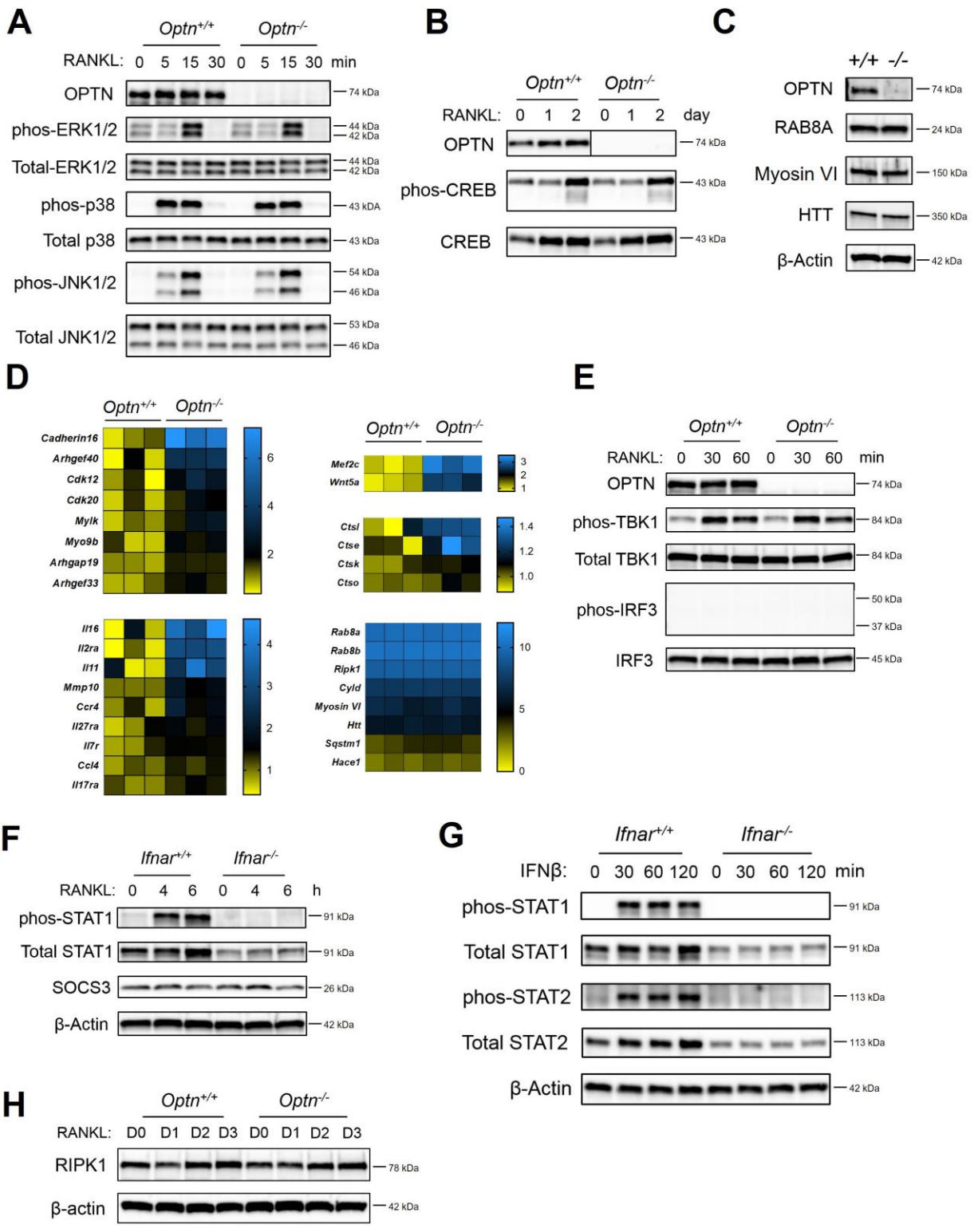

Figure 2.9 *Optn*$^{-/-}$ osteoclasts display no defect in common osteoclastic signaling pathways.

(A) Western blot of OPTN, phos-ERK1/2, Total ERK1/2, phos-p38, Total ps38, phos-JNK1/2,

and total JNK1/2 in *Optn*$^{+/+}$ and *Optn*$^{-/-}$ OC precursors treated with RANKL from 0 to 30 minutes. (B) Western blot of OPTN, phos-CREB, and Total CREB in *Optn*$^{+/+}$ and *Optn*$^{-/-}$ OC precursors treated with RANKL from 0 to 2 days; the OPTN lane was run on the same gel, but were noncontiguous (C) Western blot of OPTN, RAB8A, Myosin V, and HTT in *Optn*$^{+/+}$ and *Optn*$^{-/-}$ OC. (D) Microarray analysis of *Optn*$^{+/+}$ and *Optn*$^{-/-}$ OC on day 3 post-RANKL treatment. Heat map representing color-coded expression levels of differentially expressed genes in the type I IFN signature (log2 values) of biological triplicate samples of *Optn*$^{+/+}$ and *Optn*$^{-/-}$ OC. (E) Western blot of OPTN, phos-TBK1, Total TBK1, phos-IRF3, and Total IRF3 expression in *Optn*$^{+/+}$ and *Optn*$^{-/-}$ OC precursors treated with RANKL from 0 to 30 minutes. (F) Western blot of phos-STAT1, Total STAT1, and SOCS3 expression in *Ifnar*$^{+/+}$ and *Ifnar*$^{-/-}$ OC precursors treated with RANKL from 0 to 6 hours. (G) Western blot of phos-STAT1, Total STAT1, phos-STAT2, and Total STAT2, in *Ifnar*$^{+/+}$ and *Ifnar*$^{-/-}$ OC precursors treated with IFNβ from 0 to 120 minutes. (H) Western blot of RIPK1 in *Optn*$^{+/+}$ and *Optn*$^{-/-}$ OC precursors treated with RANKL from 3 days.

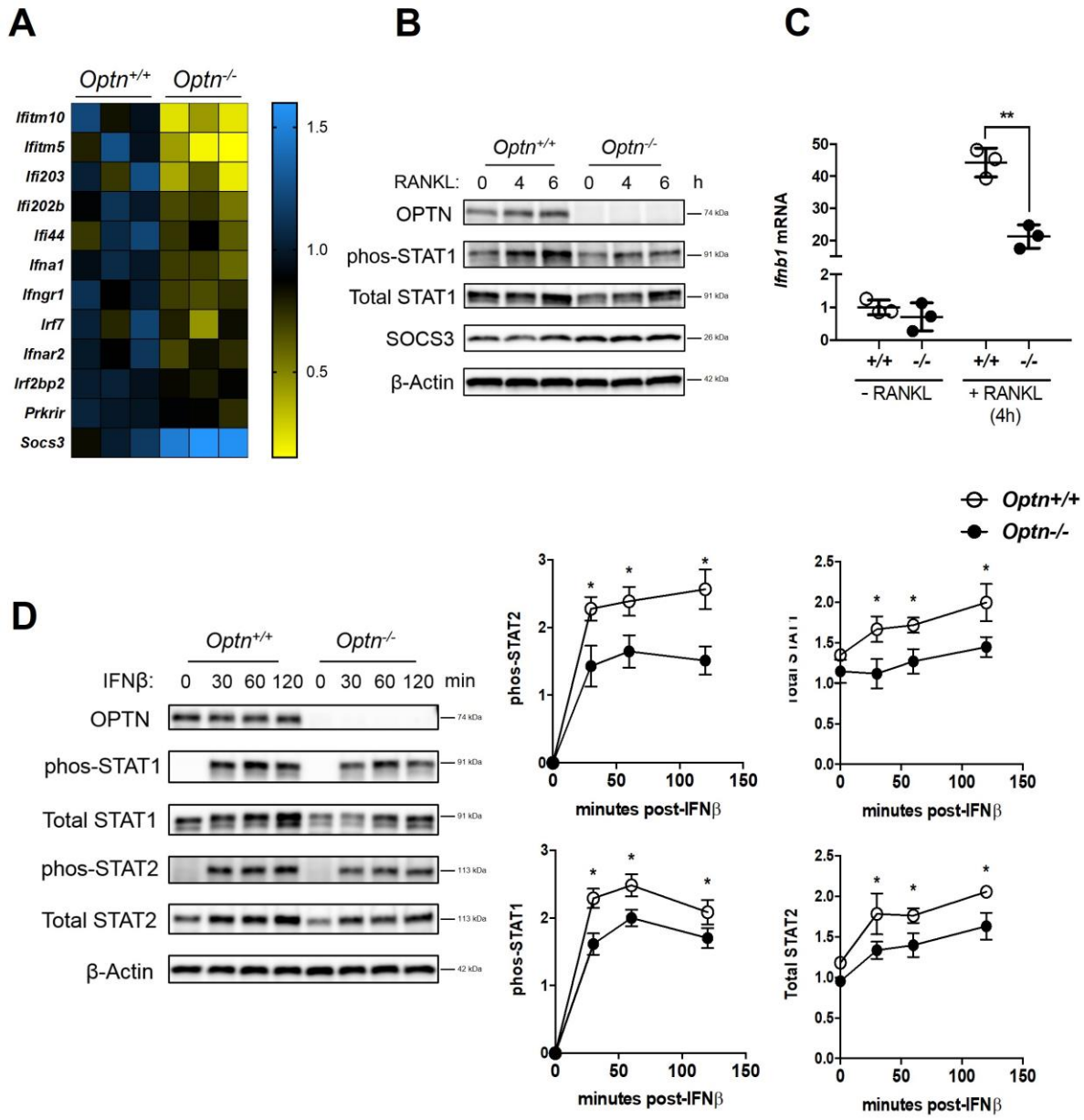

Figure 2.10 OPTN deficiency affects RANKL induced IFNβ production and type I IFN activation. (A) Microarray analysis of *Optn*$^{+/+}$ and *Optn*$^{-/-}$ OC on day 3 post-RANKL treatment. Heat map representing color-coded expression levels of differentially expressed genes in the type I IFN signature (log2 values) of biological triplicate samples of *Optn*$^{+/+}$ and *Optn*$^{-/-}$ OC. (B) Western blot of OPTN, phos-STAT1, Total STAT1, and SOCS3 expression in *Optn*$^{+/+}$ and *Optn*$^{-/-}$ OC precursors treated with RANKL at 4 and 6 hours. (C) The mRNA level of *Ifnb1* in OC

precursors treated with RANKL at 4 hours was determined using qPCR. (* $p < 0.05$, n = 3 wells). (D) *Optn*$^{+/+}$ and *Optn*$^{-/-}$ OC precursors from 8-12 week old mice were treated with IFNβ and assessed for type I IFN signaling via Western blot for phos-STAT1, phos-STAT2, Total STAT1, and Total STAT2. Densitometry was calculated with ImageJ (* $p < 0.05$, n = 3 blots).

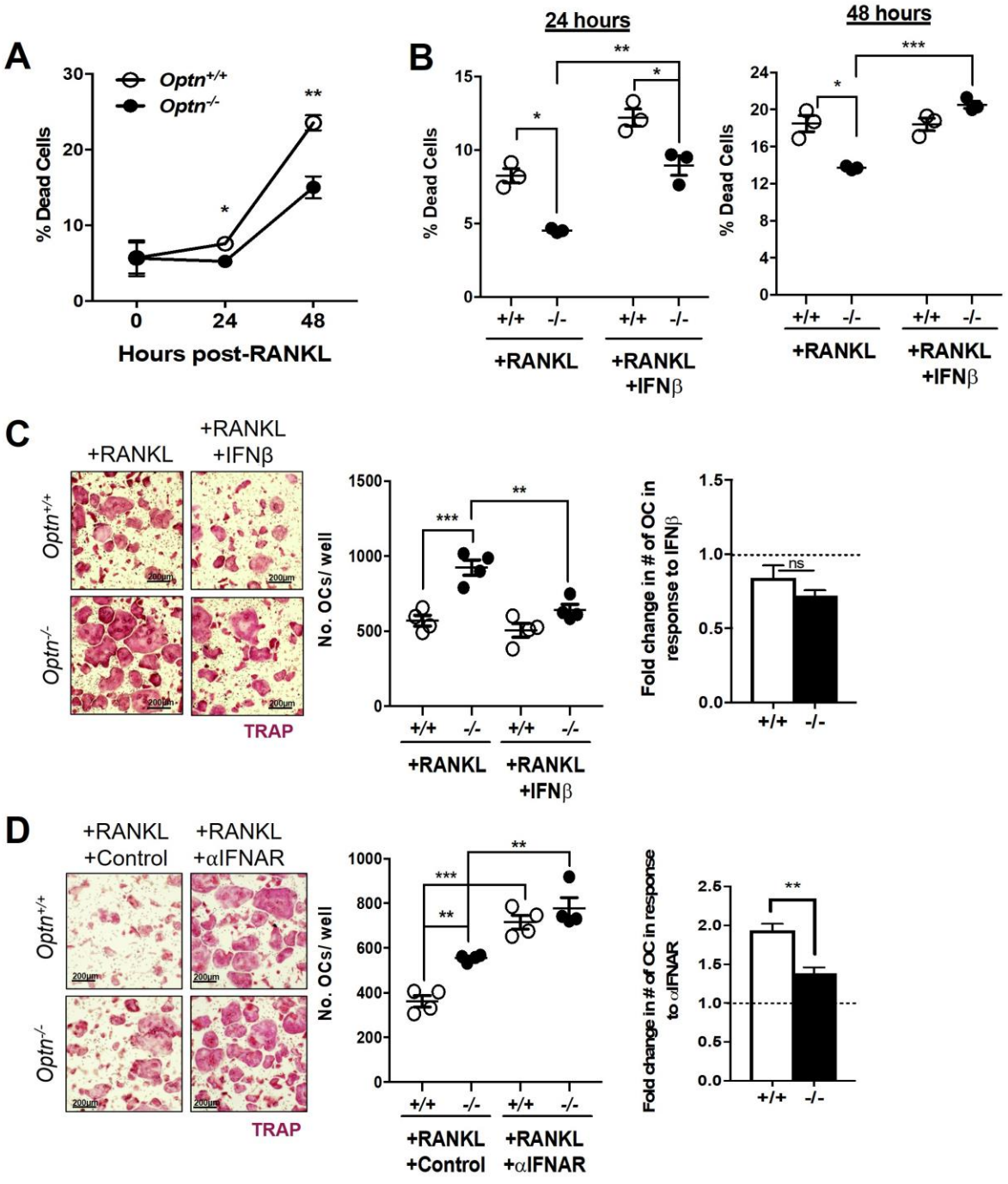

Figure 2.11 Recombinant IFNβ can rescue hyper-osteoclastogenesis observed during OPTN deficiency. (A) *Optn*$^{+/+}$ and *Optn*$^{-/-}$ OC precursors from 8-12 week old mice treated with RANKL, and cells were harvested at 0, 24, and 48 hours post-RANKL treatment and analyzed by flow cytometry for cell death by Annexin V and Zombie-Red. %Dead Cells calculated as percentage

Annexin V^+ Zombie-Red^+ of $CD45^+$ cells (* $p < 0.05$, ** $p < 0.01$, n = 6 wells). (B) *Optn*$^{+/+}$ and *Optn*$^{-/-}$ OC precursors treated with RANKL with or without IFNβ, and cells were harvested at 24 and 48 hours post-RANKL/ IFNβ treatment and analyzed by flow cytometry for cell death by Annexin V and Zombie-Red. %Dead Cells calculated as percentage Annexin V^+ Zombie-Red^+ of $CD45^+$ cells (* $p < 0.05$, *** $p < 0.001$, n = 3 wells). (C) TRAP staining of *Optn*$^{+/+}$ and *Optn*$^{-/-}$ osteoclast precursors treated with RANKL with or without IFNβ for 3 days to assess OC formation (** $p < 0.01$, n = 4 wells). (H) TRAP staining of osteoclast precursors under osteoclastogenic conditions with control or IFNα/βR blocking (αIFNAR) antibody for 3 days (* $p < 0.05$, * $p < 0.01$, *** $p < 0.001$, n = 4 wells)

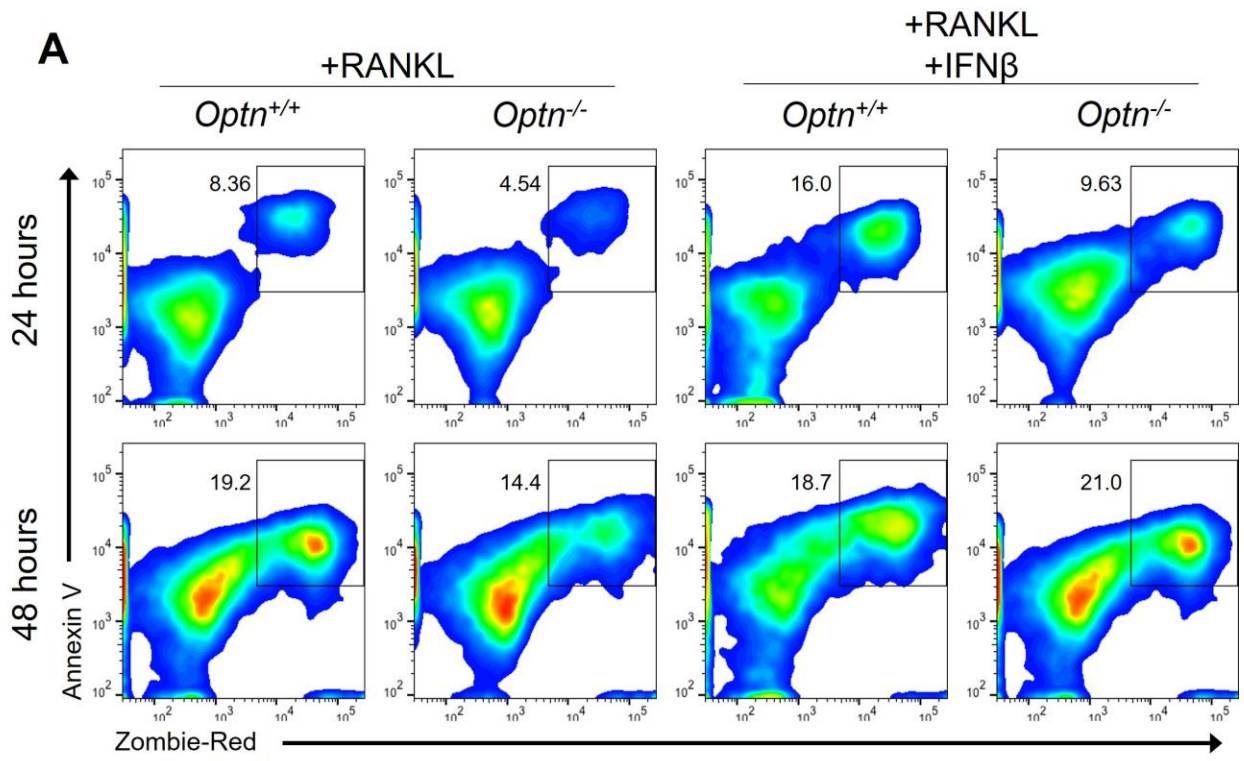

Figure 2.12 *Optn*$^{-/-}$ osteoclast precursors display a survival advantage during differentiation.

(A) *Optn*$^{+/+}$ and *Optn*$^{-/-}$ OC precursors treated with RANKL with or without IFNβ, and cells were harvested at 24 and 48 hours post-RANKL/ IFNβ treatment and analyzed by flow cytometry for cell death by Annexin V and Zombie-Red. Representative flow cytometry plots are shown.

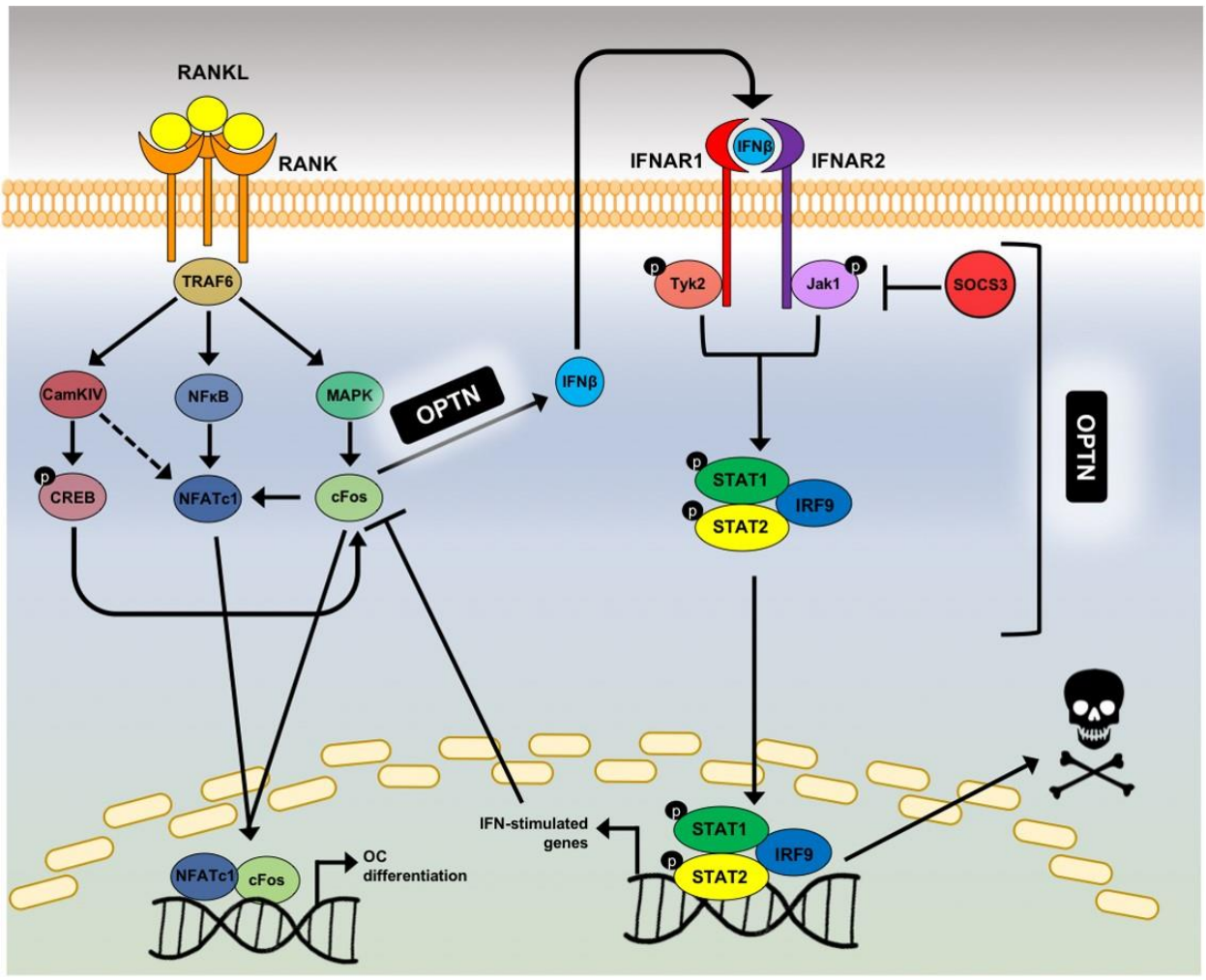

Figure 2.13 Schematic of the dual role of OPTN in mediating negative regulation of osteoclastogenesis. During RANKL-mediated osteoclastogenesis, OPTN is required for optimal IFNβ production, which is critical for inhibition of cFos, promotion of the IFNα/βR signaling cascade, and induction of cell death.

CHAPTER 3: A NON-CANONICAL ROLE FOR AUTOPHAGY MACHINERY IN OSTEOCLAST DIFFERENTIATION

Introduction

Autophagy is an evolutionally conserved intracellular system that forms double-membraned autophagosomes to engulf cytoplasmic materials and to deliver them to lysosomes for degradation. Usually, the term "autophagy" implies macroautophagy, which is a catabolic process that non-selectively digests intracellular components for the nutrients recycling. While autophagy has been well known as a survival mechanism triggered by harsh environment, such as nutrient starvation and stresses to maintenance the cell viability, it is also highly activated during embryonic development and cell differentiation (Mizushima and Levine 2010). Multiple lines of evidence shows that autophagy is involves in the terminal differentiation and maturation of many types of cells, including the immunes cells (B and T lymphocytes) (Clarke and Simon 2019), skins (keratinocytes) (Akinduro et al. 2016), and smooth muscles (myofibrobalsts) (Bernard et al. 2014).

Osteoclasts are myeloid-derived multinucleate cells that degrade mature bone for bone remodeling. Under homeostatic situations, there is an equilibrium between osteoclastic bone resorption and osteoblastic bone formation. However, over-activation of osteoclasts can lead bone loss outpacing bone formation, and hence development of osteoclast diseases, such as osteoporosis. GWA studies (Zhang et al. 2010) demonstrated that genetic variations in the core genes of autophagy pathway are associated with decreased bone mineral density, a precondition of osteoporosis. A previous study has showed that some autophagy proteins, such as ATG5, ATG7, and ATG4B, are involved in the resorptive function of osteoclast (DeSelm et al. 2011). While

Becn1 knockdown (Chung et al. 2014) and pharmacological inhibition studies (Xiu et al. 2014b) demonstrated that both depletion of an autophagy protein and blocking autophagy prohibit *in vitro* osteoclastogenesis, the absence of ATG5 seems to not interfere with osteoclast differentiation both *in vivo and in vitro*. Therefore, it remains unknown whether the autophagy influx induction or certain autophagy components are involved in osteoclast different and underlying mechanisms by which autophagy machinery functions in osteoclastogenesis remain elusive. Here, we studied the role of different autophagy proteins in osteoclast differentiation. We found that the only certain autophagy core proteins, such Beclin-1, VPS34, ATG14 and FIP200 are involved in osteoclast differentiation. Similarly, we observed an osteopetrosis phenotype caused by osteoclastopenia in mice with myeloid deficiency of *Becn1*. Mechanistically, Beclin-1 are required for noncanonical NF-kB activation and preventing DNA damages and cell death during osteoclast development. Therefore, we identified the non-canonical role of autophagy machinery for osteoclast development.

Material and Methods

Animals

Rubcn$^{flox/flox}$ mice were cross with *LysM-Cre*$^{+}$ mice (Peter Murray, St. Jude Children's Research Hospital) to generate myeloid restricted conditional knockout mice, *Rubcn*$^{LM/LM}$, in C57BL/6 background, respectively. Other autophagy gene conditional knockout mice in C57BL/6 background are provided: *LysM-Cre*$^{+}$ *Becn1*$^{flox/flox}$, (*Becn1*$^{LM/LM}$) from Edmund Rucker, University of Kentucky), *LysM-Cre*$^{+}$ *Atg5*$^{flox/flox}$ (*Atg5*$^{LM/LM}$), from Thomas A. Ferguson, Washington University, *LysM-Cre*$^{+}$ *Fip200*$^{flox/flox}$, (*Fip200*$^{LM/LM}$) from Jun-Lin Guan, University of Michigan, *LysM-Cre*$^{+}$ *Atg14*$^{flox/flox}$ (*Atg14*$^{LM/LM}$) from Herbert Virgin, Washington University, *LysM-Cre*$^{+}$

Vps34$^{flox/flox}$ (*Vps34*$^{LM/LM}$) from Richard Flavell, Yale University. Male mice were used for both *in vivo* and *ex vivo* studies. All animal procedures were approved by Institutional Animal Care and Use Committees at the NIEHS.

Micro-CT Scanning and Dual Energy X-Ray Absorptiometry (DEXA)

Femurs and Tibiae were harvested, fixed in 10% paraformaldehyde, and scanned by MicroCT Scanco 40 (Scanco Medical, Bassersdorf, Switzerland) in 10 μm resolution (E = 70kVa; I = 145 μA). Regions of interest of the trabecular and cortical bone was measured, 0.60 mm distal to metaphysis of tibia and 0.6 mm proximal to the distal tibio-fibular junction, respectively. The reconstructed solid 3D images were used for visualizing trabecular bone microarchitecture. We measured whole body bone mineral content (BMC) and bone mineral density (BMD) by DEXA using LUNAR PIXImus bone densitometer (GE Healthcare, Fairfield, CT USA).

Slide staining

Bones were decalcified in 10% EDTA for 3 weeks and then processed, paraffin embedded, and sectioned at thickness of 5 μm. Sections were stained with hematoxylin and eosin (H&E) for general histology, and with tartrate-resistant acid phosphatase (TRAP) straining to detect $TRAP^+$ cells.

Osteoclast differentiation and Immunofluorescence

Tibias and femurs were harvested from 8-10 weeks old male mice after euthanasia by CO_2. Bone marrow cells were flushed into phenol free α-MEM medium, supplemented with 10% FBS, L-Glutamine, non-essential amino acids, and penicillin/streptomycin. Unattached cells were

harvest after overnight and re-plated at a density of 1.5×10^5 cells/cm^2 in presence of 30 ng/mL M-CSF for 2-3 days to prepare for osteoclast precursor cells (R&D Systems, Minneapolis, MN USA). To stimulate osteoclastogenic differentiation, osteoclast precursors are treated with 10 ng/mL RANKL and 30 ng/mL M-CSF in the cell culture medium for 3 continuous days (R&D Systems Minneapolis, MN USA). Cells were fixed 10% formalin and stained with tartrate-resistant acid phosphatase (TRAP) to detect $TRAP^+$ multinucleated cells. For immunofluorescence staining, non-adherent bone marrow cells were cultured and stimulated in chamber slides with 4% formaldehyde fixation. After fixation, cells were blocked and perforated in block buffer (0.1% Triton X-100 and 1% BSA in PBS), and then incubated with 1/200 diluted primary antibodies overnight at 4°C. Cell were rinsed by PBS and incubated with Alex Fluor-conjugated secondary antibodies (Invitrogen).

Antibodies and Western Blot Analysis

The following antibodies were from Cell Signaling (Beverly, MA USA): Fip200 (Cat. #), Vps34 (Cat. #), Atg14 (Cat. #), Rubicon (Cat. #), c-Fos (Cat. #4384), LC3B (Cat. #2775), p62 (Cat. #5114), ATG5 (Cat. #12994), ATG7 (Cat. #2631), TRAF3 (Cat. #), p65 (Cat. #8242), phospho-p65 (Cat. #3033), p100/p52 (Cat. #4882), IκBα (Cat. #4814), phospho -p38 (Cat. #9215), p38 (Cat. #9212), phospho -ERK1/2 (Cat. #4370), ERK1/2 (Cat. #4695), phospho -JNK (Cat. #4668), JNK (Cat. #9252), phospho -CREB (Cat. #9198), CREB (Cat. #4820). The following antibodies were from Santa Cruz Biotechnology Inc. (Dallas, TX USA): NFATc1 (Cat. #sc-7294), Beclin-1 (Cat. #), and Actin (Cat. #sc-1616). Secondary antibodies were from Jackson Immuno-Research (West Grove, PA, USA).

Proteins were harvested, and protein concentration was measured as previously described (Lee et al. 2015). 5-10 µg of total protein lysate was resolved by Criterion TGX precast gel (Biorad, Hercules, CA, USA) and transferred to nitrocellulose membrane using the Trans-Blot Turbo Transfer System (Bio-rad, Hercules, CA, USA) and immunodetected using appropriate primary and peroxidase-coupled secondary antibodies (Jackson Immunoresearch, West Grove, PA USA). Proteins were visualized by enhanced chemiluminescence (ECL, Amersham Bioscience, Little Chalfont, UK).

RNA isolation and Microarray

Total RNA was isolated using the RNeasy plus mini kit (Qiagen, Hilden, Germany) according manufacturer's protocol. RNA was isolated from *Becn1*$^{WT/WT}$ and *Becn1*$^{LM/LM}$ bone-marrow-derived osteoclasts as described above, and gene expression analysis was conducted using Affymetrix Mouse Genome 430 2.0 GeneChip® arrays (Affymetrix, Santa Clara, CA). Arrays were scanned in an Affymetrix Scanner 3000 and preliminary analyses were performed with OmicSoft Array Studio (Version 9.0) software.

Assay for transposase accessible chromatin with high-throughput sequencing (ATAC-seq)

ATAC-seq was performed as previously described. Briefly, the harvested cell pellet was re-suspended in Greenleaf lysis buffer and placed on ice for 5 min. Then crude nuclei were pelleted by centrifuge for 5 min at 500 × g, 4°C. Nuclei pellet were re-suspended in transposition mix (Illumia cat# FC-121-1030), and DNA were purified by the Qiagen MinElute PCR purification kit. ATAC-seq library was generated by PCR amplification and sequenced on the NextSeq

(Illumina). Biological triplicates were performed, and combined reads were used for further analysis.

Flow Cytometry

To assess cell death, osteoclast precursors were harvested 24 and 48 hours after treatment with RANKL in the presence or absence of IFNβ and stained with Annexin-V (1:50), Zombie-Violet (1:1000), and CD45 (1:200), as previously described (Dillon et al. 2014). All antibodies were from Biolegend (San Diego, CA USA).

Statistical Analysis

For all *in vitro* studies, three independent experiments were performed. Data are presented as mean ± SD. Student's T test or Analysis of Variance (ANOVA) was used to determine the differences among groups. A *p value* less than 0.05 is considered statistically significant.

Results

Upregulation of autophagy proteins and induction of autophagy during *ex vivo* osteoclastogenesis.

To examine the temporal expression of autophagy components during *ex vivo* osteoclastogenesis, we generated osteoclast precursors from bone marrow-derived macrophage cells (BMMs), followed by 3 days of RANKL stimulation (Figures 3.1A), which resulted in fully differentiated, multinucleated osteoclasts, as detected by tartrate-resistant acid phosphatase (TRAP) staining (Figures 3.1B). The expression levels of multiple classical proteins in the autophagy pathway, including FIP200, Beclin-1, VPS34, ATG14, and ATG5 were elevated during osteoclast differentiation, peaking at 3 days post-RANKL stimulation (Figures 3.1D). In addition,

an induction of autophagic flux was detected during osteoclast differentiation, indicated by the transformation of LC3-I to LC3-II and a gradual degradation of p62, both canonical markers for autophagy (Figures 3.1D). Immunofluorescence staining further demonstrated the presence of LC3-II puncta in the cytoplasm of fully differentiated osteoclasts (Figures 3.1C). As autophagy is activated during osteoclastogenesis, we hypothesized that the autophagy machinery may play a role in osteoclast development.

Ablation of *Becn1* in osteoclast precursors resulted in osteopetrosis and prevented age-related bone loss in mice

To investigate the significance of autophagy in osteoclast biology *in vivo*, we first performed skeletal phenotyping of mice with myeloid lineage restricted deficiency of *Becn1*, a core component of the Class III PI3K complex of the autophagy machinery. Western blot confirmed approximately 70% reduction of Beclin-1 in bone marrow cell derived BMMs and osteoclasts from *LysM-Cre*$^{+}$ *Becn1*$^{flox/flox}$ (hereafter *Becn1*$^{LM/LM}$) mice compared to that from *Becn1*$^{WT/WT}$ mice (data no shown). At 2-months of age, *Becn1*$^{LM/LM}$ mice exhibited a strong osteopetrosis phenotype (Figures 3.2A, B), characterized by increased bone mass and density. 3D reconstruction of the tibiae by microcomputed tomographic analysis revealed both trabecular and cortical bone parameters were significantly increased *Becn1*$^{LM/LM}$ mice compared to *Becn1*$^{WT/WT}$ littermates (Figures 3). Furthermore, H&E staining also confirmed an increased trabecular bone component in *Becn1*$^{LM/LM}$ mice (Figures 3.2C). As *Becn1* deletion is restricted to the osteoclast, not osteoblast, lineage in the *Becn1*$^{LM/LM}$ mice, we next examined osteoclast formation *in vivo* via TRAP staining. Compared to wild type littermates, *Becn1*$^{LM/LM}$ mice exhibited a significantly decreased number of TRAP^{+} osteoclasts around the growth plate of femurs (Figures 3.2D), suggesting that the osteopetrotic phenotype is caused by osteoclastopenia.

During the aging process, there is a natural loss of the bone, so we next asked if aged *Becn1*$^{LM/LM}$ mice were protected from aged-induced bone loss. Similar to 2-month old mice, 1-year old *Becn1*$^{LM/LM}$ mice exhibited an increased bone mass and decreased bone loss compared to *Becn1*$^{WT/WT}$ mice (Figures 3.2E), indicating that *Becn1*$^{LM/LM}$ mice were indeed protected against age-related bone loss. However, a higher basal bone volume in *Becn1*$^{LM/LM}$ mice may contribute to this protection. Collectively, our results suggest that autophagy is required for osteoclast formation *in vivo*.

Differential requirements for autophagic components during osteoclastogenesis *ex vivo*

To confirm the role of autophagy in osteoclast development, we performed primary *ex vivo* osteoclastogenesis using bone marrow cells from the long bones of *Becn1*$^{LM/LM}$ and *Becn1*$^{WT/WT}$ mice. Compared to *Becn1*$^{WT/WT}$ OCs, *Becn1*$^{LM/LM}$ OCs displayed an accumulation of p62 and a decrease in LC3-II conversion (Figures 3.3A), indicating that autophagic flux is defective during differentiation of *Becn1*$^{LM/LM}$ osteoclasts. Importantly, *Becn1*-deficiency resulted in significantly decreased numbers of TRAP^{+} osteoclasts (Figures 3.3B). In parallel with this reduction in TRAP^{+} ploykaryons, *Becn1*$^{LM/LM}$ precursor cells expressed significantly lower levels of c-Fos and NFATc1, two essential osteoclastic transcription factors, following RANKL treatment (Figure 3.3C). These data confirm that autophagy induction and Beclin-1 may be needed for osteoclastogenesis.

Beclin-1 is a core protein in the Class III PI3K complex, so we next asked if its binding partners in the Class III PI3K Complex are also required for osteoclast differentiation. Similar to the phenotype of *Becn1*$^{LM/LM}$ osteoclasts, we found the absence of either *Vps34* or *Atg14* resulted in significantly decreased numbers of OCs, as well as defective autophagy flux in the *Vps34*- or

Atg14-deficient OCs (Figures 3.3D, E). Intriguingly, myeloid deficiency of *Uvrag*, which can also be associated with the Class III PI3K Complex (Figures 3.3F), or *Rubcn*, an essential component of LC3-associated phagocytosis (LAP) and negative regulator for autophagy, did not result in defective osteoclastogenesis, demonstrating that these molecules are not required.

In addition, we examined the requirement for the pre-initiaion complex, upstream of the Class III PI3K complex, in osteoclastogenesis. Deletion of *Rb1cc1*, which encodes FIP200, blocked autophagic flux in differentiating osteoclasts, and significantly decreased *ex vivo* osteoclastogenesis (Figures 3.4A). However, deletion of *Atg5*, a component of the ubiquitin-like conjugation system downstream of the Class III PI3K complex, did not affect osteoclast formation, with BMM from both $Atg5^{WT/WT}$ and $Atg5^{LM/LM}$ mice generating equivalent $TRAP^{+}$ osteoclasts and equivalent levels of c-Fos and NFATc1 (Figures 3.4B). As expected, however, $Atg5^{LM/LM}$ OCs displayed an intrinsic defect in autophagic flux, compared to $Atg5^{WT/WT}$ OCs (Figures 3.4B). Collectively, these data indicate that upstream canonical autophagy proteins in the pre-initiation complex (FIP200) and Class III PI3K complex, (Beclin-1, VPS34 and ATG14) display autophagic defects and are required for osteoclast differentiation *ex vivo*, while proteins downstream in the autophagy pathway (such as ATG5), display autophagic defects yet are not required for osteoclastogenesis. Thus, defects in autophagy *per se* do not result in decreased osteoclastogenesis, therefore these required autophagic components must be functioning in a non-canonical fashion.

Becn1 deficiency does not affect common osteoclastogenic pathways

We next sought to investigate the mechanisms by which Beclin-1 functions as a positive regulator for osteoclast differentiation. As a previous study showed that *Becn1* gene knockdown in BMMs decreased RANKL induced JNK and p38 activation, we next evaluated MAP kinases activation in

Becn1$^{WT/WT}$ and *Becn1*$^{LM/LM}$ osteoclast precursors following RANKL treatment. We observed equivalent levels of phosphorylated JNK1/2, ERK1/2 and p38 in *Becn1*$^{WT/WT}$ and *Becn1*$^{LM/LM}$ BMMs post-RANKL treatment (Figures 3.5A), suggesting that *Becn1* deficiency does not alter RANKL induced MAP kinase activation. RANKL-mediated NF-κB pathway activation is prerequisite for the c-Fos-NFATc1 axis during osteoclastogenesis. We next assessed the activation of p65 and IκBα, members of the canonical NF-κB pathway, in *Becn1*$^{WT/WT}$ and *Becn1*$^{LM/LM}$ post-RANKL treatment. The levels of phosphorylated p65 and IκBα, and the degradation of the IκBα showed similar patterns in *Becn1*$^{WT/WT}$ and *Becn1*$^{LM/LM}$ BMMs post-RANKL treatment (Figures 3.5B), suggesting that *Becn1* deficiency does not affect RANKL-induced canonical NF-κB responses. As RANKL also induces a PI3K-Akt-NFATc1 signaling axis for osteoclastogenesis, we examined the phosphorylated levels of Akt in *Becn1*$^{WT/WT}$ and *Becn1*$^{LM/LM}$ BMMs in response to RANKL treatment. We observed an equivalent level of phosphorylated Akt in *Becn1*$^{WT/WT}$ and *Becn1*$^{LM/LM}$ BMMs post-RANKL treatment (Figures 3.5C). These data, therefore, suggest that Beclin-1 regulates osteoclastogenesis independently of MAP kinases, canonical NF-κB activation, or Akt activation.

Becn1 deficiency alters non-canonical NF-κB activation

Previous studies have shown that non-canonical NF-κB responses also participate in osteoclastogenesis, therefore we next evaluated if *Becn1* deficiency affects non-canonical NF-κB activations in osteoclasts. As expected, RANKL induces a robust processing of p100 to p52, which indicates non-canonical NF-κB activation, in *Becn1*$^{WT/WT}$ precursors during osteoclast development. *Becn1*$^{LM/LM}$ precursors, however, displayed a decreased level of the processed p52 protein compared to *Becn1*$^{WT/WT}$ osteoclast precursors, suggesting that *Becn1* deficiency results in

a defective non-canonical NF-κB response (Figures 3.6A). Importantly, fractionation experiments revealed that, in *Becn1*$^{WT/WT}$ osteoclast precursors, RANKL treatment results in nuclear translocation of RelB, and that RelB nuclear translocation is significantly decreased in *Becn1*$^{LM/LM}$ precursors (Figures 3.6B). Intriguingly, RANKL treatment of *Becn1*$^{WT/WT}$ precursors also induced nuclear translocation of Beclin-1, which was absent in *Becn1*$^{LM/LM}$ precursors (Figures 3.6B). To validate this observation, we performed immunofluorescence staining, and confirmed nuclear translocation of both Beclin-1 and RelB to the nucleus of RANKL-stimulated *Becn1*$^{WT/WT}$ precursors, both of which were again absent in *Becn1*$^{LM/LM}$ precursors (Figures 3.6C). Therefore, Beclin-1 is required for RANKL-induced non-canonical NF-κB activation in osteoclasts, possibly via the nuclear translocation of Beclin-1.

Nuclear Beclin-1 is required to mediate the DNA damage repair response and promote cell survival during osteoclastogenesis

To address the mechanisms underlying Beclin-1's role in osteoclastogensis, we performed genome-wide transcriptional profiling using microarray with the *Becn1*$^{WT/WT}$ and *Becn1*$^{LM/LM}$ osteoclasts at day 2 of osteoclast differentiation *ex vivo*. Microarray revealed that many critical pathways were significantly downregulated in *Becn1*$^{LM/LM}$ osteoclasts compared to *Becn1*$^{WT/WT}$ osteoclasts, including protein ubiquitination, NF-κB signaling and the DNA damage response, whereas genes related to cell death, the oxidative stress response, and the unfolded protein response were upregulated in *Becn1*$^{LM/LM}$ osteoclasts (Figures 3.7A). In parallel to the global gene profiling, we examined chromatin accessibility of day 2 *Becn1*$^{WT/WT}$ and *Becn1*$^{LM/LM}$ osteoclasts by assay for transposase-accessible chromatin with high throughput sequencing (ATAC-seq). Compared to *Becn1*$^{WT/WT}$ osteoclasts, *Becn1*$^{LM/LM}$ osteoclasts displayed increased chromatin accessibility at transcriptional start sites (TSSs) - 48.2% of TSS in *Becn1*$^{LM/LM}$ osteoclasts

compared to 3.8% of TSS in *Becn1*$^{WT/WT}$ osteoclasts, suggesting changes in chromatin corresponding to increased transcription in *Becn1*$^{LM/LM}$ osteoclasts (Figures 3.7B). In *Becn1*$^{LM/LM}$ osteoclasts, differential ATAC-seq peaks within TSSs or broader promoter regions mapped to genes encoding proteins involved in intrinsic apoptotic signaling pathway and the responses to ER stress. By contrast, differential ATAC-seq peaks in *Becn1*$^{WT/WT}$ osteoclasts were clustered to genes encoding proteins involved in the negative regulation of apoptotic signaling pathways and genes responded to DNA damage (Figures 3.7B). Therefore, our data from accessible chromatin profile matches temporal transcription pattern in *Becn1*$^{LM/LM}$ osteoclasts, suggesting that the differentiating *Becn1*$^{LM/LM}$ osteoclasts exhibit transcriptional signatures associated with unresolved DNA damage and cell death.

Nuclear Beclin-1 maintains genomic integrity to promote cell survival during osteoclast differentiation

A recent study demonstrated that nuclear translocation of Beclin-1 is required for radiation-induced DNA damage repair. As our transcriptional profiling demonstrated that *Becn1*$^{LM/LM}$ osteoclasts had defects in DNA damage repair pathways, we next asked if *Becn1*-deficiency resulted in compromised genomic integrity during osteoclast differentiation. After one day of RANKL stimulation, both *Becn1*$^{WT/WT}$ and *Becn1*$^{LM/LM}$ precursors showed increased nuclear staining of phosphorylated histone H2.AX (phospho-γH2.AX), which is a biomarker for DNA double-strand breaks (DSBs) (Figures 3.8A). After 2 days of RANKL treatment, *Becn1*$^{WT/WT}$ precursors displayed reduced phos-γH2.AX levels, concurrently with increased levels of phosphorylated ATM (phospho-ATM), a key regulator of the DNA damage response. *Becn1*$^{LM/LM}$ precursors, however, exhibited increased levels of phospho-γH2.AX and significantly decreased levels of phospho-ATM (Figures 3.8B). Taken together, these results indicate that *Becn1*$^{LM/LM}$

osteoclast precursors have an intrinsic defect in repairing DNA damage incurred during osteoclastogenic differentiation.

Unresolved DNA damage may elicit cyto-destructive cell death as a mechanism to eliminate damaged cells. We next accessed if *Becn1*-deficiency affects the survival advantage of differentiating osteoclasts. Treatment of *Becn1*$^{LM/LM}$ precursors with RANKL, a TNF superfamily member, resulted in a significantly increased percentage of apoptotic and necrotic cells, as indicated by Annexin and Zombie-Violet double positivity, compared to *Becn1*$^{WT/WT}$ precursors (Figures 3.8C). Taken together, these results demonstrate that Beclin-1 serves a non-canonical role by preserving genomic integrity and preventing cell death during osteoclast development.

Discussion

It is well known that lysosomal pathways and autophagy function in cell survival and intracellular quality control. In recent decades, however, emerging evidence has revealed non-canonical roles for autophagy machinery. In this study, we demonstrated the importance of autophagy proteins, including Beclin-1, FIP200, VPS34, and ATG14 in osteoclast development, yet their requirement does not seem linked to canonical autophagy, as *Atg*5-deficiency does not impair osteoclastogenesis despite a defect in autophagic flux.

Previous studies show that downstream autophagy, but Atg5 deficient OC precursors can undergo normal osteoclast differentiation, although defects in autophagy flux found in Atg5 deficient osteoclasts. While we agree with the previous study that the absence of Atg5 does not affect osteoclast differentiation, our study highlighted that the proteins in the upstream pre-initiation complex and PI3KC3 complex are dispensable for osteoclast formation, suggesting that the entire autophagy pathway may be instrumental for both osteoclast differentiation and function,

through different components exert different control over each process. Coincidently, studies showed that the differentiation of osteoblasts, counterparts of osteoclast, depends on upstream autophagic machinery FIP200 (Liu et al. 2013), while the ATG5 functions in the mineralized role of osteoblasts (Nollet et al. 2014). However, the normal osteoclast differentiation from ATG5 deficient precursors cannot totally excluded that autophgic flux is unneeded for osteoclastogenesis, as studies have proven the existence of Atg5-independent non-canonical autophagy, which depends on the Rab9 to form autophagosomes (Nishida et al. 2009). Therefore, future studies need to address whether molecules in Atg5-independent autophagy pathways is involved in osteoclastogenesis.

Although it has been shown that the upregulation of autophagy genes, *BECN1*, *ATG5* and *LC3*, depends on the IKK-β and IKK-α, components of NF-κB pathways (Comb et al. 2011), whether autophagy machinery mediates NF-κB responses remains elusive. Our data showed *Becn1* deficient osteoclasts had by reduced expression of p52 and diminished nuclear translocation of RelB, thus indicating Beclin-1 is required for RANKL induced non-canonical NF-κB activations. While a recent study suggests applications of lysosomal inhibitor chloroquine reduced the degradation of TRAF3, a negative regulator for non-canonical NF-κB pathway, thereby diminishing its activations, we did not find a changed TRAF3 levels in the Becn1 deficient osteoclast, suggesting that Beclin-1 regulates noncanonical NF-κB pathway independent of TRAF3.

Interestingly, we observed a nuclear translocation of Beclin-1 during osteoclastogenesis, and it is reasonable to speculate it re-distribution may mediate non-canonical NF-κB activation in osteoclasts. While a recent study has identified an alternative function of Beclin-1 for DNA DSBs repair, our data agree with the previous study, showing a sustained DNA damage response in the

Becn1 deficiency differentiating osteoclasts, due to a decreased activity of ATM, a critical kinase for DSBs repair. As ATM along with NEMO have been shown as central players in nuclear-initiated NF-κB signaling pathway (Miyamoto 2011), the decreased levels phosphorylated ATM in *Becn1* deficient osteoclasts may cause an alteration of noncanonical NF-κB response and hence an decreased osteoclastogensis.

Taken together, our study delineates the mechanisms by which autophagy components mediate osteoclast differentiation. At the molecular level, autophagy machinery FIP200, Beclin-1, VPS34 and ATG14 are involved in osteoclastogenesis, which seems to be dispensable of autophagic flux. Furthermore, Beclin-1 employed a noncanonical role to maintain gemone integerity and prevent necrobiosis for proper noncaonical NF-κB responses during osteoclastogenesis (Figure 3.9).

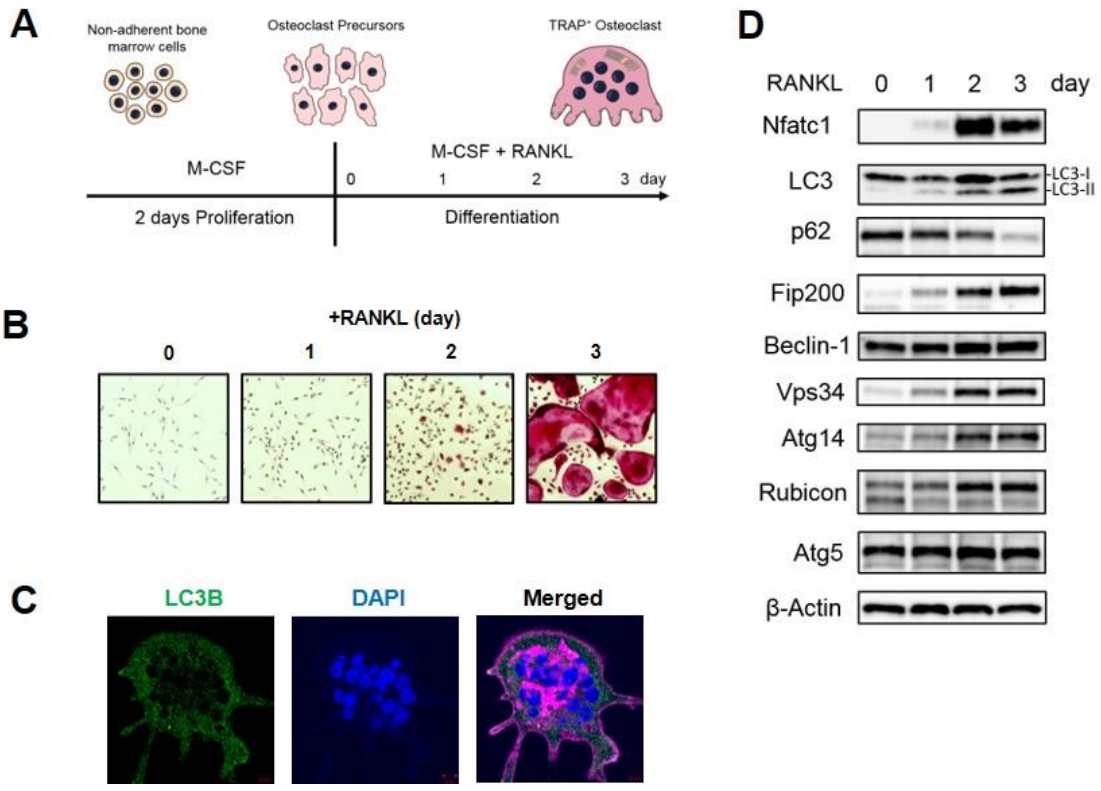

Figure 3.1 Expression of autophagy proteins during osteoclast differentiation. (A) A schematic picture for *ex vivo* osteoclastogenesis. (B) TRAP and Hematoxylin staining of day 0 to day 3 of RANKL induced osteoclastogenesis from bone marrow macrophages (BMMs). 3 days post-RANKL stimulations, $TRAP^{+}$ multinucleated osteoclasts are formed (20X). (C) Immunofluorescent staining of LC3B (green), DAPI (blue) and phalloidin (far red) for BMMs derived osteoclasts. (D) Expression of the osteoclastogenic marker and autophagy proteins in day 0 to day 3 of RANKL-induced osteoclast differentiation *ex vivo* from BMMs assessed by immunoblotting.

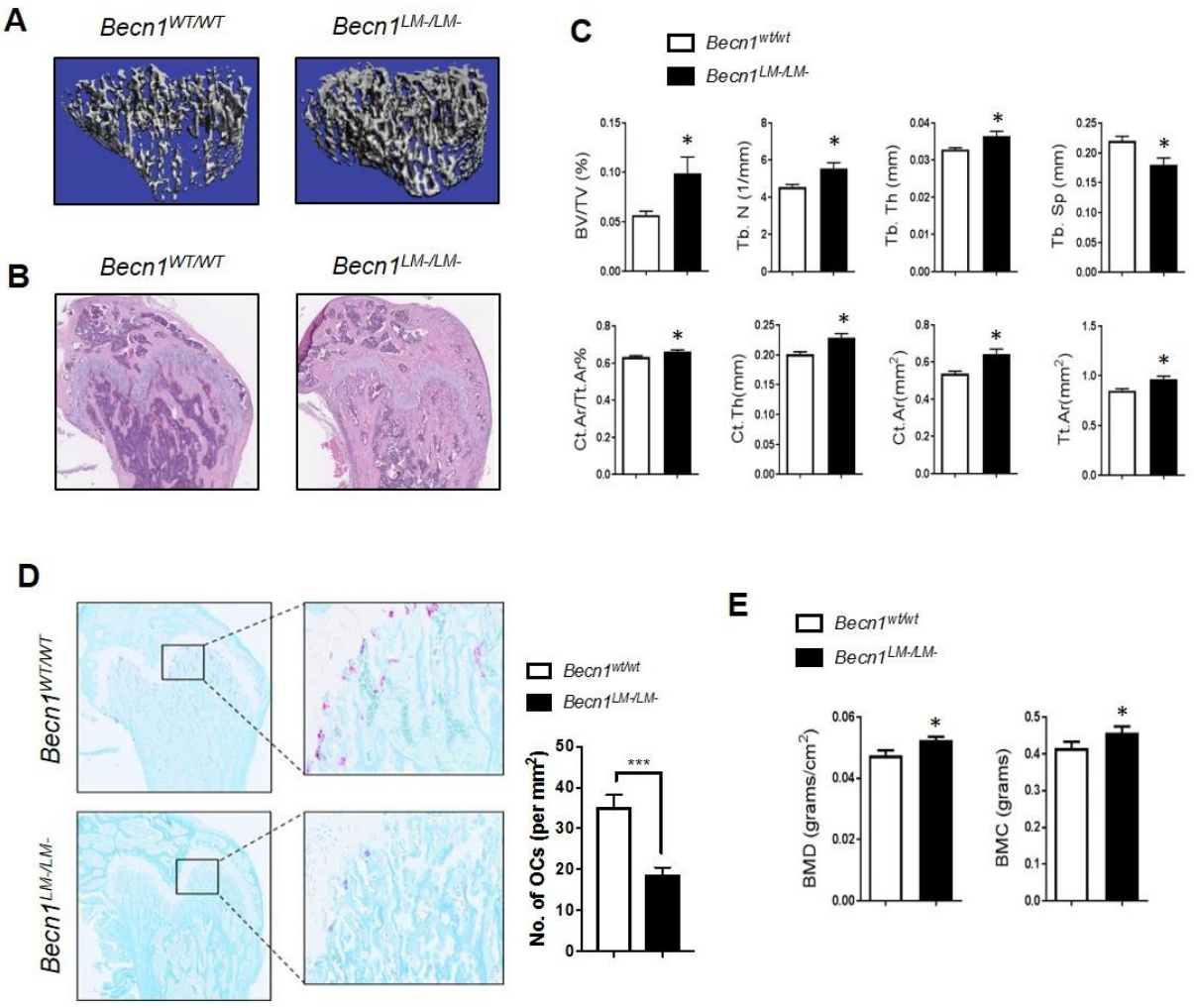

Figure 3.2 *Becn1*$^{LM/LM}$ mice exhibit an osteopetrosis phenotype and have reduced age-related bone loss (A) Representative micro CT rendering pictures of tibia trabeculae of 2-month-old *Becn1*$^{WT/WT}$ and *Becn1*$^{LM/LM}$ mice. (B) Representative H&E staining of femurs of 2-month-old *Becn1*$^{WT/WT}$ and *Becn1*$^{LM/LM}$ mice. (C) Trabecular and cortical bone morphometric analysis from the tibiae of 2-month-old mice; BV/TV, bone volume / total volume; Tb. N, trabecular number; Tb. Th, trabecular thickness; Tb. Sp, trabecular spacing; Tt. Ar, total area; Ct. Ar, cortical area; Ct. Ar/Tt. Ar, cortical area / total area; Ct. Th, cortical thickness. (n= 6-7 male mice per genotype). (D) Representative TRAP staining of femurs of 2-month-old *Becn1*$^{WT/WT}$ and *Becn1*$^{LM/LM}$ mice.

(E) Whole body bone mineral density (BMD) of 1-year-old *Becn1*$^{WT/WT}$ and *Becn1*$^{LM/LM}$ mice (n=5 male mice per genotype).

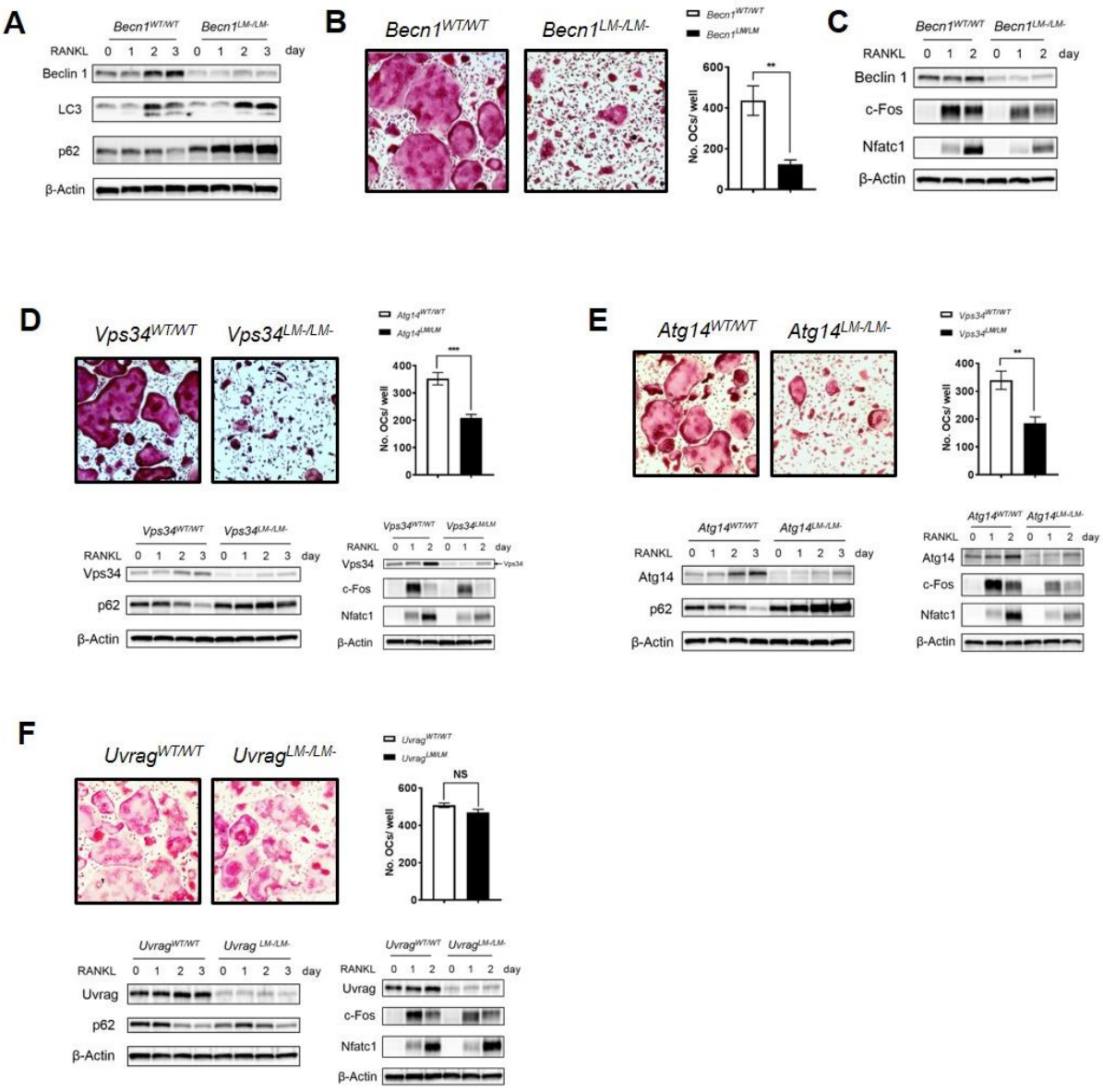

Figure 3.3 Differential requirements for PI3KC3 components during osteoclastogenesis *ex vivo*. (A) *Becn1*$^{WT/WT}$ and *Becn1*$^{LM/LM}$ BMMs were cultured under osteoclastogenic conditions, and Beclin-1 knockout efficacy and autophagic influx was assessed by immunobloting on days 0-3 post-RANKL treatment. Protein lysates were probed for Beclin-1, LC3 and p62. (B) (A) *Becn1*$^{WT/WT}$ and *Becn1*$^{LM/LM}$ BMMs were cultured under osteoclastogenic conditions, and osteoclast (OC) differentiation was assessed by quantification of the number of TRAP^{+} multinucleated (≥3 nuclei) cells on day 3 post-RANKL treatment. Representative images are

shown. (** $p < 0.01$, n = 5 wells). (C) Immunoblotting of c-Fos, and NFATc1 in *Becn1*$^{WT/WT}$ and *Becn1*$^{LM/LM}$ OC at days 0-2 of OC differentiation. (D) *Vps34*$^{WT/WT}$ and *Vps34*$^{LM/LM}$ BMMS were cultured under osteoclastogenic conditions, and OC differentiation the number of TRAP^{+} multinucleated (≥3 nuclei) cells on day 3 post-RANKL treatment (*** $p < 0.001$, n = 5 wells). Cell protein lysates were probed for VPS34 and p62 in *Vps34*$^{WT/WT}$ and *Vps34*$^{LM/LM}$ OC at days 0-3 of OC differentiation, and for c-Fos, and NFATc1 in *Vps34*$^{WT/WT}$ and *Vps34*$^{LM/LM}$ OC at days 0-2 of OC differentiation. (E) *Atg14*$^{WT/WT}$ and *Atg14*$^{LM/LM}$ BMMS were cultured under osteoclastogenic conditions, and OC differentiation the number of TRAP^{+} multinucleated (≥3 nuclei) cells on day 3 post-RANKL treatment (n = 5 wells). Cell protein lysates were probed for ATG14 and p62 in *Atg14*$^{WT/WT}$ and *Atg14*$^{LM/LM}$ OCs at days 0-3 of OC differentiation, and for c-Fos, and NFATc1 in *Atg14*$^{WT/WT}$ and *Atg14*$^{LM/LM}$ OCs at days 0-2 of OC differentiation. (F) *Uvrag*$^{WT/WT}$ and *Uvrag*$^{LM/LM}$ BMMS were cultured under osteoclastogenic conditions, and OC differentiation the number of TRAP^{+} multinucleated (≥3 nuclei) cells on day 3 post-RANKL treatment (NS = no significance, 0.0001, n = 5 wells). Cell protein lysates were probed for ATG14 and p62 in *Uvrag*$^{WT/WT}$ and *Uvrag*$^{LM/LM}$ OCs at days 0-3 of OC differentiation, and for c-Fos, and NFATc1 in *Uvrag*$^{WT/WT}$ and *Uvrag*$^{LM/LM}$ OCs at days 0-2 of OC differentiation.

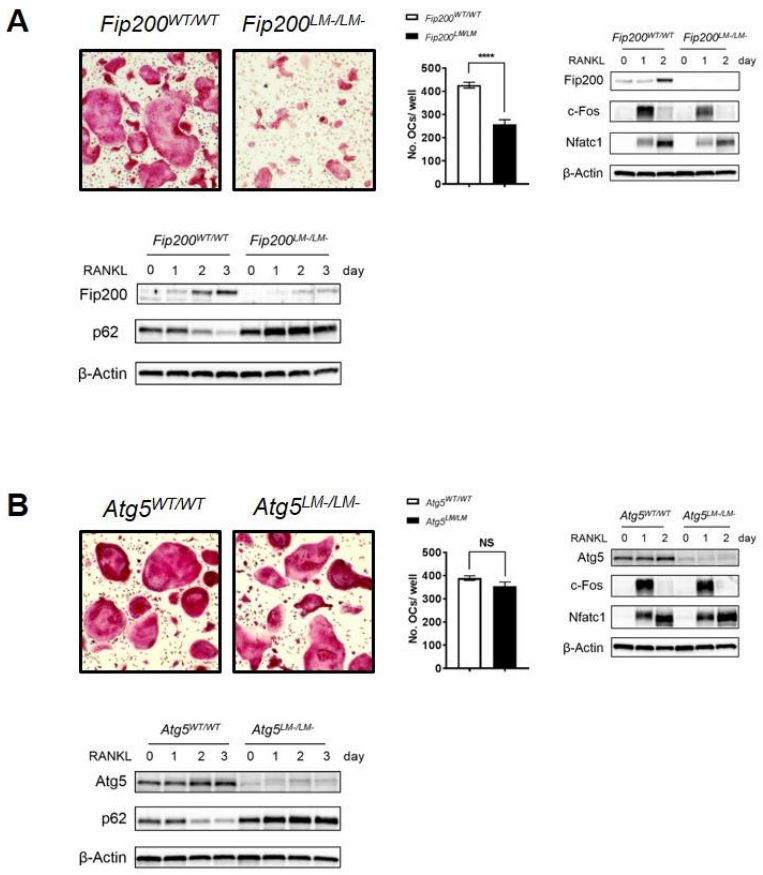

Figure 3.4 Differential requirements for autophagy components during osteoclastogenesis *ex vivo*. (A) *Fip200*$^{WT/WT}$ and *Fip200*$^{LM/LM}$ BMMS were cultured under osteoclastogenic conditions, and OC differentiation the number of TRAP^{+} multinucleated (≥3 nuclei) cells on day 3 post-RANKL treatment (**** $p < 0.0001$, n = 5 wells). Cell protein lysates were probed for FIP200 and p62 in *Fip200*$^{WT/WT}$ and *Fip200*$^{LM/LM}$ OCs at days 0-3 of OC differentiation, and for c-Fos, and NFATc1 in *Fip200*$^{WT/WT}$ and *Fip200*$^{LM/LM}$ OCs at days 0-2 of OC differentiation. (B) *Atg5*$^{WT/WT}$ and *Atg5*$^{LM/LM}$ BMMS were cultured under osteoclastogenic conditions, and OC differentiation the number of TRAP^{+} multinucleated (≥3 nuclei) cells on day 3 post-RANKL treatment (n = 5 wells). Cell protein lysates were probed for ATG5 and p62 in *Atg5*$^{WT/WT}$ and *Atg5*$^{LM/LM}$ OCs at days 0-3 of OC differentiation, and for c-Fos, and NFATc1 in *Atg5*$^{WT/WT}$ and *Atg5*$^{LM/LM}$ OCs at days 0-2 of OC differentiation.

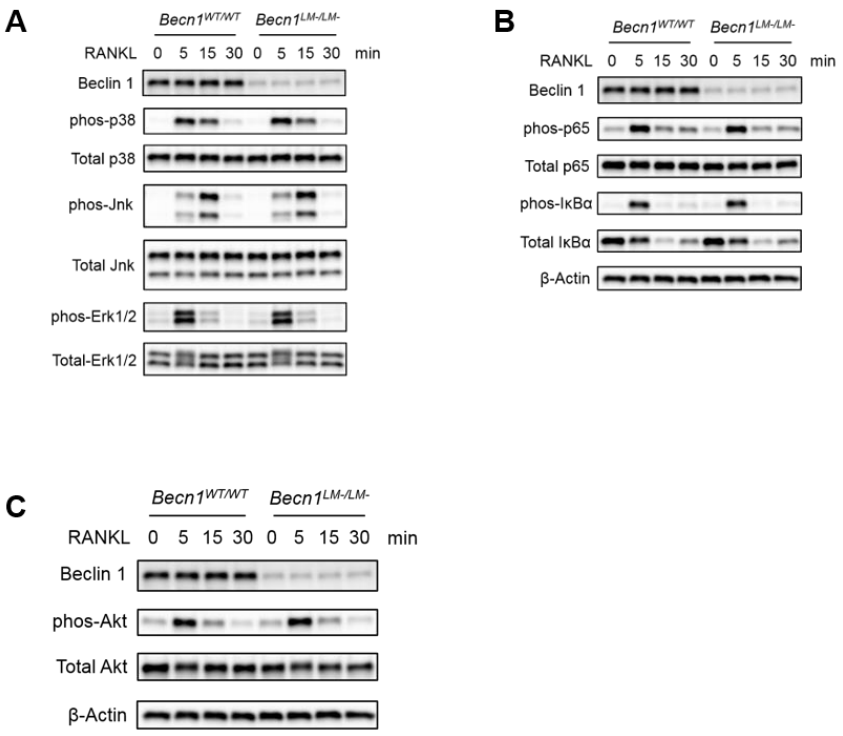

Figure 3.5 The absence of *Becn1* does not affect common osteoclastic signaling pathways in RANKL-treated BMMs. (A) Western blot of Beclin-1, phos-p38, Total p38, phos-JNK1/2, and total JNK1/2, phos-ERK1/2 and Total ERK1/2, in *Becn1*$^{WT/WT}$ and *Becn1*$^{LM/LM}$ OC precursors treated with RANKL from 0 to 30 minutes. (B) Western blot of phos-p65, Total p65, phos- IκBα, and total IκBα in *Becn1*$^{WT/WT}$ and *Becn1*$^{LM/LM}$ OC precursors treated with RANKL from 0 to 30 minutes. (C) Western blot of phos-Akt and Total Akt in *Becn1*$^{WT/WT}$ and *Becn1*$^{LM/LM}$ OC precursors treated with RANKL from 0 to 30 minutes.

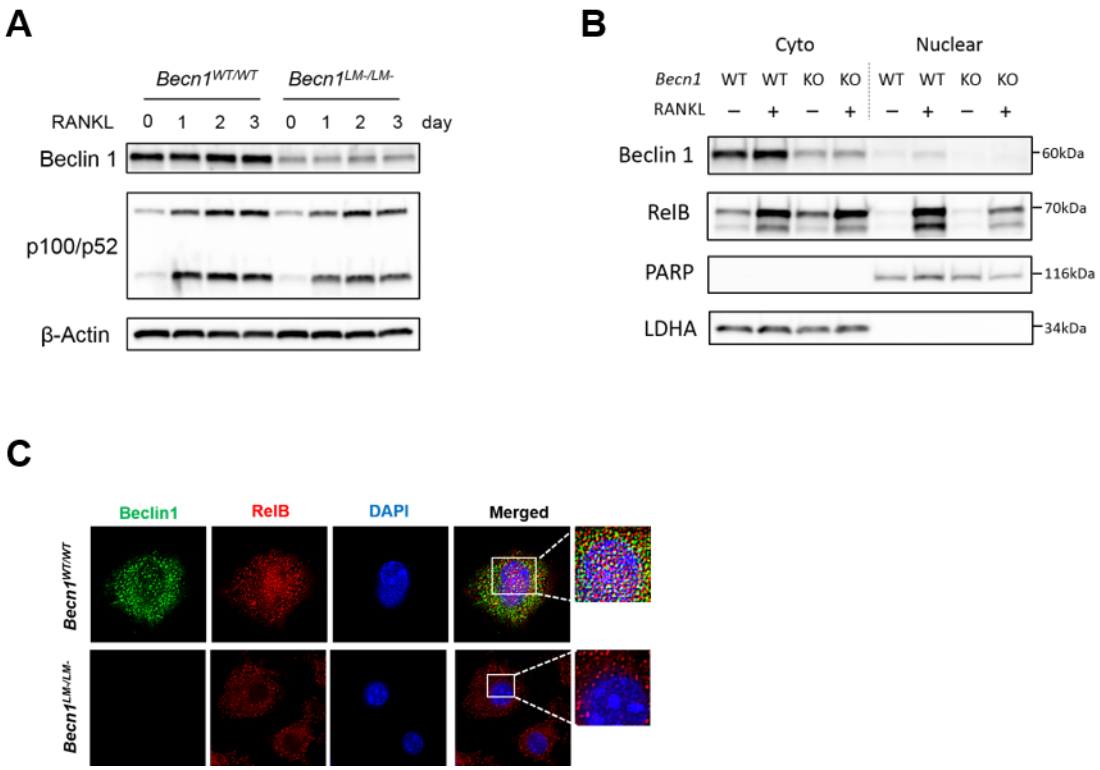

Figure 3.6 *Becn1*$^{LM/LM}$ osteoclasts display defects in non-canonical NF-κB responses. *Becn1*$^{WT/WT}$ and *Becn1*$^{LM/LM}$ OC precursors underwent osteoclastogenesis after RANKL treatment. (A) Total protein lysates were immunoblotted for p100/p52 to access non-canonical NF-κB activations. (B) Cytoplasmic (Cyto) and nuclear fractions were extracted from *Becn1*$^{WT/WT}$ and *Becn1*$^{LM/LM}$ OC precursors 1 day post-RANKL treatment. Cytoplasmic (Cyto) and nuclear levels of Beclin-1 and RelB are accessed by Western immunoblotting. LDHA was used as a cytoplasmic housekeeping and PARP was used as a nuclear housekeeping. (C) Immunofluorecent staining for the subcellular localization of Beclin-1 (green) and RelB in BMMs 1 day following RANKL stimulations. These cells were co-stained with DAPI (blue).

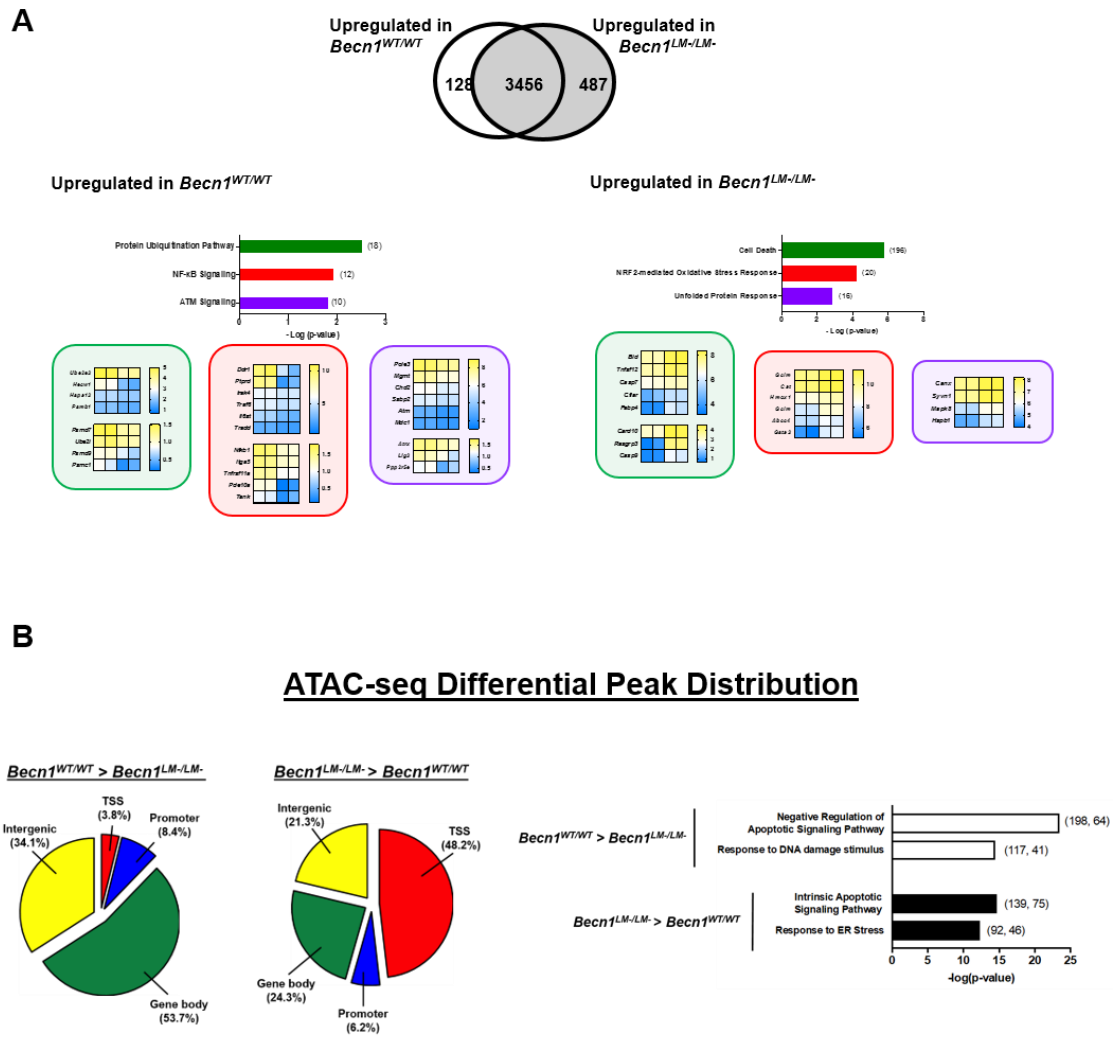

Figure 3.7 *Becn1*$^{LM/LM}$ osteoclasts display transcriptional profiles associated with unresolved DNA damage and cell death. (A) Microarray analysis of *Becn1*$^{WT/WT}$ and *Becn1*^{LM} OC on day 2 post-RANKL stimulation followed by gene set enrichment analyses. Alterations of signaling pathways were summarized by the Ingenuity Pathway Analysis TM software. Heat map representing of hierarchically clustered differentially expressed genes related to the biological pathways of biological duplicate samples of *Becn1*$^{WT/WT}$ and *Becn1*^{LM} OC. (B) Open chromatin assessments of *Becn1*$^{WT/WT}$ and *Becn1*^{LM} OC on day 2 post-RANKL stimulation using ATAC-Seq.

Comparison of the proportions of the ATAC-seq peak regions identified in *Becn1*$^{WT/WT}$ and *Becn1*^{LM} OCs that represent the various genome annotations. Significantly enriched genes of differentially accessible regions nearby genes from gene set enrichment analysis.

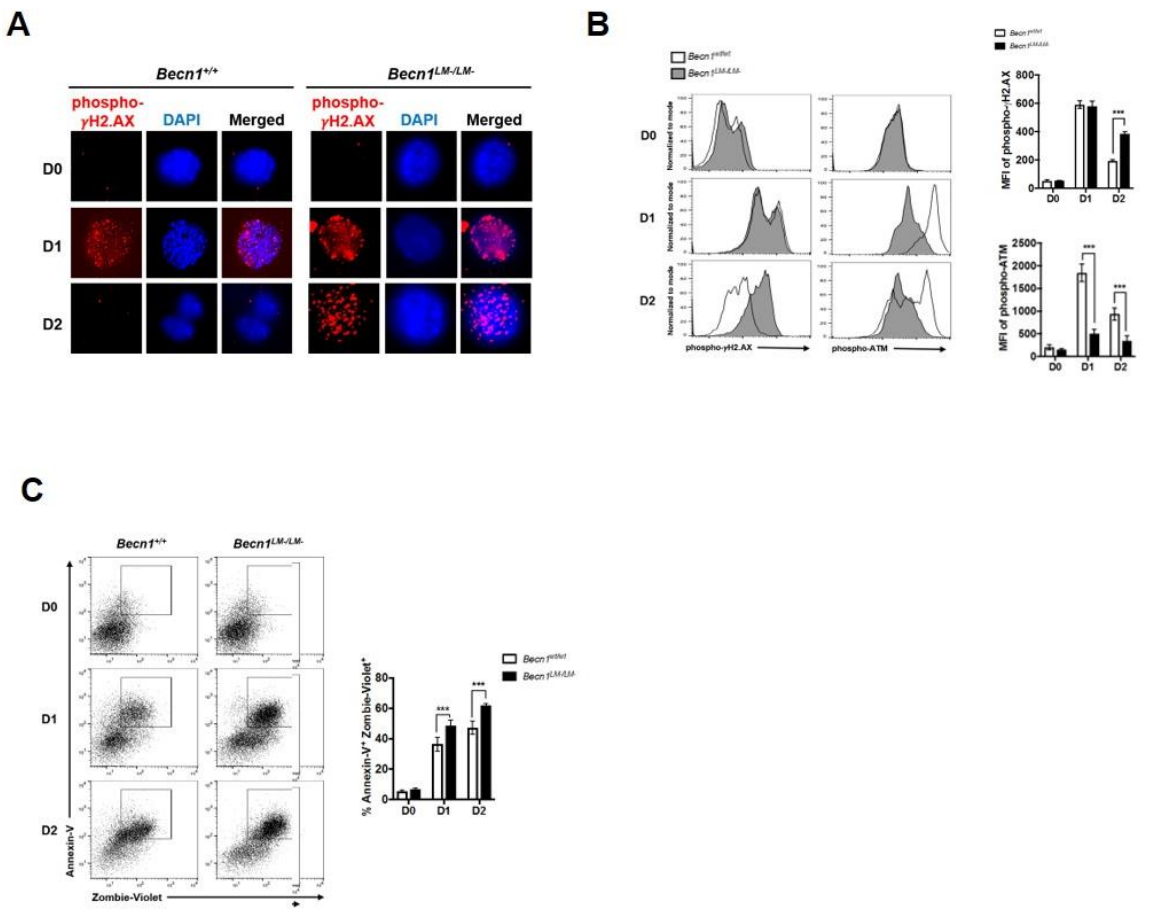

Figure 3.8 *Becn1*$^{LM/LM}$ osteoclasts display defects in DNA repair and an increase of cell death.

(A) Immunofluorescence staining of phospho-γH2.AX (red) and DAPI (blue) for *Becn1*$^{WT/WT}$ and *Becn1*$^{LM/LM}$ OC precursors with day 0-2 RANKL stimulations. (B) *Becn1*$^{WT/WT}$ and *Becn1*$^{LM/LM}$ OC precursors treated with RANKL. Adherent cells were harvested at 0, 1, and 2 days post-RANKL stimulation and were analyzed by cytometry of intracellular phospho-γH2 and phospho-ATM. (C) *Becn1*$^{WT/WT}$ and *Becn1*$^{LM/LM}$ OC precursors treated with RANKL and both non-adherent and adherent cells were harvested at 0, 1, and 2 days following RANKL stimulation and were analyzed for cell death by cytometry of Annexin V and Zombie-Red. Percentage of dead cells calculated percentage Annexin V and Zombie-Red double positive of CD45 positive cells.

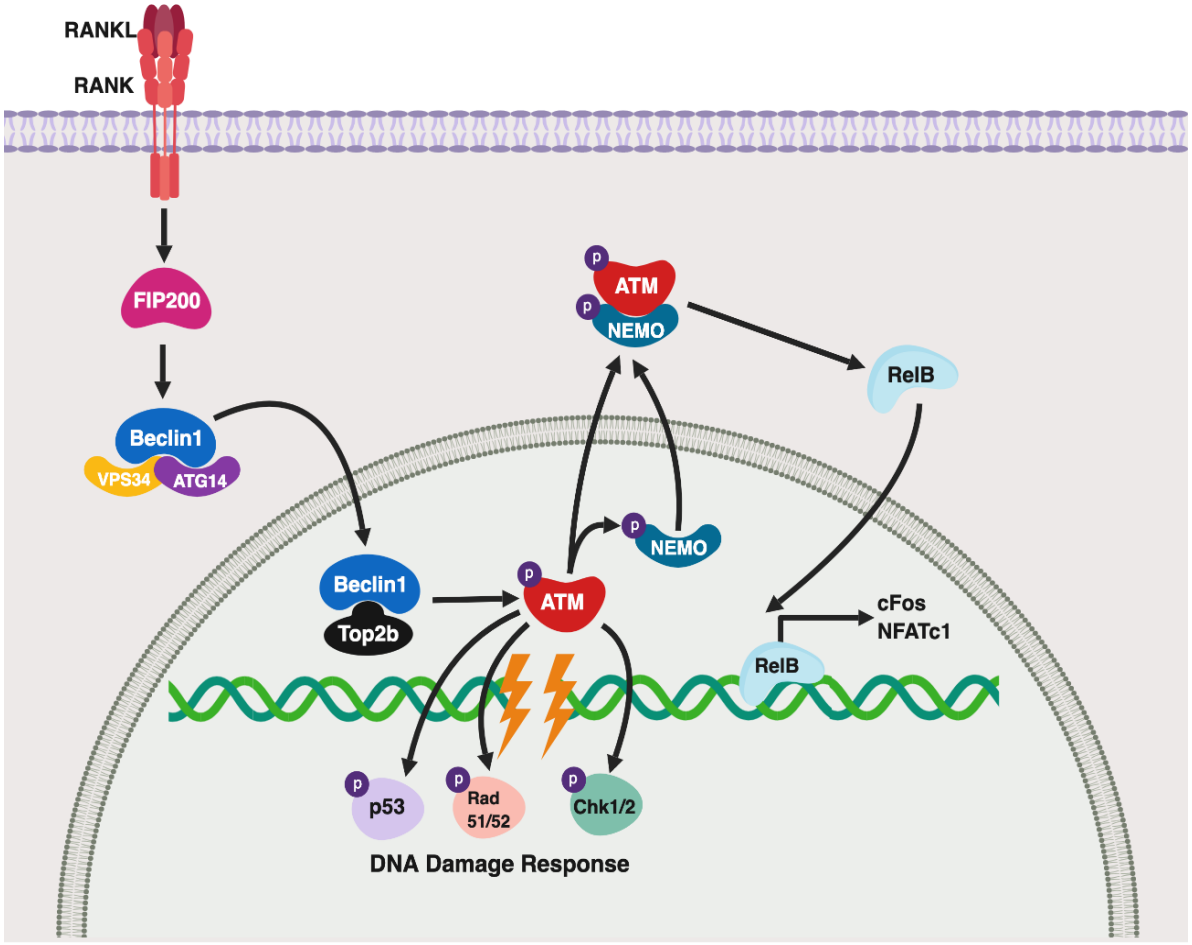

Figure 3.9 Schematic picture of the role of autophagy machinery in the regulation of osteoclast differentiation. The upstream core autophagy proteins, Fip200, Beclin-1, VPS34, and ATG14 are required for RANKL-induced osteoclastogenesis. During osteoclast differentiation, Beclin-1 is relocated to the nucleus to protect against DNA damage response, to promote cell survival and to augment nuclear mediated NF-κB responses.

CHAPTER 4: FUTURE DIRECTIONS

Osteoclast disease, such as Paget's disease of the bone and osteoporosis, is a group of disorder featured with imbalanced bone remodeling with a shift toward a net of bone loss caused by increased osteoclastogenesis. In this study, we uncovered the role of autophagy machinery in osteoclast differentiation and their implications in osteoclast disease pathogenesis comprehensively using a sophisticated osteoclast primary culture system and different strains of global and conditional autophagy gene knockout mice.

In the second chapter, we describe a novel and clinical relevant Paget's disease mouse model with global deficiency of the autophagy receptor OPTN. We also delineate the molecular mechanisms by which OPTN negatively regulates osteoclast differentiation, and identify IFNβ as a novel therapeutic target for PDB from *in vitro* rescue experiments. Though many experiments completed, more opening questions come up and require us to address in the future. While IFNβ recombinant protein could rescue the hyperactivated phenotype in OPTN deficient *osteoclasts in vitro*, can it prevent or treat the osteolytic lesions in OPTN global knockout mice *in vivo*? How does OPTN regulate RANKL-induced IFNβ production and mediate type I IFN response? Besides interferon signal, does OPTN modulate other signaling pathways to regulate osteoclastogensis?

In the third chapter, we elucidate the molecular mechanisms by which autophagy machinery mediates osteoclast development. We identify certain upstream autophagy components, including FIP200, Beclin-1, ATG14 and VPS34 are required for autophagic induction and the differentiation of osteoclasts. Intriguingly, the absence of ATG5 blocks autophagic induction in

osteoclasts but does not affect their differentiation, suggesting ATG5 deficient osteoclasts might employ an ATG5-independent alternative autophagy to complete the differentiation process. The ATG5-independent autophagy relies on Rab9 for autophagosome formation. While Rab9 has been shown highly expressed in the mature osteoclasts (Zhao et al. 2002), future study about its role in osteoclast differentiation is needed. While we have studied six different autophagy proteins in osteoclast differentiation, future studies should access if other upstream autophagy proteins, such as ULK1, ULK2 or ATG13 is involved in the osteoclastogeneis.

REFERENCES

Abu-Amer Y. 2013. Nf-kappab signaling and bone resorption. Osteoporos Int. 24(9):2377-2386.

Akinduro O, Sully K, Patel A, Robinson DJ, Chikh A, McPhail G, Braun KM, Philpott MP, Harwood CA, Byrne C et al. 2016. Constitutive autophagy and nucleophagy during epidermal differentiation. J Invest Dermatol. 136(7):1460-1470.

Al Nofal AA, Altayar O, BenKhadra K, Qasim Agha OQ, Asi N, Nabhan M, Prokop LJ, Tebben P, Murad MH. 2015. Bone turnover markers in paget's disease of the bone: A systematic review and meta-analysis. Osteoporos Int. 26(7):1875-1891.

Albagha OM. 2015. Genetics of paget's disease of bone. Bonekey Rep. 4:756.

Albagha OM, Visconti MR, Alonso N, Langston AL, Cundy T, Dargie R, Dunlop MG, Fraser WD, Hooper MJ, Isaia G et al. 2010. Genome-wide association study identifies variants at csf1, optn and tnfrsf11a as genetic risk factors for paget's disease of bone. Nature genetics. 42(6):520-524.

Alexander DE, Leib DA. 2008. Xenophagy in herpes simplex virus replication and pathogenesis. Autophagy. 4(1):101-103.

Altman RD, Bloch DA, Hochberg MC, Murphy WA. 2000. Prevalence of pelvic paget's disease of bone in the united states. J Bone Miner Res. 15(3):461-465.

Anderson DM, Maraskovsky E, Billingsley WL, Dougall WC, Tometsko ME, Roux ER, Teepe MC, DuBose RF, Cosman D, Galibert L. 1997. A homologue of the tnf receptor and its ligand enhance t-cell growth and dendritic-cell function. Nature. 390(6656):175-179.

Asagiri M, Sato K, Usami T, Ochi S, Nishina H, Yoshida H, Morita I, Wagner EF, Mak TW, Serfling E et al. 2005. Autoamplification of nfatc1 expression determines its essential role in bone homeostasis. Journal of Experimental Medicine. 202(9):1261-1269.

Bernard M, Dieude M, Yang B, Hamelin K, Underwood K, Hebert MJ. 2014. Autophagy fosters myofibroblast differentiation through mtorc2 activation and downstream upregulation of ctgf. Autophagy. 10(12):2193-2207.

Bilezikian JP. 2019. Primer on the metabolic bone diseases and disorders of mineral metabolism. Hoboken, NJ: Wiley-Blackwell.

Burman C, Ktistakis NT. 2010. Regulation of autophagy by phosphatidylinositol 3-phosphate. FEBS Lett. 584(7):1302-1312.

Cao HL, Yu SB, Yao Z, Galson DL, Jiang Y, Zhang XY, Fan J, Lu BF, Guan YF, Luo M et al. 2010. Activating transcription factor 4 regulates osteoclast differentiation in mice. Journal of Clinical Investigation. 120(8):2755-2766.

Chalasani ML, Radha V, Gupta V, Agarwal N, Balasubramanian D, Swarup G. 2007. A glaucoma-associated mutant of optineurin selectively induces death of retinal ganglion cells which is inhibited by antioxidants. Invest Ophthalmol Vis Sci. 48(4):1607-1614.

Chibalina MV, Poliakov A, Kendrick-Jones J, Buss F. 2010. Myosin vi and optineurin are required for polarized egfr delivery and directed migration. Traffic. 11(10):1290-1303.

Chibalina MV, Roberts RC, Arden SD, Kendrick-Jones J, Buss F. 2008. Rab8-optineurin-myosin vi: Analysis of interactions and functions in the secretory pathway. Methods Enzymol. 438:11-24.

Chung PY, Beyens G, Boonen S, Papapoulos S, Geusens P, Karperien M, Vanhoenacker F, Verbruggen L, Fransen E, Van Offel J et al. 2010. The majority of the genetic risk for paget's disease of bone is explained by genetic variants close to the csf1, optn, tm7sf4, and tnfrsf11a genes. Human genetics. 128(6):615-626.

Chung YH, Jang Y, Choi B, Song DH, Lee EJ, Kim SM, Song Y, Kang SW, Yoon SY, Chang EJ. 2014. Beclin-1 is required for rankl-induced osteoclast differentiation. J Cell Physiol. 229(12):1963-1971.

Clarke AJ, Simon AK. 2019. Autophagy in the renewal, differentiation and homeostasis of immune cells. Nature Reviews Immunology. 19(3):170-183.

Comb WC, Cogswell P, Sitcheran R, Baldwin AS. 2011. Ikk-dependent, nf-kappa b-independent control of autophagic gene expression. Oncogene. 30(14):1727-1732.

Darnay BG, Haridas V, Ni J, Moore PA, Aggarwal BB. 1998. Characterization of the intracellular domain of receptor activator of nf-kappa b (rank) - interaction with tumor necrosis factor receptor-associated factors and activation of nf-kappa b and c-jun n-terminal kinase. Journal of Biological Chemistry. 273(32):20551-20555.

David JP, Sabapathy K, Hoffmann O, Idarraga MH, Wagner EF. 2002. Jnk1 modulates osteoclastogenesis through both c-jun phosphorylation-dependent and -independent mechanisms. Journal of Cell Science. 115(22):4317-4325.

De Duve C, Wattiaux R. 1966. Functions of lysosomes. Annu Rev Physiol. 28:435-492.

Deosaran E, Larsen KB, Hua R, Sargent G, Wang YQ, Kim S, Lamark T, Jauregui M, Law K, Lippincott-Schwartz J et al. 2013. Nbr1 acts as an autophagy receptor for peroxisomes. Journal of Cell Science. 126(4):939-952.

DeSelm CJ, Miller BC, Zou W, Beatty WL, van Meel H, Takahata Y, Klumperman J, Tooze SA, Teitelbaum SL, Virgin HW. 2011. Autophagy proteins regulate the secretory component of osteoclastic bone resorption. Dev Cell. 21(5):966-974.

Dillon CP, Weinlich R, Rodriguez DA, Cripps JG, Quarato G, Gurung P, Verbist KC, Brewer TL, Llambi F, Gong YN et al. 2014. Ripk1 blocks early postnatal lethality mediated by caspase-8 and ripk3. Cell. 157(5):1189-1202.

Eghbali-Fatourechi G, Khosla S, Sanyal A, Boyle WJ, Lacey DL, Riggs BL. 2003. Role of rank ligand in mediating increased bone resorption in early postmenopausal women. Journal of Clinical Investigation. 111(8):1221-1230.

Garnero P, SornayRendu E, Chapuy MC, Delmas PD. 1996. Increased bone turnover in late postmenopausal women is a major determinant of osteoporosis. Journal of Bone and Mineral Research. 11(3):337-349.

Grigoriadis AE, Wang ZQ, Cecchini MG, Hofstetter W, Felix R, Fleisch HA, Wagner EF. 1994. C-fos - a key regulator of osteoclast-macrophage lineage determination and bone remodeling. Science. 266(5184):443-448.

Hanada R, Hanada T, Sigl V, Schramek D, Penninger JM. 2011. Rankl/rank-beyond bones. J Mol Med (Berl). 89(7):647-656.

Hayman AR, Jones SJ, Boyde A, Foster D, Colledge WH, Carlton MB, Evans MJ, Cox TM. 1996. Mice lacking tartrate-resistant acid phosphatase (acp 5) have disrupted endochondral ossification and mild osteopetrosis. Development. 122(10):3151-3162.

Herbert BA, Valerio MS, Gaestel M, Kirkwood KL. 2015. Sexual dimorphism in mapk-activated protein kinase-2 (mk2) regulation of rankl-induced osteoclastogenesis in osteoclast progenitor subpopulations. PLoS One. 10(5):e0125387.

Hofbauer LC, Khosla S, Dunstan CR, Lacey DL, Spelsberg TC, Riggs BL. 1999. Estrogen stimulates gene expression and protein production of osteoprotegerin in human osteoblastic cells. Endocrinology. 140(9):4367-4370.

Iotsova V, Caamano J, Loy J, Yang Y, Lewin A, Bravo R. 1997. Osteopetrosis in mice lacking nf-kappa b1 and nf-kappa b2. Nature Medicine. 3(11):1285-1289.

Itakura E, Kishi C, Inoue K, Mizushima N. 2008. Beclin 1 forms two distinct phosphatidylinositol 3-kinase complexes with mammalian atg14 and uvrag. Mol Biol Cell. 19(12):5360-5372.

Ito Y, Ofengeim D, Najafov A, Das S, Saberi S, Li Y, Hitomi J, Zhu H, Chen H, Mayo L et al. 2016. Ripk1 mediates axonal degeneration by promoting inflammation and necroptosis in als. Science. 353(6299):603-608.

Ivashkiv LB, Donlin LT. 2014. Regulation of type i interferon responses. Nat Rev Immunol. 14(1):36-49.

Jaco I, Annibaldi A, Lalaoui N, Wilson R, Tenev T, Laurien L, Kim C, Jamal K, Wicky John S, Liccardi G et al. 2017. Mk2 phosphorylates ripk1 to prevent tnf-induced cell death. Mol Cell. 66(5):698-710 e695.

Johnell O, Kanis JA. 2006. An estimate of the worldwide prevalence and disability associated with osteoporotic fractures. Osteoporos Int. 17(12):1726-1733.

Kanis JA, Alexeeva L, Bonjour JP, Burkhardt P, Christiansen C, Cooper C, Delmas P, Johnell O, Johnston C, Kanis JA et al. 1994. Assessment of fracture risk and its application to screening for postmenopausal osteoporosis - synopsis of a who report. Osteoporosis Int. 4(6):368-381.

Khosla S, Atkinson EJ, Melton LJ, Riggs BL. 1997. Effects of age and estrogen status on serum parathyroid hormone levels and biochemical markers of bone turnover in women: A population-based study. J Clin Endocr Metab. 82(5):1522-1527.

Khosla S, Melton LJ, 3rd, Atkinson EJ, O'Fallon WM, Klee GG, Riggs BL. 1998. Relationship of serum sex steroid levels and bone turnover markers with bone mineral density in men and women: A key role for bioavailable estrogen. J Clin Endocrinol Metab. 83(7):2266-2274.

Khosla S, Riggs BL. 2005. Pathophysiology of age-related bone loss and osteoporosis. Endocrin Metab Clin. 34(4):1015-+.

Kim YM, Jung CH, Seo M, Kim EK, Park JM, Bae SS, Kim DH. 2015. Mtorc1 phosphorylates uvrag to negatively regulate autophagosome and endosome maturation. Mol Cell. 57(2):207-218.

Krebs DL, Hilton DJ. 2000. Socs: Physiological suppressors of cytokine signaling. J Cell Sci. 113 (Pt 16):2813-2819.

Kukita A, Chenu C, McManus LM, Mundy GR, Roodman GD. 1990. Atypical multinucleated cells form in long-term marrow cultures from patients with paget's disease. J Clin Invest. 85(4):1280-1286.

Kurihara N, Zhou H, Reddy SV, Garcia Palacios V, Subler MA, Dempster DW, Windle JJ, Roodman GD. 2006. Expression of measles virus nucleocapsid protein in osteoclasts induces paget's disease-like bone lesions in mice. J Bone Miner Res. 21(3):446-455.

Lamark T, Kirkin V, Dikic I, Johansen T. 2009. Nbr1 and p62 as cargo receptors for selective autophagy of ubiquitinated targets. Cell Cycle. 8(13):1986-1990.

Lamothe B, Lai YJ, Hur L, Orozco NM, Wang J, Campos AD, Xie M, Schneider MD, Lockworth CR, Jakacky J et al. 2012. Deletion of tak1 in the myeloid lineage results in the spontaneous development of myelomonocytic leukemia in mice. PloS one. 7(12).

Lazarou M, Sliter DA, Kane LA, Sarraf SA, Wang C, Burman JL, Sideris DP, Fogel AI, Youle RJ. 2015. The ubiquitin kinase pink1 recruits autophagy receptors to induce mitophagy. Nature. 524(7565):309-314.

Lee DJ, Tseng HC, Wong SW, Wang Z, Deng M, Ko CC. 2015. Dopaminergic effects on in vitro osteogenesis. Bone Res. 3:15020.

Lee SH, Rho J, Jeong D, Sul JY, Kim T, Kim N, Kang JS, Miyamoto T, Suda T, Lee SK et al. 2006. V-atpase v-0 subunit d2-deficient mice exhibit impaired osteoclast fusion and increased bone formation. Nature Medicine. 12(12):1403-1409.

Lehtonen A, Matikainen S, Julkunen I. 1997. Interferons up-regulate stat1, stat2, and irf family transcription factor gene expression in human peripheral blood mononuclear cells and macrophages. J Immunol. 159(2):794-803.

Li XT, Udagawa N, Itoh K, Suda K, Murase Y, Nishihara T, Suda T, Takahashi N. 2002. P38 mapk-mediated signals are required for inducing osteoclast differentiation but not for osteoclast function. Endocrinology. 143(8):3105-3113.

Liang C, Feng P, Ku B, Dotan I, Canaani D, Oh BH, Jung JU. 2006. Autophagic and tumour suppressor activity of a novel beclin1-binding protein uvrag. Nat Cell Biol. 8(7):688-699.

Liang C, Lee JS, Inn KS, Gack MU, Li Q, Roberts EA, Vergne I, Deretic V, Feng P, Akazawa C et al. 2008. Beclin1-binding uvrag targets the class c vps complex to coordinate autophagosome maturation and endocytic trafficking. Nat Cell Biol. 10(7):776-787.

Lin NY, Beyer C, Giessl A, Kireva T, Scholtysek C, Uderhardt S, Munoz LE, Dees C, Distler A, Wirtz S et al. 2013. Autophagy regulates tnfalpha-mediated joint destruction in experimental arthritis. Ann Rheum Dis. 72(5):761-768.

Liu F, Fang F, Yuan HB, Yang DY, Chen YQ, Williams L, Goldstein SA, Krebsbach PH, Guan JL. 2013. Suppression of autophagy by fip200 deletion leads to osteopenia in mice through the inhibition of osteoblast terminal differentiation. Journal of Bone and Mineral Research. 28(11):2414-2430.

Mao K, Klionsky DJ. 2017. Xenophagy: A battlefield between host and microbe, and a possible avenue for cancer treatment. Autophagy. 13(2):223-224.

Martinez J, Malireddi RK, Lu Q, Cunha LD, Pelletier S, Gingras S, Orchard R, Guan JL, Tan H, Peng J et al. 2015. Molecular characterization of lc3-associated phagocytosis reveals distinct roles for rubicon, nox2 and autophagy proteins. Nat Cell Biol. 17(7):893-906.

Maruyama K, Fukasaka M, Vandenbon A, Saitoh T, Kawasaki T, Kondo T, Yokoyama KK, Kidoya H, Takakura N, Standley D et al. 2012. The transcription factor jdp2 controls bone homeostasis and antibacterial immunity by regulating osteoclast and neutrophil differentiation. Immunity. 37(6):1024-1036.

Matsunaga K, Saitoh T, Tabata K, Omori H, Satoh T, Kurotori N, Maejima I, Shirahama-Noda K, Ichimura T, Isobe T et al. 2009. Two beclin 1-binding proteins, atg14l and rubicon, reciprocally regulate autophagy at different stages. Nature Cell Biology. 11(4):385-U369.

McHugh KP, Hodivala-Dilke K, Zheng MH, Namba N, Lam J, Novack D, Feng X, Ross FP, Hynes RO, Teitelbaum SL. 2000. Mice lacking beta 3 integrins are osteosclerotic because of dysfunctional osteoclasts. Journal of Clinical Investigation. 105(4):433-440.

Meena NP, Zhu G, Mittelstadt PR, Giardino Torchia ML, Pourcelot M, Arnoult D, Ashwell JD, Munitic I. 2016. The tbk1-binding domain of optineurin promotes type i interferon responses. FEBS Lett. 590(10):1498-1508.

Menaa C, Reddy SV, Kurihara N, Maeda H, Anderson D, Cundy T, Cornish J, Singer FR, Bruder JM, Roodman GD. 2000. Enhanced rank ligand expression and responsivity of bone marrow cells in paget's disease of bone. J Clin Invest. 105(12):1833-1838.

Miyamoto H, Suzuki T, Miyauchi Y, Iwasaki R, Kobayashi T, Sato Y, Miyamoto K, Hoshi H, Hashimoto K, Yoshida S et al. 2012. Osteoclast stimulatory transmembrane protein and dendritic cell-specific transmembrane protein cooperatively modulate cell-cell fusion to form osteoclasts and foreign body giant cells. J Bone Miner Res. 27(6):1289-1297.

Miyamoto S. 2011. Nuclear initiated nf-kappab signaling: Nemo and atm take center stage. Cell research. 21(1):116-130.

Miyauchi Y, Ninomiya K, Miyamoto H, Sakamoto A, Iwasaki R, Hoshi H, Miyamoto K, Hao W, Yoshida S, Morioka H et al. 2010. The blimp1-bcl6 axis is critical to regulate osteoclast differentiation and bone homeostasis. Journal of Experimental Medicine. 207(4):751-762.

Mizukami J, Takaesu G, Akatsuka H, Sakurai H, Ninomiya-Tsuji J, Matsumoto K, Sakurai N. 2002. Receptor activator of nf-kappa b ligand (rankl) activates tak1 mitogen-activated protein kinase kinase kinase through a signaling complex containing rank, tab2, and traf6. Molecular and cellular biology. 22(4):992-1000.

Mizushima N, Levine B. 2010. Autophagy in mammalian development and differentiation. Nat Cell Biol. 12(9):823-830.

Morissette J, Laurin N, Brown JP. 2006. Sequestosome 1: Mutation frequencies, haplotypes, and phenotypes in familial paget's disease of bone. J Bone Miner Res. 21 Suppl 2:P38-44.

Munch C, Dikic I. 2018. Hitchhiking on selective autophagy. Nat Cell Biol. 20(2):122-124.

Munitic I, Giardino Torchia ML, Meena NP, Zhu G, Li CC, Ashwell JD. 2013. Optineurin insufficiency impairs irf3 but not nf-kappab activation in immune cells. J Immunol. 191(12):6231-6240.

Naito A, Azuma S, Tanaka S, Miyazaki T, Takaki S, Takatsu K, Nakao K, Nakamura K, Katsuki M, Yamamoto T et al. 1999. Severe osteopetrosis, defective interleukin-1 signalling and lymph node organogenesis in traf6-deficient mice. Genes Cells. 4(6):353-362.

Nishida Y, Arakawa S, Fujitani K, Yamaguchi H, Mizuta T, Kanaseki T, Komatsu M, Otsu K, Tsujimoto Y, Shimizu S. 2009. Discovery of atg5/atg7-independent alternative macroautophagy. Nature. 461(7264):654-U699.

Nollet M, Santucci-Darmanin S, Breuil V, Al-Sahlanee R, Cros C, Topi M, Momier D, Samson M, Pagnotta S, Cailleteau L et al. 2014. Autophagy in osteoblasts is involved in mineralization and bone homeostasis. Autophagy. 10(11):1965-1977.

Obaid R, Wani SE, Azfer A, Hurd T, Jones R, Cohen P, Ralston SH, Albagha OME. 2015. Optineurin negatively regulates osteoclast differentiation by modulating nf-kappab and interferon signaling: Implications for paget's disease. Cell Rep. 13(6):1096-1102.

Okamoto K, Nakashima T, Shinohara M, Negishi-Koga T, Komatsu N, Terashima A, Sawa S, Nitta T, Takayanagi H. 2017. Osteoimmunology: The conceptual framework unifying the immune and skeletal systems. Physiol Rev. 97(4):1295-1349.

Padman BS, Nguyen TN, Uoselis L, Skulsuppaisarn M, Nguyen LK, Lazarou M. 2019. Lc3/gabaraps drive ubiquitin-independent recruitment of optineurin and ndp52 to amplify mitophagy. Nat Commun. 10(1):408.

Peck WA, Burckhardt P, Christiansen C, Fleisch HA, Genant HK, Gennari C, Martin TJ, Martini L, Morita R, Ogata E et al. 1993. Consensus development conference - diagnosis, prophylaxis, and treatment of osteoporosis. Am J Med. 94(6):646-650.

Ralston SH, Albagha OM. 2014. Genetics of paget's disease of bone. Current osteoporosis reports. 12(3):263-271.

Rebel A, Basle M, Pouplard A, Malkani K, Filmon R, Lepatezour A. 1980. Bone tissue in paget's disease of bone. Ultrastructure and immunocytology. Arthritis Rheum. 23(10):1104-1114.

Rebel A, Malkani K, Basle M, Bregeon C. 1976. Osteoclast ultrastructure in paget's disease. Calcif Tissue Res. (2):187-199.

Richter B, Sliter DA, Herhaus L, Stolz A, Wang CX, Beli P, Zaffagnini G, Wild P, Martens S, Wagner SA et al. 2016. Phosphorylation of optn by tbk1 enhances its binding to ub chains and promotes selective autophagy of damaged mitochondria. P Natl Acad Sci USA. 113(15):4039-4044.

Riggs BL, Khosla S, Melton LJ. 1998. A unitary model for involutional osteoporosis: Estrogen deficiency causes both type i and type ii osteoporosis in postmenopausal women and contributes to bone loss in aging men. Journal of Bone and Mineral Research. 13(5):763-773.

Roodman GD, Windle JJ. 2005. Paget disease of bone. J Clin Invest. 115(2):200-208.

Saftig P, Hunziker E, Wehmeyer O, Jones S, Boyde A, Rommerskirch W, Moritz JD, Schu P, von Figura K. 1998. Impaired osteoclastic bone resorption leads to osteopetrosis in cathepsin-k-deficient mice. P Natl Acad Sci USA. 95(23):13453-13458.

Sato K, Suematsu A, Nakashima T, Takemoto-Kimura S, Aoki K, Morishita Y, Asahara H, Ohya K, Yamaguchi A, Takai T et al. 2006. Regulation of osteoclast differentiation and function by the camk-creb pathway. Nat Med. 12(12):1410-1416.

Sil P, Wong SW, Martinez J. 2018. More than skin deep: Autophagy is vital for skin barrier function. Frontiers in Immunology. 9.

Singer FR. 2015. Paget's disease of bone-genetic and environmental factors. Nat Rev Endocrinol. 11(11):662-671.

Singer FR, Mills BG, Gruber HE, Windle JJ, Roodman GD. 2006. Ultrastructure of bone cells in paget's disease of bone. J Bone Miner Res. 21 Suppl 2:P51-54.

Slowicka K, Vereecke L, Mc Guire C, Sze M, Maelfait J, Kolpe A, Saelens X, Beyaert R, van Loo G. 2016a. Optineurin deficiency in mice is associated with increased sensitivity to salmonella but does not affect proinflammatory nf-kappab signaling. Eur J Immunol. 46(4):971-980.

Slowicka K, Vereecke L, van Loo G. 2016b. Cellular functions of optineurin in health and disease. Trends Immunol. 37(9):621-633.

Song Z, An L, Ye Y, Wu J, Zou Y, He L, Zhu H. 2014. Essential role for uvrag in autophagy and maintenance of cardiac function. Cardiovasc Res. 101(1):48-56.

Suda T, Takahashi N, Udagawa N, Jimi E, Gillespie MT, Martin TJ. 1999. Modulation of osteoclast differentiation and function by the new members of the tumor necrosis factor receptor and ligand families. Endocr Rev. 20(3):345-357.

Sun Q, Zhang J, Fan W, Wong KN, Ding X, Chen S, Zhong Q. 2011. The run domain of rubicon is important for hvps34 binding, lipid kinase inhibition, and autophagy suppression. The Journal of biological chemistry. 286(1):185-191.

Sundaram K, Shanmugarajan S, Rao DS, Reddy SV. 2011. Mutant p62p392l stimulation of osteoclast differentiation in paget's disease of bone. Endocrinology. 152(11):4180-4189.

Swarnkar G, Karuppaiah K, Mbalaviele G, Chen T, Abu-Amer Y. 2015. Osteopetrosis in tak1-deficient mice owing to defective nf-kappa b and notch signaling. P Natl Acad Sci USA. 112(1):154-159.

Swarnkar G, Shim K, Nasir AM, Seehra K, Chen HP, Mbalaviele G, Abu-Amer Y. 2016. Myeloid deletion of nemo causes osteopetrosis in mice owing to upregulation of transcriptional repressors. Sci Rep-Uk. 6.

Takayanagi H, Kim S, Koga T, Nishina H, Isshiki M, Yoshida H, Saiura A, Isobe M, Yokochi T, Inoue J et al. 2002a. Induction and activation of the transcription factor nfatc1 (nfat2) integrate rankl signaling in terminal differentiation of osteoclasts. Dev Cell. 3(6):889-901.

Takayanagi H, Kim S, Matsuo K, Suzuki H, Suzuki T, Sato K, Yokochi T, Oda H, Nakamura K, Ida N et al. 2002b. Rankl maintains bone homeostasis through c-fos-dependent induction of interferon-beta. Nature. 416(6882):744-749.

Takeshige K, Baba M, Tsuboi S, Noda T, Ohsumi Y. 1992. Autophagy in yeast demonstrated with proteinase-deficient mutants and conditions for its induction. J Cell Biol. 119(2):301-311.

Teramachi J, Nagata Y, Mohammad K, Inagaki Y, Ohata Y, Guise T, Michou L, Brown JP, Windle JJ, Kurihara N et al. 2016. Measles virus nucleocapsid protein increases osteoblast differentiation in paget's disease. J Clin Invest. 126(3):1012-1022.

Teramachi J, Zhou H, Subler MA, Kitagawa Y, Galson DL, Dempster DW, Windle JJ, Kurihara N, Roodman GD. 2014. Increased il-6 expression in osteoclasts is necessary but not sufficient for the development of paget's disease of bone. J Bone Miner Res. 29(6):1456-1465.

Theill LE, Boyle WJ, Penninger JM. 2002. Rank-l and rank: T cells, bone loss, and mammalian evolution. Annu Rev Immunol. 20:795-823.

Toth RP, Atkin JD. 2018. Dysfunction of optineurin in amyotrophic lateral sclerosis and glaucoma. Front Immunol. 9:1017.

Tseng HC, Riday TT, McKee C, Braine CE, Bomze H, Barak I, Marean-Reardon C, John SW, Philpot BD, Ehlers MD. 2015. Visual impairment in an optineurin mouse model of primary open-angle glaucoma. Neurobiol Aging. 36(6):2201-2212.

Tsuji-Takechi K, Negishi-Koga T, Sumiya E, Kukita A, Kato S, Maeda T, Pandolfi PP, Moriyama K, Takayanagi H. 2012. Stage-specific functions of leukemia/lymphoma-related factor (lrf) in the transcriptional control of osteoclast development. P Natl Acad Sci USA. 109(7):2561-2566.

Viret C, Rozieres A, Faure M. 2018. Novel insights into ndp52 autophagy receptor functioning. Trends Cell Biol. 28(4):255-257.

Wan YH, Chong LW, Evans RM. 2007. Ppar-gamma regulates osteoclastogenesis in mice. Nature Medicine. 13(12):1496-1503.

Whang MI, Tavares RM, Benjamin DI, Kattah MG, Advincula R, Nomura DK, Debnath J, Malynn BA, Ma A. 2017. The ubiquitin binding protein tax1bp1 mediates autophagasome induction and the metabolic transition of activated t cells. Immunity. 46(3):405-420.

Wong SW, Sil P, Martinez J. 2018. Rubicon: Lc3-associated phagocytosis and beyond. Febs Journal. 285(8):1379-1388.

Xiu Y, Xu H, Zhao C, Li J, Morita Y, Yao Z, Xing L, Boyce BF. 2014a. Chloroquine reduces osteoclastogenesis in murine osteoporosis by preventing traf3 degradation. J Clin Invest. 124(1):297-310.

Xiu Y, Xu H, Zhao C, Li JB, Morita Y, Yao ZQ, Xing LP, Boyce BF. 2014b. Chloroquine reduces osteoclastogenesis in murine osteoporosis by preventing traf3 degradation. Journal of Clinical Investigation. 124(1):297-310.

Yagi M, Miyamoto T, Sawatani Y, Iwamoto K, Hosogane N, Fujita N, Morita K, Ninomiya K, Suzuki T, Miyamoto K et al. 2005. Dc-stamp is essential for cell-cell fusion in osteoclasts and foreign body giant cells. Journal of Experimental Medicine. 202(3):345-351.

Yamashita T, Yao ZQ, Li F, Zhang Q, Badell IR, Schwarz EM, Takeshita S, Wagner EF, Noda M, Matsuo K et al. 2007. Nf-kappa b p50 and p52 regulate receptor activator of nf-kappa b ligand (rankl) and tumor necrosis factor-induced osteoclast precursor differentiation by activating c-fos and nfatc1. Journal of Biological Chemistry. 282(25):18245-18253.

Zhang L, Guo YF, Liu YZ, Liu YJ, Xiong DH, Liu XG, Wang L, Yang TL, Lei SF, Guo Y et al. 2010. Pathway-based genome-wide association analysis identified the importance of regulation-of-autophagy pathway for ultradistal radius bmd. J Bone Miner Res. 25(7):1572-1580.

Zhao HB, Ettala O, Vaananen HK. 2002. Intracellular membrane trafficking pathways in bone-resorbing osteoclasts revealed by cloning and subcellular localization studies of small gtp-binding rab proteins. Biochem Bioph Res Co. 293(3):1060-1065.

Zhong Y, Wang QJ, Li X, Yan Y, Backer JM, Chait BT, Heintz N, Yue Z. 2009. Distinct regulation of autophagic activity by atg14l and rubicon associated with beclin 1-phosphatidylinositol-3-kinase complex. Nat Cell Biol. 11(4):468-476.

Zhu G, Wu CJ, Zhao Y, Ashwell JD. 2007. Optineurin negatively regulates tnfalpha- induced nf-kappab activation by competing with nemo for ubiquitinated rip. Curr Biol. 17(16):1438-1443.